

ornl

ORNL/Sub/92-SL807/1

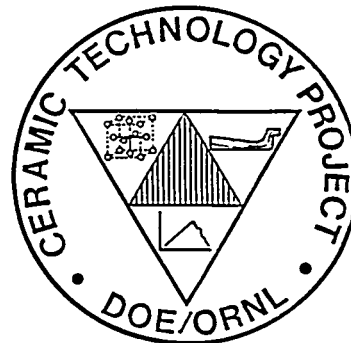
OAK RIDGE NATIONAL LABORATORY

MARTIN MARIETTA

High-Speed, Low-Damage Grinding of Advanced Ceramics Phase 1

J. A. Kovach
S. Malkin

CERAMIC TECHNOLOGY PROJECT



Prepared by
The Eaton Corporation
Manufacturing Technologies Center
Willoughby Hills, Ohio

MANAGED BY
MARTIN MARIETTA ENERGY SYSTEMS, INC.
FOR THE UNITED STATES
DEPARTMENT OF ENERGY

RECEIVED

MAY 10 1995

OSTI

This report has been reproduced directly from the best available copy.

Available to DOE and DOE contractors from the Office of Scientific and Technical Information, P.O. Box 62, Oak Ridge, TN 37831; prices available from (615) 576-8401, FTS 626-8401.

Available to the public from the National Technical Information Service, U.S. Department of Commerce, 5285 Port Royal Rd., Springfield, VA 22161.

This report was prepared as an account of work sponsored by an agency of the United States Government. Neither the United States Government nor any agency thereof, nor any of their employees, makes any warranty, express or implied, or assumes any legal liability or responsibility for the accuracy, completeness, or usefulness of any information, apparatus, product, or process disclosed, or represents that its use would not infringe privately owned rights. Reference herein to any specific commercial product, process, or service by trade name, trademark, manufacturer, or otherwise, does not necessarily constitute or imply its endorsement, recommendation, or favoring by the United States Government or any agency thereof. The views and opinions of authors expressed herein do not necessarily state or reflect those of the United States Government or any agency thereof.

DISCLAIMER

Portions of this document may be illegible in electronic image products. Images are produced from the best available original document.

Metals and Ceramics Division
HIGH-SPEED, LOW-DAMAGE GRINDING OF
ADVANCED CERAMICS PHASE 1

J. A. Kovach
Eaton Corporation

S. Malkin
University of Massachusetts

Date Published: March 1995

FINAL REPORT

Prepared by
The Eaton Corporation
Manufacturing Technologies Center
Willoughby Hills, Ohio
Subcontract No. 86X-SL807C

Funded by
Propulsion System Materials Program
Office of Transportation Technologies
the Assistant Secretary for
Energy Efficiency and Renewable Energy
U.S. Department of Energy
EE 51 05 00 0

for
OAK RIDGE NATIONAL LABORATORY
Oak Ridge, Tennessee 37831-6285
managed by
MARTIN MARIETTA ENERGY SYSTEMS, INC.
for the
U.S. DEPARTMENT OF ENERGY
under Contract DE-AC05-84OR21400

MASTER

DISTRIBUTION OF THIS DOCUMENT IS UNLIMITED *ble*

TABLE of CONTENTS

	<u>PAGE</u>
ABSTRACT.	1
1.0 INTRODUCTION and OBJECTIVES	1
2.0 BACKGROUND	3
3.0 TECHNICAL APPROACH	4
4.0 RESULTS and DISCUSSION	6
4.1 THERMAL MEASUREMENTS DURING GRINDING	6
4.1.1 Grinding Tests	6
4.1.2 Temperature Measurements with Thermocouples	7
4.1.3 Infrared Temperature Measurement System	9
4.1.4 Calibration of a Two-Color Detector System	10
4.1.5 Measurement with the Two-Color Detector System	12
4.2 HSLD GRINDING FEASIBILITY TESTS	13
4.2.1 Grinding Conditions	13
4.2.2 Surface Inspection Technique	14
4.2.3 Relationship of Surface Quality to Grinding Conditions	15
4.2.4 Relationships Between Lab Tests and Calculations	17
5.0 PRODUCTION IMPLEMENTATION CONSIDERATIONS	18
5.1 Creep-Feed and Cutoff Grinding	19
5.2 I.D. Finishing	21
5.3 O.D. Finishing	24
5.4 Other Practical Implementation Concerns	26
6.0 SUMMARY	27
7.0 ACKNOWLEDGMENTS	29
8.0 REFERENCES	30

LIST of FIGURES

<u>FIGURE</u>		<u>PAGE</u>
1	Grinding forces vs. removal rate (S/RBSN)	32
2	Grinding power vs. material removal rate (S/RBSN)	33
3	Specific energy vs. material removal rate (S/RBSN)	34
4	Surface roughness vs. depth of cut (S/RBSN)	35
5	Grinding forces vs. removal rate (SN-220)	36
6	Grinding power vs. material removal rate (SN-220)	37
7	Specific energy vs. material removal rate (SN-220)	38
8	Lab setup for embedded thermocouple measurement system	39
9	Max. temperature rise vs. depth into workpiece (1.25 mm hole)	40
10	Max. temperature rise vs. depth into workpiece (1.0 mm hole)	41
11	Temperature results: 16% energy partition, 25 ms time constant	42
12	Temperature results: 18% energy partition, 25 ms time constant	43
13	Temperature results: 18% energy partition, 37 ms time constant	44
14	Experimental setup for two-color infrared measurement system	45
15	Blackbody for two-color infrared measurement system calibration	46
16	Calibration setup for two-color infrared detector system	47
17	Chopped signal output from InSb cell at 380 °C	48
18	InSb and MCT cell initial calibration signals	49
19	Ratio of InSb and MCT signals from initial calibration	50
20	InSb and MCT cell signals from second calibration	51
21	Ratio of InSb and MCT signals vs. temperature (2nd calibration)	52

LIST of FIGURES (continued)

<u>FIGURE</u>	<u>PAGE</u>	
22	Transient signals from the InSb and MCT cells	53
23	Maximum signal rise from both cells vs. depth into workpiece	54
24	Signal ratio vs. depth into workpiece	55
25A	Effect of wheel speed on normal force	56
25B	Effect of wheel speed on tangential force	57
26	Effect of wheel speed on surface finish	58
27	Effect of wheel speed on pull out	59
28A	SEM photo: 43% surface fragmentation, low MRR, low V_s	60
28B	SEM photo: 12% surface fragmentation, low MRR, high V_s	61
28C	SEM photo: 16% surface fragmentation, moderate MRR, low V_s	62
28D	SEM photo: 9% surface fragmentation, moderate MRR, high V_s	63
29	Effect of wheel speed on unit grit load	64
30	Effect of wheel speed on grinding zone temperature	65
31	Creep feed cutoff setup	66
32	Creep feed grinding force components	67
33	Creep feed tangential grinding force vs. time	68
34A	Normal force vs. wheel speed - S/RBSN cylindrical specimens	69
34B	Power vs. wheel speed - S/RBSN cylindrical specimens	70
35A	Surface finish vs. wheel speed - S/RBSN cylindrical specimens	71
35B	Roundness vs. wheel speed - S/RBSN cylindrical specimens	72
36	Effect of wheel runout on normal force	73

LIST of FIGURES (continued)

<u>FIGURE</u>		<u>PAGE</u>
37	Normal force fluctuations for various brazed wheel conditions	74
38	Workpiece chatter as influenced by wheel speed - roundness	75
39	Workpiece chatter - lobe frequency & amplitude	76

LIST of TABLES

<u>TABLE</u>		<u>PAGE</u>
1	Material property data - S/RBSN & SN-220	77
2	HSLD surface grinding results summary	78
3	Creep feed grinding force and power summary	79
4	HSLD cylindrical grinding results summary - plated wheels	80
5	HSLD cylindrical grinding results summary - resin wheel	81

HIGH-SPEED, LOW-DAMAGE GRINDING OF ADVANCED CERAMICS

Dr. Joseph A. Kovach, Dr. Stephen Malkin

ABSTRACT

In the manufacture of structural ceramic components, it has been well documented that grinding costs can comprise up to 80% of the entire manufacturing cost. The majority of these costs arise from the conventional multi-step grinding process which generally requires numerous grinding wheels, additional capital equipment, additional perishable dressing tools, and additional labor.

In an attempt to reduce structural ceramic grinding costs, an initial feasibility investigation was undertaken to develop a single step, roughing-finishing process suitable for producing high-quality silicon nitride ceramic parts at high material removal rates and at substantially lower cost than traditional, multi-stage grinding processes. This feasibility study employed the combined use of laboratory grinding tests, mathematical grinding models, and characterization of the resultant material surface condition. More specifically, this Phase I final report provides a technical overview of **High-Speed, Low-Damage (HSLD)** ceramic grinding and the conditions necessary to achieve the small grain depths of cut necessary for low damage grinding while operating at relatively high material removal rates.

The particular issues that are addressed include determining the effects of wheel speed and material removal rate on the resulting mode of material removal (ductile or brittle fracture), limiting grinding forces, calculation of approximate grinding zone temperatures developed during HSLD grinding, and developing the experimental systems necessary for determining HSLD grinding energy partition relationships. In addition, practical considerations for production utilization of the HSLD process are also discussed.

1.0 INTRODUCTION and OBJECTIVES

With increasing demands placed on improving the performance and cost effectiveness of heat engines in a worldwide marketplace, additional emphasis is continually being placed upon maximizing manufacturing productivity while utilizing the state-of-the-art engine designs and materials. In particular, the role of structural ceramics in heat engines has evolved considerably from the onset of being an academic curiosity to the point where the primary concern is now

one of reducing final manufacturing costs. Unfortunately, the mechanical and physical characteristics which make these materials desirable from a product performance standpoint usually render them far from ideal in terms of manufacturability. Typically, structural ceramic finishing costs alone can account for up to 80% of the entire component manufacturing cost. Consequently, one of the most challenging tasks now faced by manufacturing process engineers is the development of a ceramic finishing process which maximizes part throughput rate while minimizing costs and associated scrap levels.

To maximize material removal rates in the grinding operations necessary for finishing structural ceramics, it is essential that the relationships between product performance, material behavior, and manufacturing processes are clearly defined in addition to understanding the effects of the required material removal process. Since the consequences of in-service ceramic failure can be catastrophic, extremely slow finishing operations are usually employed in an attempt to minimize process induced defects. Usually, a painstaking multi-step ceramic finishing process is deployed which requires numerous grinding wheels, additional capital equipment, additional perishable dressing tools, and additional labor. From this perspective, the development of improved grinding processes for structural ceramic heat engine components will require not only strict attention to the mechanics of the grinding process but requires a quantitative understanding of the aforementioned interrelationships.

Based on the concerns outlined above, the efforts summarized in this report represent the initial phase of a multi-phase program whose overall objective is to develop a single step, roughing-finishing process suitable for producing high-quality silicon nitride ceramic parts at high material removal rates and at substantially lower cost than traditional, multi-stage grinding processes. More specifically, the objective of this initial "Phase I" research is to undertake an exploratory feasibility investigation of **High-Speed, Low-Damage (HSLD)** grinding by using high wheel speeds and fine grit wheels to achieve the small grain depths of cut necessary for low damage grinding while operating at high material removal rates. The particular issues addressed include:

- Development of the experimental systems necessary for identifying approximate ceramic grinding zone temperatures and corresponding energy partition relationships
- Determining the effects of wheel speed and material removal rate on the resulting mode of material removal (low damage or fracture)
- Identifying what removal rates can be obtained under high speed low damage grinding conditions
- Outlining unique concerns for successful production implementation of cylindrical and surface grinding processes

2.0 BACKGROUND

Previous research on the grinding of ceramics indicates that the abrasive/workpiece interactions generally involve both ductile flow and brittle fracture. As the abrasive engages the workpiece, initial cutting action occurs by plastic or ductile flow which is followed by fracture if the grain depth of cut becomes sufficiently large. By analogy with indentation fracture mechanics, two principal types of cracks are generated: "lateral" cracks, which lead to material removal, and "radial or median" cracks, which cause strength degradation.

One implication from the past research is that fracture damage may be avoided or minimized if the grain depth of cut and/or unit grain load is kept below some critical level such that predominantly low-damage grinding occurs. The common approach to achieve this objective is to use extremely small removal rates (fine depths of cut and low workpiece velocities), which are **not** economical in production. From analytical considerations of grinding kinematics, the only apparent way to overcome this drawback, namely to achieve large removal rates while maintaining a small grain depth of cut, is through the use of high wheel speeds and fine grit wheels.

It should be noted that low damage and ductile mode grinding generally require a much higher specific energy (i.e. grinding energy input per volume of material removed) than mixed mode grinding which involves both ductile flow and fracture. This higher energy input will, in turn, lead to higher grinding zone temperatures. The results of some recent Japanese research¹ suggest that elevated grinding zone temperatures tend to inhibit fracture and promote the non-detrimental ductile mode of grinding. Moreover, the researchers achieved a "polished" surface finish (2 microinch Ra) using a fine grit wheel without impairing original material strength properties. High temperatures can thereby have a beneficial effect on the resulting surface integrity, which is contrary to the case of grinding metallic alloys.

It is hypothesized that the mechanical and thermal grinding effects can act in concert to enhance material removal rates while minimizing incipient microcracking tendencies in the ceramic workpiece. On the other hand, extreme heat can reduce diamond wheel life. In conventional grinding of metallic alloys with aluminum oxide wheels the majority of the grinding energy enters the workpiece as heat.² Conversely, when using superabrasive wheels, a large portion of the heat energy is transferred into the wheel due to its superior thermal conductivity.³ Since this "reverse" heat transfer phenomenon is even more pronounced when grinding ceramic materials with diamonds, it is important to understand the grinding "energy balance" to avoid reducing wheel life from excessive heat, while maximizing the thermal benefits arising from plastic deformation in the workpiece surface.

In order to calculate the transient temperature field in the workpiece, it is first necessary to determine what portion of the total grinding energy enters the workpiece as heat. Typically, an inverse heat transfer method is employed

whereby temperatures measured in the workpiece are used to obtain the heat input at the grinding zone.⁴ One approach is to use thermocouples embedded in close proximity to the workpiece surface. Recent work by Ueda, et al.⁵ indicates that temperatures may also be accurately measured near the workpiece surface using an infrared pyrometer with an optical fiber. Similar efforts involving infrared pyrometry are also underway at the University of Massachusetts to improve fundamental process understanding. Subsequently, through modification of the Carslaw-Jaeger⁶ moving band heat source model, a useful *thermal model* of ceramic grinding can be developed for approximate calculation of HSLD wheel/grinding zone temperatures.

Additionally, the *mechanical effects* of the unit grain load on resulting surface quality can be determined by measuring grinding forces. Typical fracture mechanics principles⁷ can be considered in combination with the aforementioned temperature effects to enhance overall HSLD process *model performance*. Ideally, it would be desirable to determine "thermal softening temperatures" and unit load combinations such that the grinding parameters can be appropriately altered to minimize wheel heating while maximizing material removal rates and plastic flow in the workpiece surface. With the above considerations in mind, the following technical approach was developed.

3.0 TECHNICAL APPROACH

The purpose of this section is to present the general approach used throughout the investigation. Many of the procedural details are provided as necessary in the following specific sections. Based on the background material presented earlier, it became apparent that a rather broad technical approach would be required to meet the feasibility objectives defined in the introduction. Owing to the large number of independent process variables and difficulty associated with on-line measurement of many of the dependent variables, an interdisciplinary approach which combines laboratory experimentation with previously established process models was employed.

The overall program utilized a team consisting of representatives from the Eaton Corporation and the University of Massachusetts. In addition, a close relationship with the High Temperature Materials Laboratory (HTML) at Oak Ridge National Laboratory (ORNL) was maintained to help develop an in-depth understanding of the resulting surface topography and its relationship to the mode(s) of material removal. Plastic flow and/or brittle fracture was determined through the use of scanning electron microscopy or, when possible, using high power optical atomic force microscopes. The majority of the laboratory grinding experimentation was conducted at Eaton's Corporate Machining Research Center (MRC) utilizing three fully instrumented grinding machines covering several grinding processes (conventional surface grinding, creep feed surface grinding, I.D. grinding, and O.D. cylindrical grinding). Where applicable, the

spindle power and grinding forces were measured. As a function of the process under examination, the following conditions were collectively varied to establish low damage grinding behavior at high material removal rates:

- Wheel speeds ranging from 5000 to 35,000 ft/min (25 - 178 m/s)
- Wide array of grinding wheel types with:
 - Various bond systems (plated, resin, etc.) and,
 - Various diamond grit sizes (ranging from 180 to 1200)
- Workpiece velocities covering:
 - Low speed creep feed conditions at 1 in/min (2.54 cm/min) to,
 - High speed O.D. grinding levels at 400+ ft/min (122 m/min)

Building on fundamental grinding kinematics and existing thermal grinding models, the University of Massachusetts, in conjunction with Eaton's MRC, utilized the above grinding data to calculate specific grinding energies, approximate unit grain loads, and corresponding grinding zone temperatures. Through modification of the Carslaw-Jaeger⁶ moving band heat source model, the long range goal is to develop a useful analytical model of HSLD grinding. Model verification will be performed through extensive analysis of the ground surface morphology. In this Phase I investigation, the University of Massachusetts developed a two-color infrared pyrometry system, described in the following section, to measure ceramic grinding zone temperatures.

The majority of tests conducted in this study utilized Eaton's newly developed sintered reaction bonded silicon nitride material (S/RBSN). Since this material is formed from elemental silicon using a high speed diffusion reaction, it offers the potential advantage of being considerably less expensive than conventional silicon nitride powder-based materials having comparable properties. Material blank fabrication was done using Eaton's pre-production manufacturing facilities at the CoRD-DC center. Documented material properties are similar to those of the Kyocera SN-220 silicon nitride material (approx. 600 MPa flexural strength, 3.25 g/cc density, 300 GPa E-modulus, etc.). As Table 1 indicates, the S/RBSN material compares favorably with the SN-220 material. In addition to material property comparisons, several grinding tests were conducted in this study to assess relative grindability as well.

4.0 RESULTS and DISCUSSION

4.1 THERMAL MEASUREMENTS DURING GRINDING

In order to calculate the temperatures generated by grinding, it is first necessary to know the fraction of the total grinding energy conducted as heat to the workpiece. In the present investigation, an inverse heat transfer method is being used to estimate the energy input to the workpiece from temperature measurements in the subsurface. This energy is then compared with the total measured energy input, obtained from the measured grinding forces and power, to determine the fraction of the grinding energy conducted as heat to the workpiece. Two types of temperature measuring systems are being used. The first utilizes a thermocouple embedded in the workpiece. The second utilizes an infrared detector and optical fiber. This latter system is more complex, but should provide much faster temperature response than the embedded thermocouple.

Before proceeding with temperature measurements, a series of grinding tests was conducted to provide a baseline to characterize the grinding behavior. The workpiece materials were sintered reaction bonded silicon nitride (S/RBSN) from Eaton Corporation and SN-220 silicon nitride from Kyocera. Temperature measurements with the embedded thermocouple technique were performed on S/RBSN. An optical infrared temperature measuring system, which utilizes a two-color (Indium Antimonide/Mercury Cadmium Telluride or InSb/MCT) detector was also developed. Subsequently, the system was set up and calibrated, and initial grinding tests were conducted.

4.1.1 Grinding Tests

Grinding tests were conducted under straight surface grinding conditions on sintered reaction bonded silicon nitride (S/RBSN). The results are summarized in Figures 1-4. Figure 1 shows the normal and tangential force components as a function of removal rate per unit width ($Q' = v_w a$). The forces were measured with a Kistler 9257A dynamometer. The removal rate was varied by altering both the workpiece velocity v_w and wheel depth of cut a . Note that both force components increase approximately linearly with removal rate and that the normal force is approximately 3-5 times larger than the tangential force. At the largest removal rate per unit width of $8.5 \text{ mm}^2/\text{s}$, the forces were initially found to be substantially above the straight line in each case. However, when the wheel was periodically cleaned with an abrasive stick between each grinding pass, the forces were reduced close to the straight lines, which suggests that the high forces were caused by loading of the wheel with workpiece material. Direct measurements of the net spindle power P are also shown in Figure 2. As expected, the product of the tangential force component

from Figure 1 and the wheel velocity v_s was found to be virtually the same as the power for each data point.

The corresponding specific grinding energy is shown in Figure 3. A trend of slightly decreasing specific energy was obtained with increasing removal rates. Although similar results were previously obtained in the UMass grinding laboratory for the grinding of hot pressed silicon nitride (HPSN) with a comparable diamond wheel, the magnitude of the specific energy in the previous tests was about 35% higher than for the present results. The lower specific energy with the S/RBSN suggests that this material may not be as tough as the HPSN.

After grinding, the surface roughness R_a was measured using a Surtronic 3P. The data are summarized in Figure 4 in terms of R_a versus depth of cut for various workpiece velocities. The results suggest that surface roughness is more strongly affected by workpiece velocity than depth of cut.

Grinding tests on the SN-220 from Kyocera were also conducted under straight grinding conditions in order to compare the results with those obtained on the S/RBSN from Eaton. Figure 5 shows the normal and tangential force components versus removal rate per unit width. Measured normal grinding force for the Kyocera material had less scatter than the measurements on sintered reaction bonded silicon nitride (S/RBSN). At the largest removal rate per unit width of $Q'=7.25 \text{ mm}^2/\text{s}$, wheel loading such as found with the S/RBSN did not occur. Figure 6 shows the direct measurements of the net spindle power P , which again are virtually the same as the product of the tangential force and the wheel velocity v_s . The corresponding specific energy is shown in Figure 7. Comparing Figure 3 with Figure 7, it can be seen that the specific energy for the Kyocera material is very close to the energy measured for the Eaton S/RBSN.

4.1.2 Temperature Measurements with Embedded Thermocouples

Temperature measurements with embedded thermocouples were conducted under straight grinding conditions on S/RBSN. The experimental setup for measuring the temperature response and grinding power is illustrated in Figure 8. Note that a hole was drilled in each specimen, and then a thermocouple (type K, 36 gauge wire) installed and held with high temperature cement. Each thermocouple junction was initially about 1.2 mm from the top surface of the workpiece. The grinding test was continued by taking successive passes under the same conditions until the thermocouple was ground and destroyed. The machine was left idle for a few minutes between successive passes in order to ensure that the temperature of the workpiece returned to the ambient temperature before the next grinding pass. The last grinding pass was taken for reference as zero depth, and the locations of the previous grinding passes were then calculated.

All grinding passes were performed in the upgrinding mode using a 5% soluble oil grinding fluid and a Norton SD150-R100BX619C grinding wheel. For the first test, a hole of 1.25 mm diameter was used. The results, summarized in

Figure 9, show a plot of the maximum temperature rise for each grinding pass versus depth into the workpiece. It can be seen that the maximum measured temperature rise from a depth of 0.2 mm to 0.7 mm was almost insensitive to the depth, which is contradictory to what was expected. It is suspected that this was caused by a combination of an oversized hole for the thermocouple, too much cement, and poor contact between the thermocouple and the workpiece at the bottom of the hole.

The next experiment used a smaller hole of 1.00 mm diameter and much less cement. The maximum temperature rise for each grinding pass versus depth in this configuration is shown in Figure 10. Although there is some scatter, the maximum grinding zone temperature obtained with each subsequent pass closer to the surface tended to increase as expected. An example of the temperature response at a depth of 0.0375 mm below the workpiece surface is shown in Figure 11. The horizontal scale is dimensionless length x/l , where x is the distance from the center of the heat source at the grinding zone (positive ahead) and l corresponds to half the theoretical geometrical wheel-workpiece contact length l_c . Using moving band heat source theory, the measured temperature response can be compared with the theoretical temperature response for the input heat flux to the workpiece ϵq , where ϵ is the fraction of the total energy transported as heat to the workpiece and q is the total heat flux at the grinding zone. The total heat flux at the grinding zone was obtained as $q=P/l_cb$, where P is the net grinding power, l_c is the geometrical wheel-workpiece contact length ($l_c=(d_s a)^{1/2}$), and b is the workpiece width. In this test the net grinding power was about 1.8 kw, which corresponds to a specific energy of about 36 J/mm³.

The theoretical temperature response in the workpiece was numerically calculated using a finite difference method with the assumption of a triangular heat source at the grinding zone. Unfortunately, correlation between the theoretical and measured temperature responses was not good, as the measured temperature response tended to lag significantly behind the theoretical response (see Figure 11 for data at a depth of 0.0375 below the surface). Therefore, a time constant τ was also introduced into the theoretical model, which essentially models the temperature measuring system as a first order system. By selecting appropriate values for τ and ϵ , the modified theoretical results can be matched to the experimental results. As shown in Figure 11, a time constant of $\tau=25$ ms and an energy partition of $\epsilon=16\%$ appear to provide a reasonable match. Figures 12 and 13 show temperature responses and theoretical results at other depths, which would indicate that the energy partition to the workpiece is about $\epsilon=18\%$. In comparison to grinding of ferrous alloys with conventional aluminum oxide wheels (where ϵ can be as high as 80 to 90%) this is a relatively low value. However, for CBN superabrasive grinding of ferrous alloys the energy partition to the workpiece ϵ is on the order of 20 to 50%. In light of the aforementioned system response issues, it is critical to conduct more tests before definitive energy partition conclusions can be drawn.

In an attempt to reduce thermal inertia and improve system response, additional embedded thermocouple tests were conducted using a smaller drilled hole (0.75mm diameter) with less cement to secure the thermocouple. However, even after several tests, the results were still not satisfactory. Based on calculations using moving heat source theory and an analysis of the measured temperature, the temperatures still did not rise as rapidly as they should have. Microscopic observations of exposed thermocouple junctions after the tests revealed insufficient bonding of the cement to the surrounding ceramic workpiece. Apparently, the smaller hole made it more difficult to apply the cement. Subsequently, another approach was evaluated using a small amount of solder instead of cement to hold the thermocouple. Improved contact between the thermocouple and ceramic was expected, however the results were again unsatisfactory. Although only a very small amount of solder was used, the thermal inertia of the thermocouple increased causing a significantly slower response.

Based on the above tests, it is felt that peak ceramic grinding temperatures can not be accurately and consistently measured in process using the thermocouple approach due to the inherent time delay problems. One possible reason is the poor contact between the thermocouple tip and the ceramic workpiece. With a metallic workpiece, the thermocouple can be welded to the workpiece, thereby providing improved contact and a faster time constant (about 5 ms). Accuracy with a ceramic workpiece may also be worse due to its lower thermal conductivity (which may induce additional thermal inertia errors) and reduced heat conduction from the junction through the thermocouple wires. For the one successful test, the thermocouple was apparently fully cemented at the bottom of the hole. Obviously, any additional temperature measurements will require a more reliable system. It is felt that an infrared system, which uses an optical fiber to conduct the signal from the workpiece to a sensor, should be more reliable and provide a faster response.

4.1.3 Infrared Temperature Measurement System Characteristics

The development of the infrared system and selection of the infrared detector focused on thermal calculations, practical mechanical aspects of the system, and calibration techniques. Thermal calculations were made to determine the strength of the signal incident on the receiving surface of the optical fiber. These calculations were made using the lowest expected signal condition (i.e. at a lowest expected temperature of about 100 °C). The attenuation of this signal through the optical fiber and the ratio of the signal to noise were also determined. Various ways of polishing the surfaces and preparing the fiber for connections to the workpiece and to the detector were considered. The ends of the fiber must be polished periodically because deterioration of the surface can occur due to inadvertent mechanically inflicted scratches, chemical reactions or deposits from fluids, and thermal damage. Although damage to the end surfaces will not obviate the signal, it will influence

the calibration of the temperature measurements. In addition, large changes in fiber curvature will influence signal conduction and have a deleterious effect on the calibration. Consequently, a 2 m optical fiber length was selected to minimize curvature change and at the same time keep the detector and other electronics away from the immediate grinding operation.

Initially a single detector system was considered, however, for improved performance a two-color detector was subsequently selected. The advantage of the two color detector is that the measured temperature is determined by the ratio of the signals received by two cells, thus the emissivity of the material is not required to estimate the temperature. It also appears that the conditions of both ends of the fiber may have less influence on the measurement. Furthermore, unlike with a single-color system, movement of the fiber will not affect the two-color system accuracy. It is also expected that the time response of the two-color detector system should be almost as fast as a single detector system. Moreover, other problems inherent with a single detector (such as calibration and transient changes in the system) are less problematic with the two-color system.

An InSb/MCT (Indium Antimonide & Mercury Cadmium Telluride) detector was selected to cover a temperature range from room temperature to about 500 °C. The InSb cell absorbs and detects radiation at wavelengths from 1.0 to 5.5 μm , while radiation with wavelengths longer than 6.0 μm are detected by the MCT cell. Optical fibers made of chalcogenide (which transmit radiation between 3 μm to 11 μm) were selected. According to the thermal calculations at 100 °C, the energy transmitted to the detector from a 2 meter chalcogenide fiber with core diameter 500 μm is about 0.819 microwatts for wavelengths from 3.0 to 5.5 μm , and is about 14.7 microwatts for wavelengths from 6 to 11 μm . At 500 °C, the input energy is about 60 microwatts for wavelengths between 4 and 5.5 μm , and 220 microwatts for wavelengths between 6 to 11 μm .

4.1.4 Development and Calibration of a Two-Color Detector System

A schematic of the experimental infrared system setup is shown in Figure 14. Note that the infrared system utilizes a hole from the under side of the workpiece, analogous to the thermocouple system. Radiation from the workpiece is transmitted by the fiber to a detector which converts the radiation energy from the fiber to an electrical signal. The two-color InSb/MCT detector system was supplied with built-in preamplifiers and an optical SMA connector in a metal dewar. The unit is operated at a temperature of 77 °K using liquid nitrogen. Two chalcogenide fibers with core diameters of 0.01 and 0.02 inch were purchased. Although a fiber with a larger cross sectional area can transmit more energy, the incident radiation comes from a larger area which tends to average the thermal data.

For calibrating the system, a blackbody (Figure 15) was made from pure copper to ensure isothermal conditions within the body during cooling. Two

thermocouples were installed in the copper body to monitor the temperature. A hole was drilled, threaded and coated with lampblack to provide high emissivity as a true blackbody. A hot plate (Omega, Chromalox Roph-204) with a maximum temperature of 500 °C was used to heat the blackbody for calibration. A 240 voltage power line was installed in the laboratory for operating the hot plate.

A special fixture was designed and built to hold the workpiece specimen and the optical fiber. Since the fiber is quite delicate, the fixture protects and guides the fiber from the workpiece to prevent fracture if the bending radius becomes too small. This fixture also adapts to a Kistler dynamometer for grinding tests.

An analog tape recorder was selected to record all the data. The tape recorder (Racal Recorder/V-Store 8) can simultaneously record up to 8 channels of data with bandwidths from DC up to 100 kHz. Recorded signals can be replayed and transmitted to a PC data acquisition system. The analog signals can be sampled and filtered at different frequencies for data analysis.

Since the infrared system used in this project employs a fiber to transmit the radiation from the workpiece to the detector, the calibration must be done with the fiber. As previously indicated, the two-color detector system consists of two infrared cells, MCT and InSb. The MCT cell has an AC amplifier, and the InSb cell has a DC amplifier. The AC-coupled cell can detect only an AC signal. Therefore, a mechanical chopper was constructed to modulate the radiation from the blackbody so that the chopped signal can be detected by the cell. The experimental setup for calibrating the system is shown in Figure 16, and a chopped signal output in Figure 17. The difference between the highest and lowest values in Figure 17 represents the sensitivity of the cell.

The system was calibrated by monitoring the temperature of the blackbody as it slowly cooled from an initial temperature after heating. Electrical signals from the two cells were recorded by a PC. In these initial tests, a fiber with 0.020 inch core diameter was used to calibrate the system. Output signals from the two cells are shown in Figure 18. The ratio of the signal from the InSb cell to the signal from the MCT cell as a function of temperature is shown in Figure 19. Unfortunately, the signal fluctuated and became weaker at temperatures below 200 °C, which greatly reduced the accuracy. After polishing the fiber end, a second calibration was conducted which resulted in more consistent data in the lower temperature range. Figure 20 shows the signals after the second calibration, while Figure 21 represents the ratio of the two signals. By comparing the results from these two calibrations, it can be seen that although the absolute values from these two calibrations are somewhat different, the ratios from both of these separate calibrations are very close. It appears that the fiber end condition did not significantly affect the ratio.

4.1.5 Temperature Measurement with the Two-Color Detector System

Once the system calibration was completed, several grinding tests were conducted on the UMass Brown & Sharpe 1236 Hi-Tech CNC grinder using 8.5 mm wide S/RBSN specimens provided by Eaton. A 12" diameter Norton ASD120-R75B56-1/8 wheel was used at a wheelspeed of 30 m/s and workspeed of 158 mm/s. The wheel depth of cut was 0.0375 mm for grinding with fluid, and 0.0254 mm for grinding without fluid. Prior to grinding, the wheel was trued using a silicon carbide brake-controlled truing device then subsequently conditioned with a silicon carbide abrasive stick. A tape recorder (Racal Recorder/V-store 8) was used to record the signals from the two detector cells, the power monitor, and the Kistler force dynamometer. One channel was used to record voice to facilitate locating data files during signal retrieval. The grinding test involved taking successive passes under the same conditions until reaching the hole with the fiber.

To protect the fiber end surface from damage during the first grinding test, the fiber was not placed in direct contact with the bottom surface of the hole. Unfortunately, only weak signals were obtained from the two cells. In order to increase the temperature, the fluid flow was turned off. This increased the output, but the signals were much smaller than expected. Again, it was suspected that the fiber tip was too far from the bottom surface of the hole.

The fiber end was then polished, and a second grinding test was conducted. This time the fiber end was placed in direct contact with the bottom surface of the hole with grinding fluid applied. At first a good signal was obtained, but became weaker as testing continued. Even after turning off the grinding fluid, the signal remained too small. The grinding test was stopped before the hole was ground through. After cleaning the fluid around the fixture and specimen, the specimen was removed from the fixture. The fiber end was found to be contaminated by grinding fluid. Apparently the fluid had gradually penetrated the interface between the specimen and the fixture, causing the signal to become too weak.

A third grinding test was performed without fluid. In this case, much stronger signals were recorded from both cells. The transient signals shown in Figure 22 were obtained from the two cells at a depth of 0.2 mm below the grinding surface. The maximum signals received from both cells versus depth into the workpiece are given in Figure 23 while the signal ratio is presented in Figure 24. Note that the ratio at shallow depths exceeded the maximum calibration value at 500 °C, indicating that the temperatures exceeded 500 °C. It should be noted that during the last few passes the signals from the MCT cell started to fluctuate. This fluctuation could be caused by degradation of the heated end of the fiber.

The results of these initial grinding tests indicate that the infrared detector can be used to measure temperatures in the workpiece subsurface during the grinding of ceramics. In order to improve performance, subsequent efforts will focus on methods to prevent grinding fluid from contaminating the fiber end and

to make the system more robust. Fibers with smaller core diameters will also be used to detect more localized temperatures on smaller areas of the workpiece. Additional thermal analyses will be conducted based on the experimental results using moving heat source theory to better estimate the energy partition to the workpiece.

4.2 HIGH-SPEED, LOW-DAMAGE GRINDING FEASIBILITY TESTS

As indicated in the introduction, this initial Phase I effort is intended to be an exploratory project directed toward determining the technical feasibility of high speed low damage grinding of Si₃N₄ (specifically Sintered RBSN). The efforts described in this section will focus primarily on surface grinding results obtained using plated wheels at speeds up to 35,000 SFM (178 m/sec) and material removal rates up to 1 in²/min (11mm²/sec). All reported grinding tests were conducted at the Eaton Manufacturing Technologies Center (MTC) Machining Research Center (MRC) using fully instrumented research grinders capable of operating under a wide variety of speeds, feeds, and configurations. Subsequent workpiece surface characterization was performed at the Oak Ridge National Laboratories (ORNL) High Temperature Materials Laboratory (HTML).

4.2.1 Grinding Conditions

Prismatic S/RBSN specimens were ground on a custom built "semi-creep feed" surface grinding machine capable of operating at workpiece velocities between 1 - 180 in/min (0.42 - 76 mm/sec) with wheel speeds up to 40,000 SFM (203 m/sec). Aside from the prismatic specimen tests, limited cylindrical grinding was performed on a modified Weldon 1632 Universal ID/OD grinder for the high speed O.D. grinding studies. Wheel speeds as high as 40,000 SFM (203 m/sec) are also attainable on the modified Weldon. As will be discussed later, the relative contact lengths and workpiece velocities developed under cylindrical grinding conditions can be much different than those seen in surface grinding thereby resulting in considerably different unit grit loads, localized workzone temperatures, and chip formation modes.

Data logging was accomplished using a PC-based data acquisition package and/or strip chart recorders. In the surface grinding modes (pendulum and creep feed) force data was measured using a standard 3-axis Kistler force dynamometer platform. Of particular interest are the normal and tangential grinding forces. In the cylindrical grinding modes, the normal force was measured using Kistler piezoelectric load washers built into the feed screws of the machine tool. In all cases, spindle power was measured using watt transducers. In subsequent tests, the temperature data will be recorded for all surface grinding tests, and where possible for some of the cylindrical grinding studies, using an infrared pyrometer equipped with an optical fiber input.

All tests discussed in this section were conducted using Eaton S/RBSN material. Material blank fabrication was done using Eaton's pre-production

manufacturing facilities at the CoRD-DC center. Building upon an agreement with Coors Golden Technologies, production material will be subsequently employed as Coors ramps-up its production S/RBSN manufacturing facility. Documented material properties are similar to those of the Kyocera SN-220 silicon nitride material (approx. 600 MPa flexural strength, 3.25 g/cc density, 300 GPa E-modulus, etc.).

These tests were designed to identify how high wheel speeds and removal rates might impact resulting grinding forces, finishes, and surface quality. A relatively coarse (120 grit) brazed diamond wheel was used. As a function of the process under examination, the following conditions were collectively varied to establish low damage grinding behavior at high material removal rates. A summary of all test data and grinding related parameters is presented in Table 2. Note that wheel speed was increased from 5000 SFM (25 m/s) to 35,000 SFM (178 m/s) in increments of 10,000 SFM (51 m/s) while the material removal rate was varied from 0.125 in²/min (1.34 mm²/s) to 1 in²/min (10.75 mm²/s) by incrementing the depth of cut and workpiece velocity as follows:

Depth of Cut inches (mm)	Part Velocity in/min (mm/s)	Removal Rate in ² /min (mm ² /s)
0.0025 (.0635)	50 (21)	0.125 (1.34)
0.0050 (.1270)	50 (21)	0.250 (2.69)
0.0025 (.0635)	100 (42)	0.250 (2.69)
0.0050 (.1270)	100 (42)	0.500 (5.38)
0.0150 (.3810)	50 (21)	0.750 (8.06)
0.0100 (.2540)	100 (42)	1.000 (10.8)

4.2.2 Surface Inspection Technique

It has been well documented that in the grinding of ceramic materials, the resulting workpiece surface is covered predominantly by machining grooves produced from the abrasive grit cutting action. Unfortunately, fragmented areas are also developed on the surface as a result of micro-fracture arising from the grinding process. These "fractured" regions have been referred to as pull-out, surface damage, pitting, grinding damage, and surface fragmentation. Such damage, may extend several micrometers into the material and are often the origin of failure in the finished ceramic component. For the purposes of these experiments, the surface quality will be given by the percent pull out or surface fragmentation. As reported by T. Bifano⁸ and J. Mayer⁹, a percent damaged area on the order of 10% to 15% was considered as the ductile mode grinding threshold.

After grinding, subsequent workpiece surface characterization was performed at the ORNL HTML. From a most fundamental perspective, all specimen surfaces were initially characterized using standard contact-type

(stylus) surface profilometry equipment (see summary data in Table 2). More importantly, the extent of plastic flow and/or brittle fracture was then determined through the use of optical and scanning electron microscopy. The method employed for quantifying surface fragmentation at the HTML is based on the point-counting technique described in Quantitative Metallography¹⁰ and by Underwood in Quantitative Stereology¹¹. Basically, a transparency with a grid consisting of one hundred points is randomly superposed on a micrograph (300 to 800X mag) of the ground surface. Points that fall within the fragmented regions are counted as 1 while points falling on the boundary between fragmented and unfragmented regions are counted as half. The total number of counts is then divided by the total number of points in the grid (100 in this case) to give a percentage. To improve statistical reliability, a grand average was obtained by repeating the procedure on micrographs obtained from 10 randomly chosen locations on each specimen. The results of these studies are described in the following section.

4.2.3 Relationship of Surface Quality to Grinding Conditions

Under the conditions outlined above, it can be seen that the grinding forces decrease considerably with increased wheel speed and/or reduced material removal rate (see Figures 25A & 25B). In general, the grinding forces are reduced by approximately a factor of two when increasing the wheel speed from conventional speeds (e.g. 5000 SFM, 25 m/s) to over 25,000 SFM (127 m/s). From a production grinding standpoint this can be significant when rough grinding a relatively weak or difficult to fixture component. Somewhat surprisingly at the highest removal rates (1 in²/min, 10.75 mm²/s) the normal force tended to increase slightly at 35,000 SFM (178 m/s). This is most likely the result of some observed wheel loading. As expected, however, the grinding forces decrease nearly linearly with decreased removal rate.

Figure 26 illustrates the wheel speed effects on surface finish for the Eaton S/RBSN material. This graph shows a tendency toward improved surface finish as wheel speed is increased. Hypothetically, this is a direct result of increased workzone temperatures which tend to promote increased ductile/glassy flow. Additional tests will be conducted to confirm this hypothesis. Note however, in several cases, the surface roughness increased somewhat at the highest wheel speed (35,000 SFM, 178 m/s). This is most likely the result of a slight wheel imbalance which was observed at the highest speed.

More interesting is the improved surface finish achieved by going to high material removal rates - - even while operating at conventional wheel speeds. Realize that typical industrial ceramic roughing rates do not go much beyond 0.125 in²/min (1.34 mm²/s). However, by dramatically increasing the removal rate, an improved surface is developed. Again, it is speculated that this may be a result of increased workzone temperatures which promote plastic flow. From an industrial perspective, this suggests that the emphasis on minimizing stock envelopes via near-net shape technologies may not be as critical as once

anticipated. What is not clear yet are the material removal rate and wheel speed interactions and their effect on wheel life.

Possibly the most significant findings to date are graphically illustrated in Figure 27. The data imply two notable trends:

- Increasing wheel speed, while operating at a relatively low material removal rate of 0.125 in²/min (1.34 mm²/s) or less, can dramatically reduce surface fragmentation. A five fold wheel speed increase from 5000 SFM (25 m/s) to 25,000 SFM (127 m/s) reduced "pull out" by almost a factor of four. To a lesser extent, the same trend is true at higher material removal rates. Surface fragmentation was reduced 2.5 fold by increasing wheel speeds when operating at 1 in²/min (10.75 mm²/s).

- Alternatively, increasing the material removal rate was also shown to reduce surface fragmentation. Approximately a three fold reduction in "pullout" was achieved by increasing removal rates from 0.125 in²/min (1.34 mm²/s) to 1.0 in²/min (10.75 mm²/s) while operating at conventional wheel speeds. At 35,000 SFM (178 m/s) a two fold reduction in surface fragmentation was achieved by increasing the material removal rate.

SEM photomicrographs illustrating the above observations are also provided in Figures 28A through 28D. Figure 28A shows the resulting workpiece surface after grinding at 0.125 in²/min (1.34 mm²/s) with a wheel speed of 5000 SFM (25 m/s). The "white-frosted" areas represent regions of surface fragmentation. In this case, roughly 43% of the surface was "fragmented". However, by increasing the wheel speed to 35,000 SFM (178 m/s), while keeping all other conditions constant, surface fragmentation was reduced to 12% (see Fig. 28B) - - which is indicative of "low damage" grinding. Alternatively, by contrasting Figures 28A & C, or 28B & D, it can be seen that increasing the material removal rate from 0.125 in²/min (1.34 mm²/s) to 0.5 in²/min (5.38 mm²/s) can also reduce the degree of surface fragmentation without increasing the wheel speed. Again, some "pullout" reduction is also evident by going to higher wheel speeds even while operating at relatively high material removal rates (compare Figures 28C & 28D). As indicated by the data in Table 2, the lowest level of surface fragmentation (6%) was achieved at the highest removal rate and highest wheel speed.

Although extensive MOR testing was not performed*, these results tend to suggest that a transition from a "brittle fracture" mode of grinding to a low damage "ductile" grinding mode can be achieved by increasing wheel speeds and/or material removal rates. As alluded to earlier, one possible explanation for this behavior stems from the fact that the grinding force per grit (unit grit load) is reduced significantly by increasing wheel speeds (see Figure 29) which, in turn, will reduce the surface fracture tendency.

*Planned for Phase II of the effort

It should be noted that the unit grit load data was determined by measuring the actual grinding force and by counting the number of grits per unit of wheel area using photomicrographic techniques. The wheel/workpiece contact area was based strictly on the calculated geometric contact length. In this fashion, an approximate unit grit load could be calculated.

Realize however, that unit grit load considerations alone will not account for the low surface fragmentation witnessed when operating at the highest material removal rates. Additional consideration must be given to the potential effect of increased workzone temperature developed at high material removal rates and/or wheel speeds which could help to promote plastic flow within the workzone. As indicated in the Background section, it is felt that critical threshold grit load and workzone temperature combinations can be identified to avoid grinding damage.

4.2.4 Relationships Between Grinding Results and Thermal Calculation Results

In an initial attempt to gain some preliminary understanding of how the grinding parameters might affect the workzone temperatures, approximate thermal calculations were performed using the Carslaw-Jaeger moving band heat source solution as given in (4). It must be emphasized that, as with most thermal analyses, a linear heat transfer model has been used with the assumption of constant thermal properties independent of temperature. In addition, this initial model does not include convective cooling effects. Moreover, the actual fraction (ϵ) of the total grinding energy (u_{total}) which enters the workpiece as heat is yet to be identified; but, was assumed to be 50% for these calculations. Nevertheless, based on the following relationship it can be seen that increased specific grinding energy or increased material removal rates can lead to increased temperature rise (Θ_m) within the workzone.

$$\Theta_m = \frac{1.13\alpha^{1/2} a^{3/4} V_w^{1/2} (\epsilon U_{total})}{kde^{1/4}}$$

Where;

- Θ_m = maximum grinding zone temperature rise
- α = thermal diffusivity = 0.016 in²/sec = 0.10cm²/sec
- a = depth of cut
- V_w = workpiece velocity
- ϵ = fraction of total grinding energy conducted as heat into the workpiece, assumed to be 50% in this case

U_{total} = total specific grinding energy

k = thermal conductivity = 17.34 BTU/hr.ft.^{°R} = 30 Watt/m^{°K}

d_e = equivalent grinding wheel diameter, which equals the wheel diameter for surface grinding (12 in. (305 mm) in these tests).

General temperature trends were subsequently plotted in Figure 30 by using the above relationship with mean thermal property data and the actual grinding test data as given in Table 2. Recognize that the primary purpose of this graph is *not* to predict absolute workzone temperatures, but rather to illustrate maximum grinding zone temperature trends as a function of wheel speed and material removal rate. From this perspective, the graph clearly shows the tendency toward increased workzone temperatures at elevated wheel speeds and material removal rates. Interestingly, the lowest level of surface fragmentation (6%) occurred under the highest temperature conditions (i.e. highest MRR, highest wheel speed) while the lowest temperatures resulted in the highest surface fragmentation (43%). Follow-on efforts will focus on refining the model to better predict surface fragmentation (Fig. 27) under varying wheel speeds and removal rates based on the combined effects of reduced unit grit load (Fig. 29) and the resulting thermal behavior (Fig. 30).

Recalling the force and surface finish graphs discussed earlier, a production processing strategy for a thin, near-net component may utilize high grinding wheel speeds to minimize fragmentation and maintain material properties. On the other hand, for more robust components having a larger stock envelope, increasing the material removal rate per pass while operating at conventional wheel speeds may be the most attractive. Again, the process economic trade-offs between wheel life, throughput, and resulting surface integrity must yet be examined.

5.0 PRODUCTION IMPLEMENTATION CONSIDERATIONS

In addition to the testing discussed above, numerous tests were performed in the Eaton Machining Research Center (MRC) to address potential concerns/limitations associated with the HSLD grinding process. These included a series of HSLD tests designed to increase cutoff rates by creep-feed grinding and precision bore finishing rates using alternative single stroke honing processes. In addition, data clearly show the influence of wheel roundness and system balance on the resulting ceramic surface while operating at increased wheel speeds.

5.1 Creep-Feed and Cutoff Grinding

In the finishing of structural ceramics, parting operations (i.e. cutoff) are often required to achieve correct component length. From a fundamental perspective, this process is somewhat analogous to surface creep feed grinding. Accordingly, the initial Eaton test series was focused on HSLD cutoff operations using creep feed grinding. The primary objective was to identify potential process limitations with respect to material removal rate and resulting surface finish. During this study, approximately 30 S/RBSN specimens were "slit" lengthwise under full-depth, creep feed grinding conditions using 0.0625" (1.6 mm) wide wheels. The rectangular specimens, provided by Coors Golden Technologies, were approximately 4.0 " long x 0.370" wide x 0.430" deep (101.6 x 9.4 x 10.9 mm).

A schematic representation of the test setup is shown in Figure 31. Note that the specimen is mounted to the "fixture base" by using a cyanoacrylate adhesive. Upon conclusion of the test, the resulting halves are dis-mounted by using either a hot plate (to melt the glue) or a solvent (to soften the glue). In all cases, the fixture base is mounted to a Kistler 3-axis dynamometer to measure forces. In addition, a spindle power monitor was used to help determine the "effective" tangential & normal forces developed under full-depth creep feed grinding conditions. To accurately determine the actual grinding power and forces developed during deep slitting operations, it is important to subtract the forces arising from fluid impact, frictional rubbing on the sides of the wheel, as well as any hydrodynamic forces arising from coolant in the slot. This is done by performing several "dead" passes to characterize the parasitic loss components. During these tests approximately 0.75 H.P. (3 lbs. horizontal force) was consumed by the parasitic losses, which can account for about 25% of the total power.

It is also important to note that under full-depth creep feed grinding conditions the forces measured by the dynamometer (horizontal and vertical forces) are **not** equivalent to the actual tangential and normal forces. As shown in Figure 32, the horizontal and vertical force vectors must be resolved to determine the total tangential and normal forces which effectively act at the location given by the angle γ . (Since all tests were conducted in the "up" grinding direction, the force vectors shown in Figure 32 apply to up grinding.) In these tests the depth of cut was quite large (0.430"), consequently the angle γ was also quite large (approx. 16°). Note that the angle γ can be determined by equating the measured power with the measured horizontal and vertical forces. Alternatively, by assuming a triangular force distribution, it can be shown that γ acts at a point approximately 2/3 of the way up the arc-length-of-contact¹³. Interestingly, the 2/3 approximation was good to within 2% for the majority of these creep-feed ceramic grinding tests.

As an initial starting point, a Norton resin bonded diamond wheel (SD100 - R 50 B 69, 8" O.D.) was utilized at a feed rate of 0.5 in/minute (12.7 mm/min) at

a full depth of 0.430" (10.9 mm) and a wheel speed of 10,000 SFM (50.8 m/s). Once the wheel reached the full arc-length-of-cut at approximately 2.25" (57.15 mm) into the cut, the power spiked dramatically, which in turn actually set the resin wheel on fire. This power spiking phenomenon, known as "burn-out", is commonly observed in full-depth creep feed grinding of metallic alloys, and can be attributed to boiling of the coolant within the workzone. In an attempt to reduce "burn-out", the feed rate was reduced by a factor of two (to 0.25 in/min, 6.4 mm/min). However, once again, the power spiked thereby igniting the resin bond in the wheel. As shown in Table 3, the specific energy ranged from 51×10^6 in-lbs/in³ (351 joule/cu mm) to 154×10^6 in-lbs/in³ (1060 joule/cu mm).

To improve the initial cutting effectiveness, the wheel was pre-conditioned by taking a series of 36 up-grinding passes through a 5" (127 mm) long Norton 37 C 150 H11 VKPM abrasive stick purchased from the Sticks & Stones Company. A feed rate of 10 in/min (254 mm/min) was used at a depth of 0.300" (7.62 mm). Wheel speed remained constant at 10,000 SFM (50.8 m/s). Just as in the case of the grinding tests, Cimperial 1011 (at a 10:1 ratio) was applied through two nozzles at 40 PSI (0.2769 MPa) and 7.5 GPM (28.4 l/min) per nozzle. This conditioning approach was used for the balance of the tests.

Once having re-conditioned the wheel, the test was repeated. Both the specific energy and heat flux dropped considerably. Moreover, burn-out was not observed. However, wheel wear was a concern with the resin bonded wheel. Therefore, in an effort to improve G-Ratios, the wheel was changed to a Regal metal bonded wheel (MD 80 N 50 M).

Using the Regal MD 80 N 50 M wheel, the feed rate was increased until "burn-out" occurred. As shown in Figure 33 the tangential force develops considerable spiking when the fluid begins to boil in the workzone. A similar burn-out spiking behavior was observed for the power and normal force. Note, however, that after burn-out occurs the forces and power return to a value lower than before the spike. Since the power and forces reach extremely high values during the spike, the wheel can self-sharpen (i.e. high forces breakdown the wheel to expose fresh cutting edges). Alternatively, due to the extreme heat, slight expansion of the wheel and/or workpiece can occur to momentarily increase the amount of stock removed, after which time the effective stock removal is temporarily reduced when the wheel/workpiece return to their normal dimensions. The net effect in either case is a subsequent reduction in force.

It should be noted that during spiking (burn-out) an orange fire-band temporarily developed around the periphery of the metal bonded wheel. However, unlike the resin wheel, the metal wheel did not catch on fire. In addition, the burn-out heat flux (140,186 in-lb/in²-sec, 24.65 joule/mm²-sec) was considerably higher for the metal wheel than for the resin wheel (81,161 to 120,132 in-lb/in²-sec, 14.8 to 22 joule/mm²-sec). Therefore, it was decided to continue to use the metal bonded wheel owing to its higher temperature capabilities and potential for higher material removal rates.

In an attempt to further reduce the propensity for burn-out at increased feed rates, a coolant induction channel was added to the setup (see Figure 31) to assist in directing coolant into the workzone. By introducing additional coolant into the workzone, additional heat energy can be convected away before any vapor barrier forms from fluid boiling. Ideally, a transition from pool boiling to forced flow boiling can be developed in the workzone to increase heat transfer. As Table 3 indicates, by adding the coolant channel, burn-out was eliminated with the metal wheel at the 0.6 in/min (15.2 mm/min) feed rate. Subsequently, the feed rate was increased to 1.0 in/min (25.4 mm/min). Again, burn-out was not observed. Note, however, the maximum heat flux did not exceed 125,863 in-lb/in²-sec (23 joule/mm²-sec). Consequently, it appears that the threshold burn-out heat flux appears to be on the order of 140,186 in-lb/in²-sec (24.65 joule/mm²-sec) for the MD 80 N 50 M metal bonded wheel. To date, feed rates have been increased to 2.0 in/min (50.8 mm/min) at full depth.

5.2 I.D. Finishing

In addition to addressing the challenges associated with creep feed grinding, the complexities of creating an I.D. of precise dimension, form and surface finish were also investigated. Initially, tests at Eaton's Manufacturing Technologies Center (MTC) examined the possibility of increasing material removal rates by HSLD I.D. grinding. It must be realized, however, that conventional I.D. grinding suffers from several limitations. First of all, even with a spindle speed of 60,000 RPM it is difficult to exceed 7800 SFM (40 m/s) on small diameter I.D. wheels (e.g. 0.5", 12.7 mm). Secondly, the I.D. grinding quill is not very rigid which, in turn, seriously limits material rates. Lastly, due to the "flexible" quill, precision dressing of the diamond I.D. wheel is severely hampered. As a consequence of these factors acting in concert, the resulting bore surface exhibited extreme taper (0.005", 0.127 mm) even at relatively low material removal rates.

Therefore, the possibility of using a single stroke diamond honing process as a substitute for I.D. grinding was investigated. In these tests all honing was done on a Maho MH-700-S five axis CNC machining center using the horizontal spindle. The objective was to generate an ID to +/- 0.0002 in (+/- 0.005 mm), with a roundness tolerance of 0.000118 in (0.003 mm) and have a surface finish better than 8 μinches R_a (0.2 micron). Two materials were used for the study, Eaton S/RBSN and Kyocera SN-220. Diamond sleeves, used to produce the ID's, ranged in grit sizes from 100, for roughing, to 1200 for superfinishing.

The tool consisted of a tool holder, mandrel, abrasive sleeve, pilot and adjustment screw. The majority of the tool components were purchased from Sunnen Products in St. Louis, MO. The size of the tool could be set by turning the adjustment screw one indicating notch for every 0.0001 in (0.0025 mm) of stock off the diameter to be removed. The adjustment screw draws the sleeve up the tapered mandrel, causing the sleeve to expand.

All tests were conducted using RD2 265M coolant from Master Chemical of Perrysburg, OH, mixed at a 20:1 dilution ratio. Coolant was applied using a "through the tool" technique and an external flood. Coolant was fed along the shaft from jets 90 degrees apart at the end of the tool holder. The external flood was applied 180 degrees apart. This allowed a direct flow of coolant into the work zone. A feed rate of 30 in/min (12.7 mm/sec) was used to feed the tool through the part. The tool was retracted at 472 in/min (200 mm/sec). The surface speed of the sleeve at 125 ft/min (0.64 m/s).

Two methods of material removal were tried. The first was a fixed stage approach. In other words, the total stock removal would occur over a predetermined number of passes, from roughing to finishing. The number of stages (passes) was determined as a function of the stock envelope and the recommended depths of cut. For the Eaton parts, with an average stock envelope of 0.027 in (0.70 mm), eleven stages were required. Only nine stages were needed to remove the 0.018 in (0.47 mm) stock envelope on the Kyocera material.

Abrasive Sleeve Descriptions

<u>Tool Type</u>	<u>Grit Size</u>	<u>Material Removal Range - Off Diameter</u>	
		<u>(inches)</u>	<u>(millimeters)</u>
Roughing	100	0.001 - 0.004	0.03 - 0.10
Semi-Roughing	220	0.0005 - 0.003	0.013 - 0.076
Semi-Finishing	400	0.00005 - 0.0005	0.001 - 0.013
Finishing	800	0.000025 - 0.0002	0.0006 - 0.051
Super-Finishing	1200	0.000025 - 0.00005	0.0006 - 0.0013

The material removal rate (MRR) was determined by assuming that a cylinder of material was being removed per unit time per unit abrasive width (i.e. length of hone). The length of the sleeve was six inches (150 mm) and the duration of the grind was 0.20 min (12 seconds). It should be realized that since the I.D. honing tools are approximately 12 times longer than typical I.D. wheels, the calculated MRR appears rather low. Nevertheless, in a production setting, this process lends itself to low-cost multi-spindle machines. Cycle times on the order of 12 seconds can be expected, versus 2 minutes with traditional I.D. grinding. The following table lists the maximum material removal rate for a given depth of cut.

Material Removal Rates

<u>Depth of Cut Off Diameter</u>		<u>Max. Material Removal Rate at Depth of Cut</u>	
<u>(inch)</u>	<u>(mm)</u>	<u>(in³/in/min)</u>	<u>(mm³/mm/sec)</u>
0.004	0.10	0.0032	0.034
0.003	0.08	0.0024	0.026
0.0005	0.013	0.00041	0.0044
0.0003	0.008	0.00025	0.0027
0.0002	0.005	0.00017	0.0018
0.0001	0.003	0.000066	0.00071

Initially, this fixed stage approach appeared desirable since it could easily be transformed into a production process. The number of machines, cycle times, and other production variables could all be clearly identified. Unfortunately, the parts have to be near final size. If a part has a large stock envelope, large depths of cut are required. In our tests, this method proved unsatisfactory due to excessive chipping at the exit end of the bore. The relatively large depths of cut, 0.003 - 0.004 in (0.08 - 0.10 mm) off the diameter, caused unacceptable chipping. It was shown that the Eaton S/RBSN material had more pronounced chipping than did the Kyocera SN -220 material.

Subsequently, a fixed material removal approach was used with less abusive depths of cut. Roughing was initially tried at 0.001 in. (0.025 mm) off the diameter. Although this approach reduced the exit chipping, deep scratches were developed in the workpiece surface. Based on visual examination, it appeared as though the scratches were more pronounced in the Kyocera material than in the Eaton material. This may be due to the fact that the Eaton material is more porous than the Kyocera material, thus "masking" the apparent scratch depth.

In the next set of tests, the roughing depth of cut was changed to 0.0005 in (0.013 mm) per pass, with finishing at 0.0002 in (0.005 mm) and superfinishing at 0.00005 in (0.001 mm) per pass. Chipping was significantly reduced on the Eaton material, to the point where it could be removed by lightly surface grinding the chipped face. Unfortunately, the main problem with this fixed material removal approach is the extreme number of steps required to finish the bore. Including all passes for grinding and tool sizing, a total of 45 steps was required to finish the bores.

Little appreciable wear of the abrasive sleeves was observed, with the exception of the 400 grit sleeve. Power increased from the indistinguishable level in the early tests, to approximately 0.12 HP (0.089 kW). Another indication of tool wear was an improvement in surface finish. With a new 400 grit sleeve, the best attainable R_a was 8 μ inch (0.2 micron). After 0.0476 in³ of combined Eaton S/RBSN and Kyocera SN-220 stock removal with the 400 grit sleeve, the

R_a improved to 3.4 microinch (0.09 micron). Based on the observed honing tool wear, this translates to an approximate G-Ratio of over 6000.

From a roundness tolerance perspective, the objective was to develop bore roundness on the order of 118 μ inches (3.0 microns) with a surface finish of 7.9 μ inches (0.2 microns). Measurements were made at the entrance, middle, and exit of the bore. Roundness was worst at the entrance, but in all cases was well within the desired roundness tolerance limits as given in the table below.

Average Roundness at the Entrance, Middle and Exit of Bore

<u>Units</u>	<u>Entrance</u>	<u>Middle</u>	<u>Exit</u>
μ inch	65.4	19.7	33.5
micron	1.66	0.50	0.85

In general, the single stroke honing process was able to create parts that exceeded typical ceramic journal bore tolerances and surface finishes. Some investigation must continue, however, to determine why the entrances of the bores were more likely to be out of round, while the middle of the bore was six times better (on average) than the required bore roundness tolerance. One possibility is due to runout of the tool (the mandrel ranout about 0.002" at the tip). Also, improved material removal rates and optimal abrasive surface feeds need to be determined. Perhaps by lowering the unit grit load (by increasing surface speed), chipping and light scratching can be eliminated. It should also be noted that although the G-Ratios were quite good at conventional honing speeds, the process economics may not compare favorably with I.D. grinding when considering the relatively high honing tooling costs. Additional economic studies are planned for the Phase II follow-on effort.

5.3 O.D. Finishing

One of the final series of tests conducted during this Phase I investigation involved the generation of precision O.D. tolerances under HSLD conditions. Initially, the majority of this work took place using plated wheels. The data summarized in Table 4 pertains to O.D. grinding of cylindrical specimens using a workpiece velocity of 390 ft/min (1980 mm/s). As expected, the data shows that an improved finish and reduced surface fragmentation is achieved by using a finer grit wheel (400 vs. 120). Also note that at the highest material removal rates significant reductions in grinding force are achieved by going to higher wheel speeds. However, in several cases with the 120 grit wheel, increased wheel speed tended to increase surface roughness and pullout. Although this finding is somewhat contrary to the surface grinding studies discussed previously, it lends considerable insight to the HSLD grinding process behavior. It is important to realize that several factors, listed below, can dramatically affect

localized workzone temperatures and unit grain loads, which in turn may alter the material removal mode:

- 1) The roller workpiece velocity is between 50 to 100 times greater than for the case of surface grinding. This may tend to promote increased surface fracture.
- 2) The O.D. contact length is approximately 10 to 50 times less than in surface grinding. This results in much higher contact pressures (i.e. unit grit loads) and the onset of surface fragmentation.
- 3) The maximum wheel speed used in this O.D. study was limited to 11,300 SFM (57 m/s) rather than the 35,000 SFM (178 m/s) used in the surface grinding studies. Higher wheel speeds generally result in higher specific energies, which in turn may increase workzone temperatures and plastic flow to reduce surface fragmentation.

Aside from the plated wheel studies described above, a series of HSLD O.D. grinding tests was conducted using a 400 grit, 100 concentration, resin bonded wheel from Coors to grind cylindrical specimens made by Eaton and Kyocera. All tests were performed on an instrumented Weldon 1632 grinder. Both normal force and grinding power were measured. A summary of the test conditions and results are presented in Table 5. Unlike in previous surface grinding tests with plated wheels, the wheel speed was limited to 15000 SFM to avoid de-laminating the resin bonded material from the aluminum core as well as to minimize the possibility of igniting the resin at high speeds.

The resulting normal force and grinding power as a function of wheel speed for the Eaton specimens is shown in Figure 34A and 34B. Note that the grinding power remained relatively constant (see Figure 34B) over the speed range tested; thus indicating that the tangential force decreased with increasing wheel speed. This behavior is typical of what was previously observed with plated wheels¹². Conversely, increasing the wheel speed tended to *increase* the normal force in all tests using this fine grit resin bonded wheel, which is somewhat contrary to what was observed in the previous plated wheel tests¹². Recall that with either 120 grit or 400 grit plated wheels the normal forces were reduced at higher wheel speeds. It is speculated that increasing the wheel speed increased the grinding zone temperatures, thereby softening the resin bond to the point where the abrasive was not rigidly supported and could not readily penetrate the ceramic. Consequently, perhaps only high temperature bond systems (such as vitrified, metal, etc.) should be considered for HSLD grinding processes. Future work will include thermal measurements and various bond systems to better understand this unique normal force behavior at high speeds.

Some indication of resulting surface quality is given Figures 35A & B. Note that in almost all cases, the resulting surface finish and component roundness tended to deteriorate with increased wheel speeds. For comparison,

in previous plated wheel tests utilizing 120 & 400 grit abrasive, the surface finish tended to improve with increased wheel speeds using the 120 grit plated wheel, while increasing speeds with the 400 grit wheel resulted in a poorer surface finish. In future studies, tests with a coarse 120 grit resin wheel should be conducted to better understand these potentially opposing tendencies.

5.4 Other Practical Implementation Concerns

In addition to the operations discussed above, considerable testing was performed at Eaton MTC to address potential practical HSLD concerns and to better understand the influence of wheel roundness and system balance on the resulting ceramic surface while operating at increased wheel speeds. As given in Figure 36, the relative performance of two similarly manufactured 120 grit brazed diamond wheels is compared. The new 1.0" wheel was to be used in a Phase II series of HSLD G-Ratio studies. Unfortunately, a 15 to 20 pound normal force oscillation was present with the 1.0" wheel versus only a 3 pound oscillation with the 0.5" wheel (see Fig. 36). Indicator ring measurements showed that the wheel was mounted concentric to within ± 0.0005 ". However, by expanding the time scale on the force output trace, it could be seen that the wheel had two high and two low spots on its outside diameter. The force traces presented in Figure 37 represent two revolutions of the 1.0" wide grinding wheel. Subsequently, measurements taken around the outside diameter of the wheel showed it to be out-of-round by approximately 0.002 inch.

In an attempt to "round-up" the wheel, approximately 8 in³ of S/RBSN was ground from a series of prismatic specimens. However, as shown in Figure 37, this approach essentially **doubled** the apparent force fluctuation in addition to doubling the total grinding force. As a result, the wheel was sent back to the vendor to be stripped, re-ground, and re-brazed with new abrasive. Upon receipt of the re-brazed wheel, the test was repeated. Again, however, the force fluctuation was still present (see Fig. 37). The exact reason for the out-of-round condition was not determined, but was most likely linked to the high temperature brazing process which could have led to thermal distortion of the unique hub on the 1.0" wheel. Currently, a conventional diamond plating process is being used to recoat the wheel. This new plated 1.0" wide wheel will then be employed in the HSLD G-Ratio studies in the Phase II follow-on effort.

As stated above, it is important to realize that in generating a high quality surface finish, several additional factors, aside from grit size, must be considered collectively. For example, as alluded to in Figures 36 & 37, any wheel runout can have a profound effect on force fluctuation. This effect can be manifested in reduced surface quality. Additionally, any wheel imbalance can also deteriorate surface finish. More allusive however, is the problem of regenerative chatter which encompasses system compliance, dynamics of the grinding action, as well as all of the previously mentioned factors.

Figure 38 shows the development of some regenerative chatter by going from a wheel speed of 6500 SFM to 15,000 SFM with a 400 grit resin bonded

wheel. The amplitude and frequency of the "lobbing" is provided in Figure 39. Note that at low speeds a small 3 lobed pattern is apparent with lobe heights of 0.187 microns. However, as the wheel speed is increased to 15,000 SFM, a pronounced 22 lobe pattern is generated with lobe heights of 0.702 microns.

Typically, the first source of chatter to be considered is wheel imbalance and runout. However, with a dressable resin wheel, runout was negligible. Similarly, wheel balance checks showed the system to be well within accepted levels. Recall, however, that as the wheel speed was increased the normal forces increased (see Table 5 and Figure 34A) which in turn could have contributed to vibration of the workpiece mounting arbor. In addition, it is hypothesized that increasing the wheel speed also increased the grinding zone temperatures to the point where the resin bond could not adequately support the abrasive, thereby resulting in more of a "smearing or stick/slip" cutting action rather than a smooth grinding action. From this perspective, perhaps only *dressable* high temperature bond systems (such as vitrified, metal, etc.) should be considered for HSLD grinding processes.

6.0 SUMMARY

An initial exploratory feasibility study of the **High Speed Low Damage** (HSLD) grinding process was undertaken to identify how high wheel speeds and removal rates might impact resulting grinding forces, finishes, and surface quality of silicon nitride. Using a relatively coarse (120 grit) brazed diamond wheel, tests were conducted at wheel speeds up to 35,000 SFM (178 m/sec) and material removal rates up to 1 in²/min (11mm²/sec). It was shown that the grinding forces decrease considerably with increased wheel speed and/or reduced material removal rate and that a tendency toward improved surface finish is developed as wheel speed is increased. Moreover, an improved surface finish was obtained by going to high material removal rates; even while operating at conventional wheel speeds.

It was also found that increasing wheel speed, while operating at a relatively low material removal rate, can dramatically reduce surface fragmentation. One possible explanation for this behavior stems from the fact that the unit grit load is reduced significantly by increasing wheel speeds. Alternatively, increasing the material removal rate was also shown to reduce surface fragmentation. Therefore, consideration must be also given to the effect of increased workzone temperature developed at high material removal rates and/or wheel speeds which could help to promote plastic flow within the workzone. Although extensive MOR testing is yet to be performed, these results suggest that a transition from a "brittle fracture" mode of grinding to a low damage "ductile" grinding mode can be achieved by increasing wheel speeds and/or material removal rates.

In an attempt to experimentally identify the actual grinding zone temperatures, two laboratory systems were designed, built, and evaluated. The initial system employed a thermocouple embedded in the workpiece. It was demonstrated, however, that the peak ceramic grinding temperatures could not be accurately and consistently measured in-process with this approach due to the inherent time delay problems. One possible reason is the poor contact between the thermocouple tip and the ceramic workpiece. Accuracy with a ceramic workpiece may also be worse due to its lower thermal conductivity (which may induce additional thermal inertia errors) and reduced heat conduction from the junction through the thermocouple wires.

To provide a faster temperature response and improved reliability a two-color infrared pyrometry system, which uses an optical fiber to conduct the signal from the workpiece to a sensor, was evaluated. Unlike with a single-color system, movement of the fiber will not affect accuracy, fiber end conditions have less influence on the measurement, and, most importantly, the emissivity of the material is not required to estimate the temperature. Based upon limited testing, the results indicate that the two-color infrared detector can be used to measure temperatures in the workpiece subsurface during grinding. However, in order to improve performance, subsequent efforts will focus on methods to prevent grinding fluid from contaminating the fiber end and to make the system more robust. Fibers with smaller core diameters will also be used to detect more localized temperatures on smaller areas of the workpiece. Additional thermal analyses will be conducted using moving heat source theory to better estimate the energy partition to the workpiece. In addition, future efforts will also identify grinding zone temperatures developed under a wide range of material removal rate and wheel speed combinations and the subsequent affects on MOR strength and wheel life.

In summary, possibly the most significant findings to date which demonstrate initial HSLD feasibility are given in Figure 27, in that:

- Increasing wheel speed, while operating at a relatively low material removal rate of $0.125 \text{ in}^2/\text{min}$ ($1.34 \text{ mm}^2/\text{s}$), can dramatically reduce surface fragmentation. A five fold wheel speed increase from 5000 SFM (25 m/s) to 25,000 SFM (127 m/s) reduced "pull out" by almost a factor of four. At low wheel speeds, roughly 43% of the surface was "fragmented". However, by increasing the wheel speed to 35,000 SFM (178 m/s), while keeping all other conditions constant, surface fragmentation was reduced to 12% - - which is indicative of "low damage" grinding.

- Alternatively, increasing the material removal rate was also shown to reduce surface fragmentation. Approximately a three fold reduction in "pullout" was achieved by increasing removal rates from $0.125 \text{ in}^2/\text{min}$ ($1.34 \text{ mm}^2/\text{s}$) to $1.0 \text{ in}^2/\text{min}$ ($10.75 \text{ mm}^2/\text{s}$) while operating at conventional wheel speeds. At 35,000 SFM (178 m/s) a two fold reduction in surface fragmentation was achieved by increasing the material removal rate.

7.0 ACKNOWLEDGMENTS

Research sponsored by the U.S. Department of Energy, Assistant Secretary for Energy Efficiency and Renewable Energy, Office of Transportation Technologies, as part of the Ceramic Technology Project of the Propulsion System Materials Program, under contract DE-AC05-84OR21400 with Martin Marietta Energy Systems, Inc.

In addition, the authors would like to acknowledge the efforts of the following personnel:

Eaton Manufacturing Technologies Center -
Michael R. Cooney, Sr. Laboratory Technician
Michael A. Laurich, Jr. Engineering Support
Dr. Karl R. Ziegler, Sr. Materials Engineering

University of Massachusetts -
Professor J. Edward Sunderland, Thermal Measuring Techniques
Bo Zhu, PhD Student, Thermal Testing and Analysis

Oak Ridge National Laboratory -
Dr. P. J. Blau, Technical Program Contact
Dr. S. Srinivasan, Material Surface Analysis

University of North Dakota
Dr. B. Bandyopadhyay, Material Surface Analysis

8.0 REFERENCES

- 1) Nishioka, T., et al., Development of High Strength Si₃N₄ Sintered Body for the Valve Systems of Automotive Engines, SAE Technical paper #920384, February 24 - 28, 1992.
- 2) Kovach, J.A., and Malkin, S., "Grinding Energy Relationships for Superalloy Materials", Proc. Seventeenth North American Manufacturing Engineering Research Conference, SME, May 1989, pp. 185-192
- 3) Guo, C., and Malkin, S., "Heat Transfer in Grinding", 1st International Conference on Transport Phenomena in Processing, Hawaii, 1992.
- 4) Malkin, S., Grinding Technology, Ellis Horwood series in Mechanical Engineering, 1989.
- 5) Ueda, T., Yamada, K., and Sugita, T., "Measurement of Grinding Temperature of Ceramics Using Infrared Radiation Pyrometer With Optical Fiber", Transactions of the ASME, 1992.
- 6) Carslaw, H.S., and Jaeger, J.C., Conduction of Heat in Solids, Oxford University Press, London, 1959, pp. 266-270.
- 7) Evans, A.G. and Marshall, D.B., "Wear Mechanisms in Ceramics", Fundamentals of Friction and Wear of Materials, Edited by D.A. Rigney, ASME, 1981, p. 439.
- 8) Bifano, T., Dow T., Scattergood, R. O., "Ductile-Regime Grinding of Brittle Materials", Proceedings of the International Congress for Ultraprecision Technology, Ultraprecision in Manufacturing Engineering, pp. 22-40, May 1988.
- 9) Mayer, J. E., Fang, G. P., Diamond Grinding of Silicon Nitride Ceramic, NIST Special Publication #847, Machining of Advanced Materials, July 1993, pp. 205-222.
- 10) Vander Voort, G. F., Quantitative Metallography: Principles and Practice, McGraw-Hill Publishing Company, New York, N.Y., 1984, p. 426.
- 11) Underwood, E. E., Quantitative Stereology, Addison-Wesley, Reading, MA., 1970, p. 5.
- 12) Kovach, J.A., et al., "A Feasibility Investigation of High Speed, Low Damage Grinding for Advanced Ceramics", SME Fifth International Grinding Conference, held in Cincinnati, October 26-28, 1993.

13) Guo, Krishnan, and Malkin, "Matching Forces and Power in Creep-Feed Grinding", SME Fifth International Grinding Conference, held in Cincinnati, October 26-28, 1993.

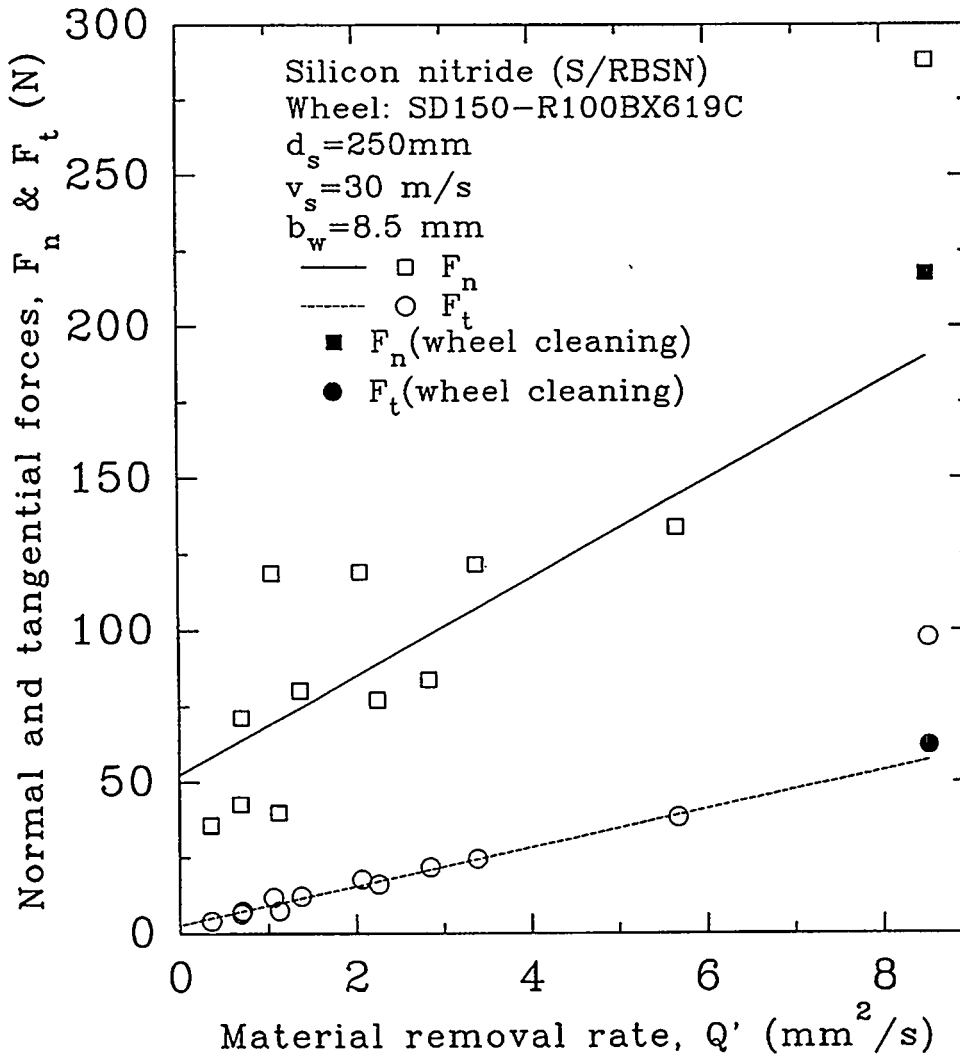


Figure 1. The normal and tangential grinding forces versus material removal rate per unit width.

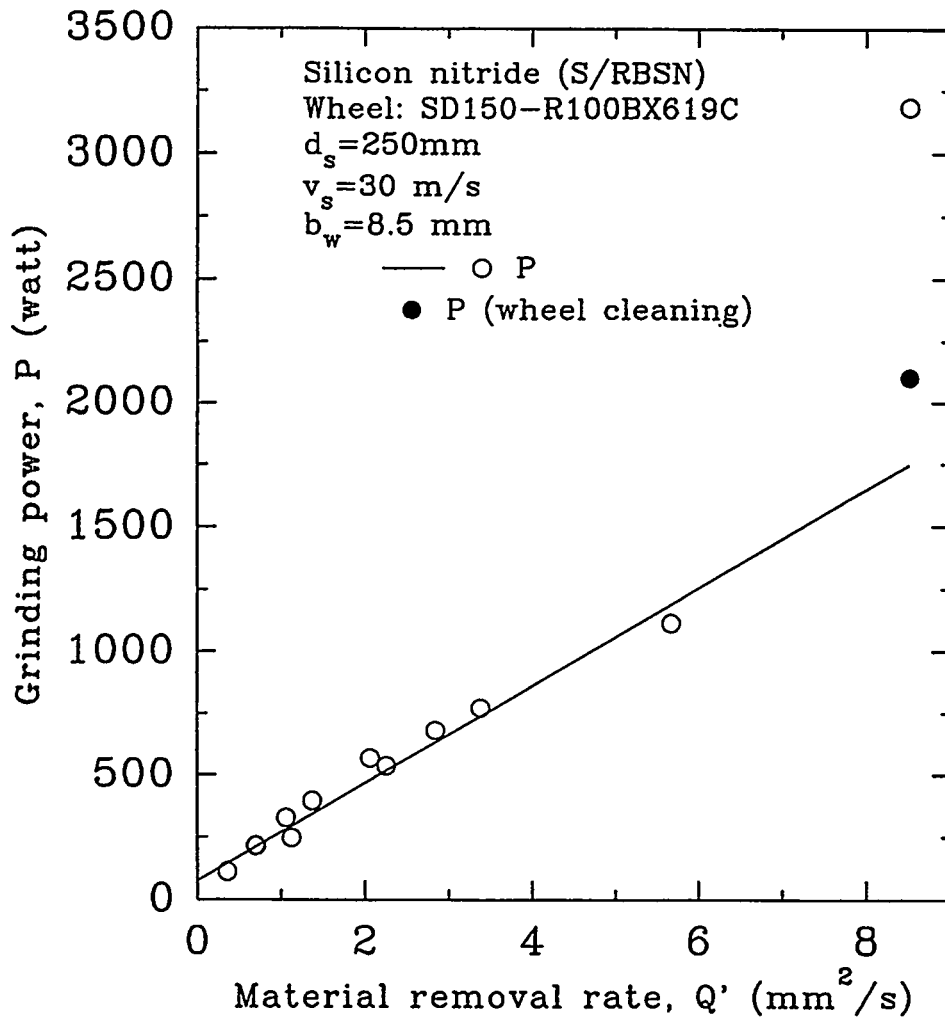


Figure 2. The grinding power versus removal rate per unit width.

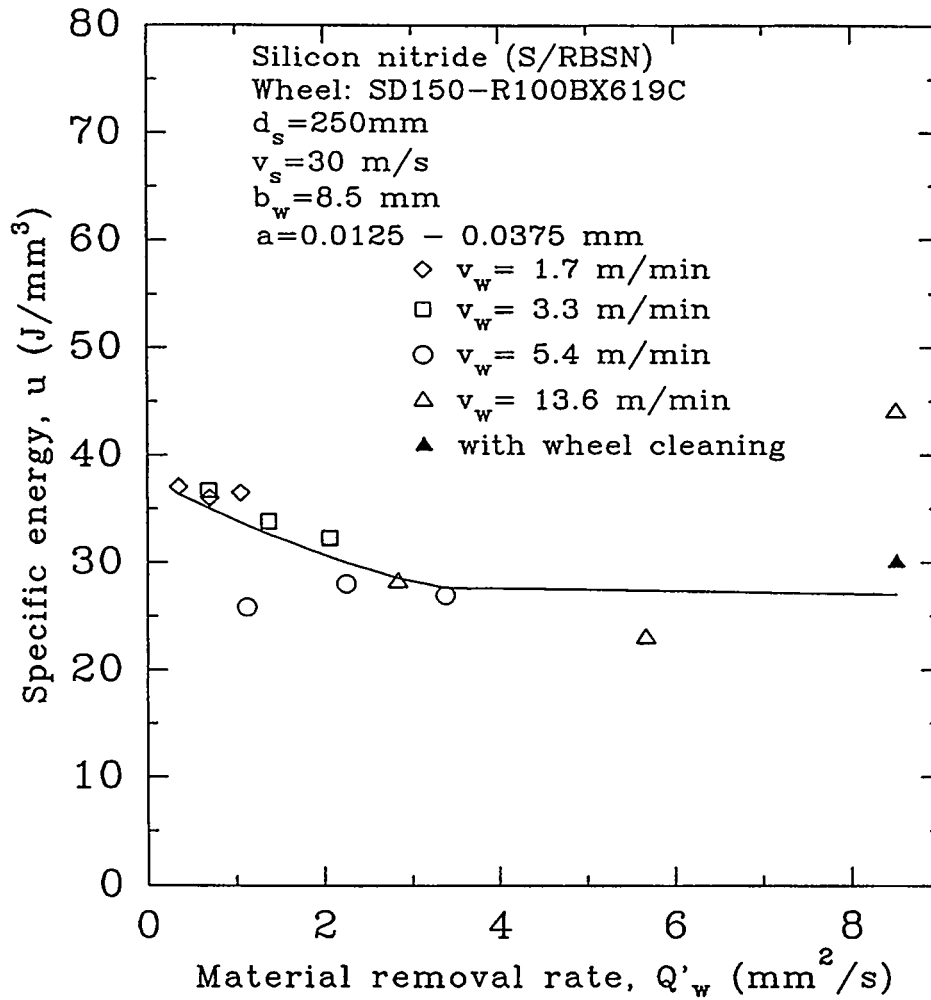


Figure 3. The specific energy versus removal rate per unit width.

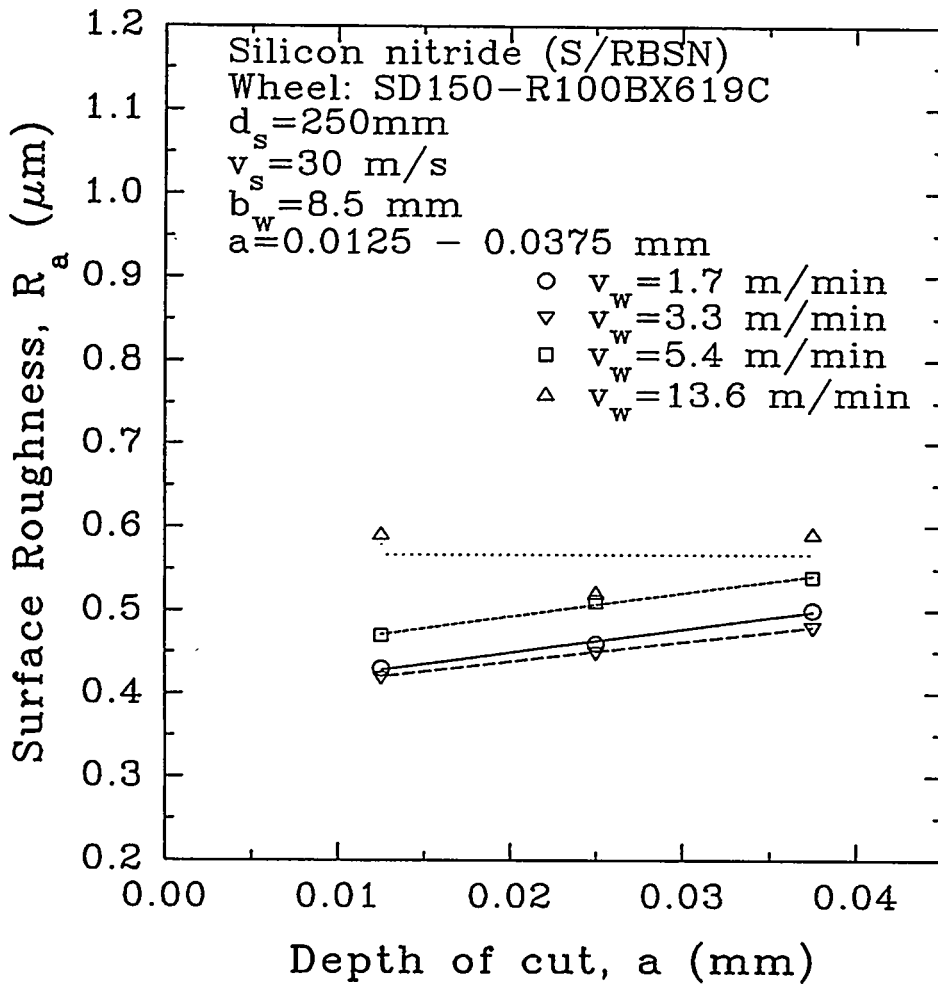


Figure 4. Surface roughness versus depth of cut.

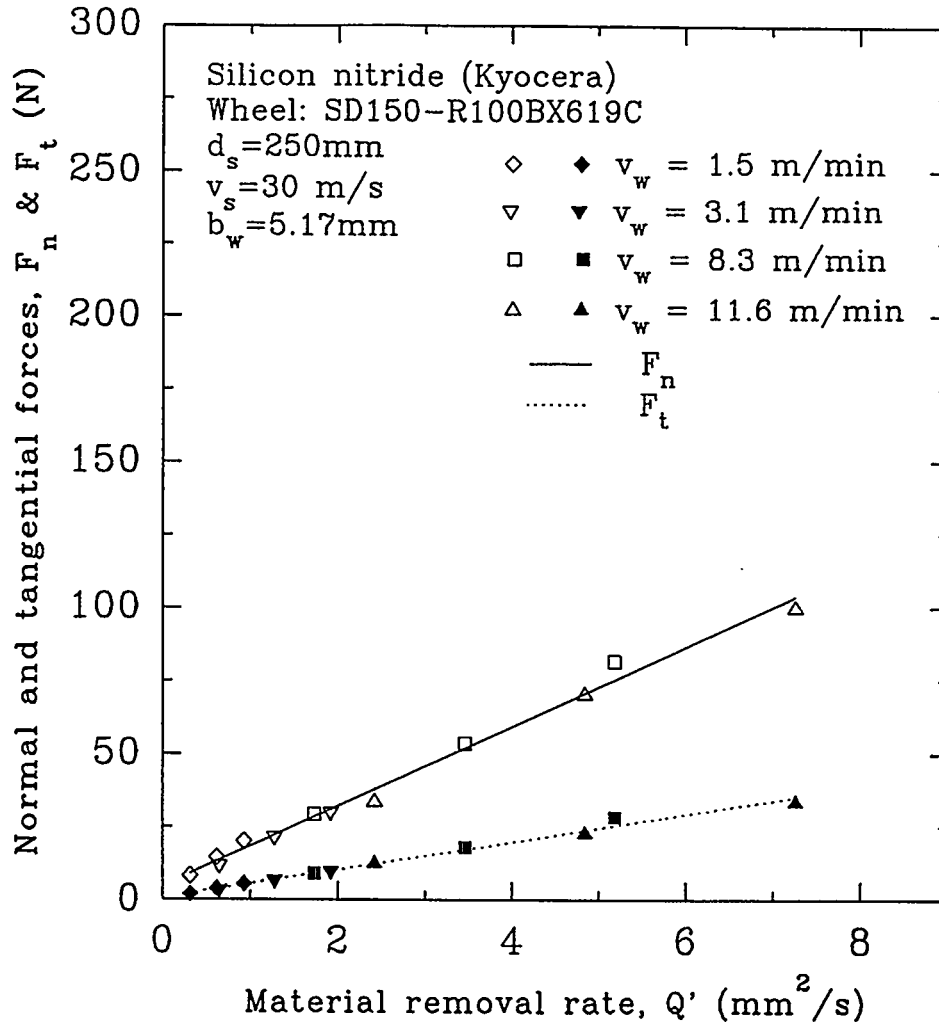


Figure 5. The normal and tangential grinding forces versus material removal rate per unit width.

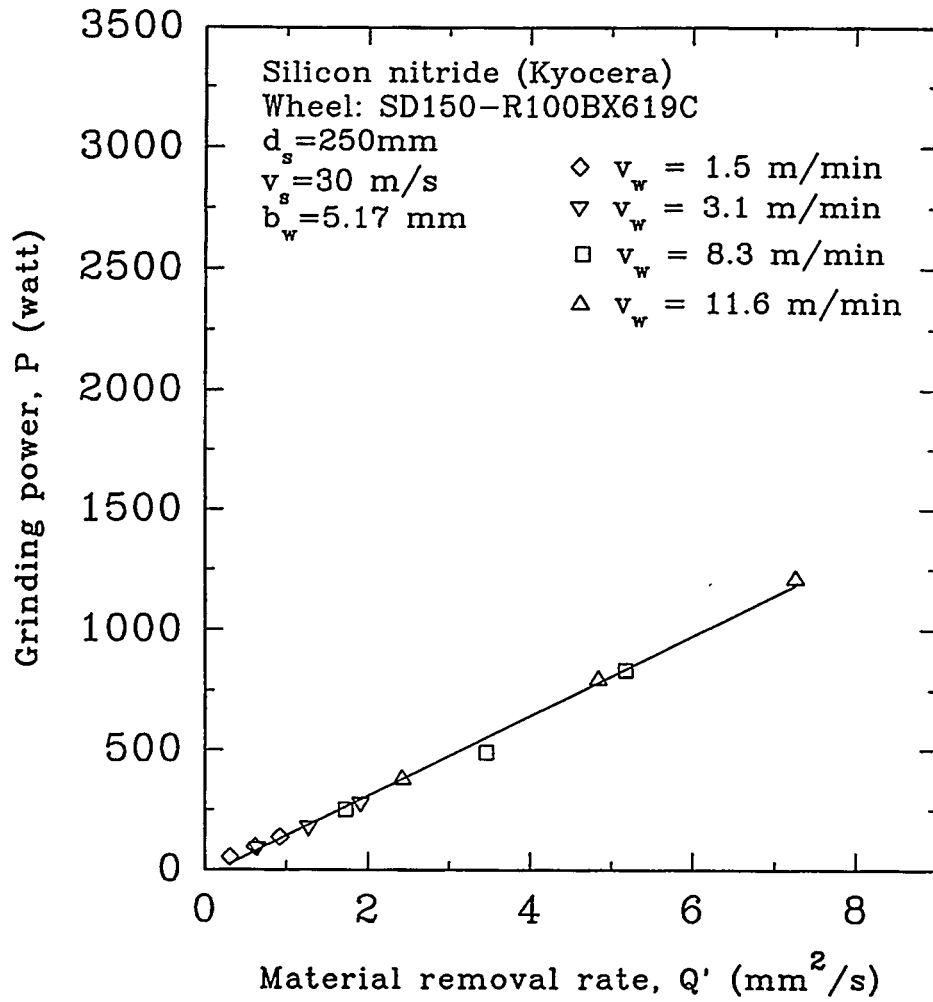


Figure 6. The grinding power versus removal per unit width.

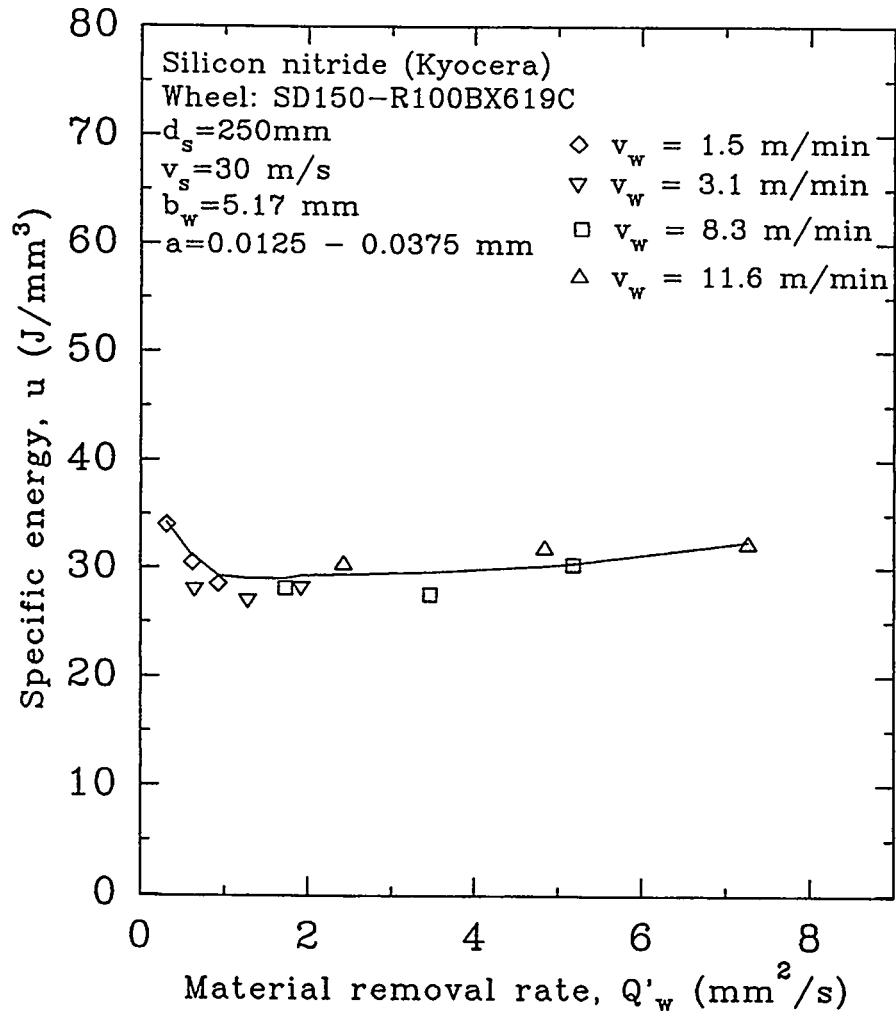


Figure 7. The specific energy versus removal rate per unit width.

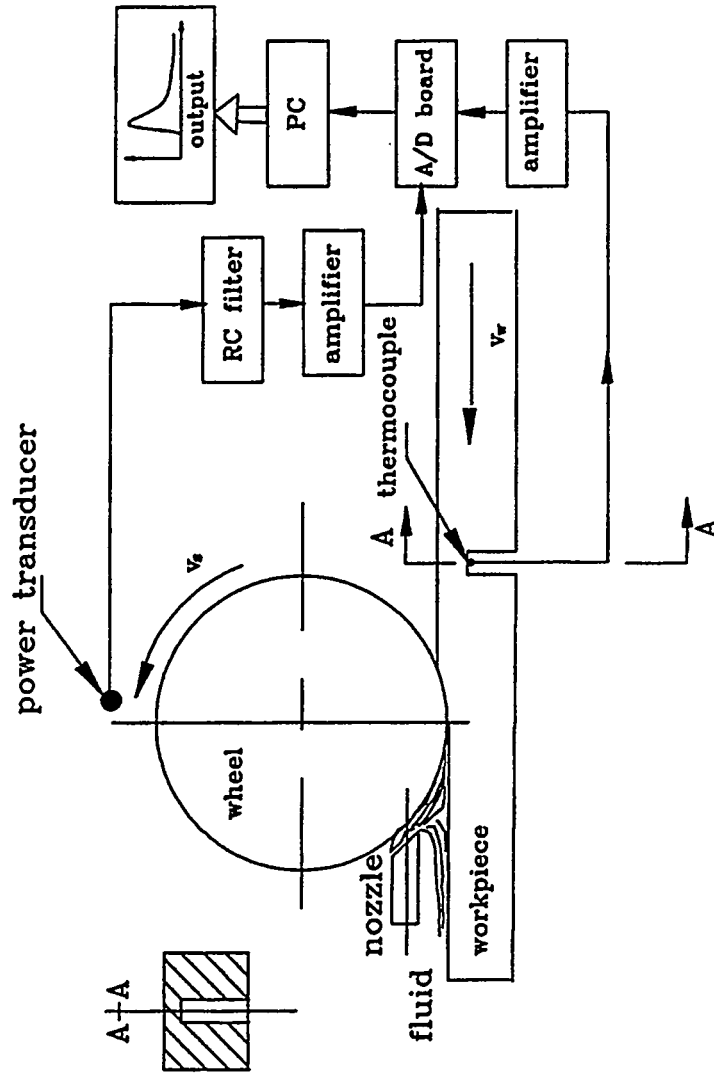


Figure 8. Experimental arrangement for grinding temperature measurement with embedded thermocouple.

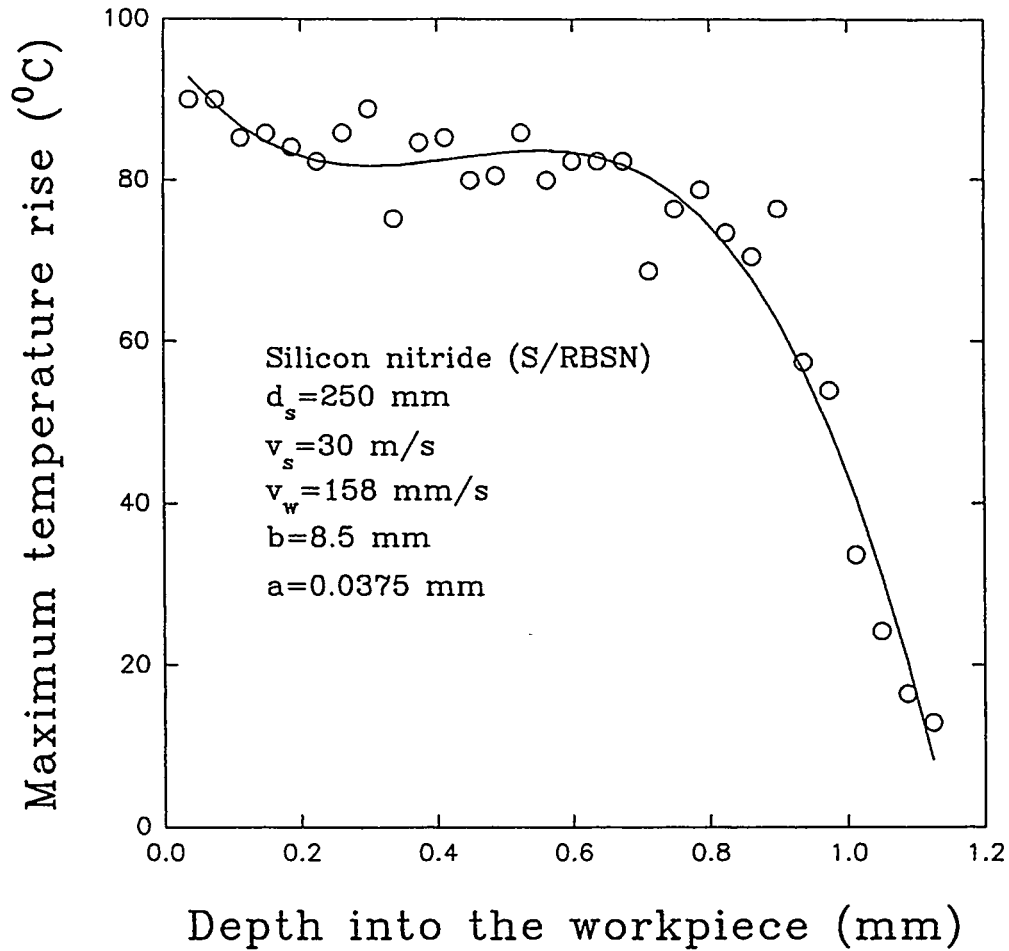


Figure 9. Maximum temperature rise versus depth into workpiece. The hole diameter for the embedded thermocouple was 1.25 mm.

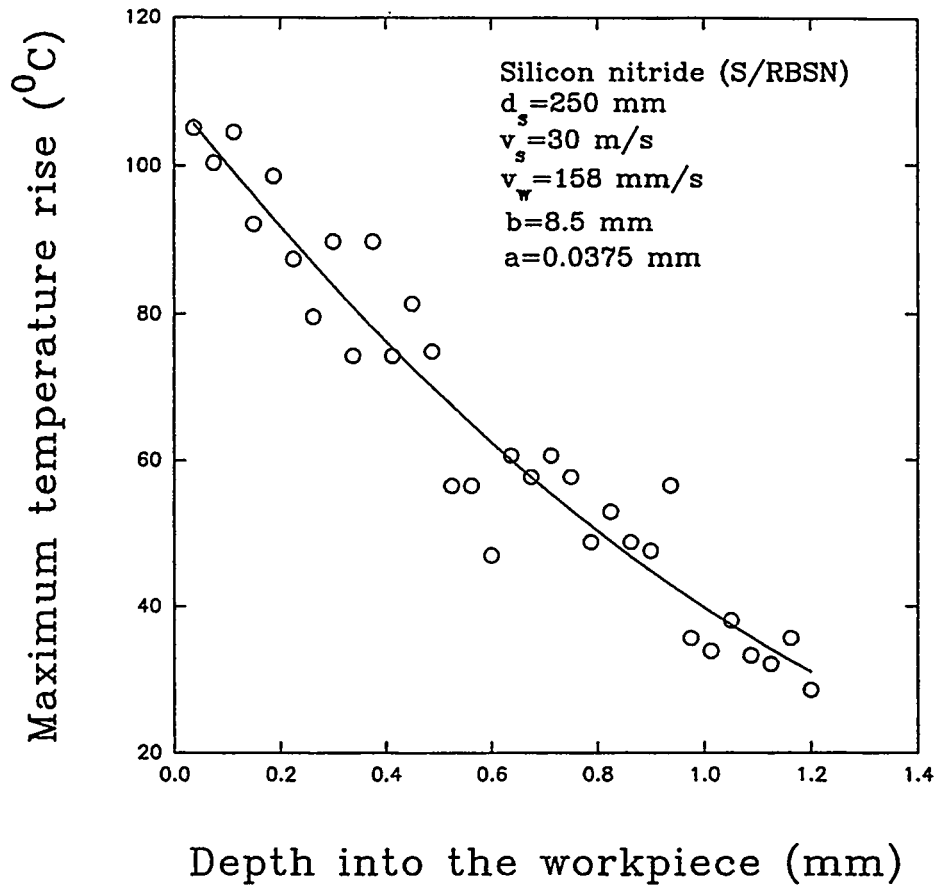


Figure 10. Maximum temperature rise versus depth into the workpiece. The hole diameter for the embedded thermocouple was 1.0 mm.

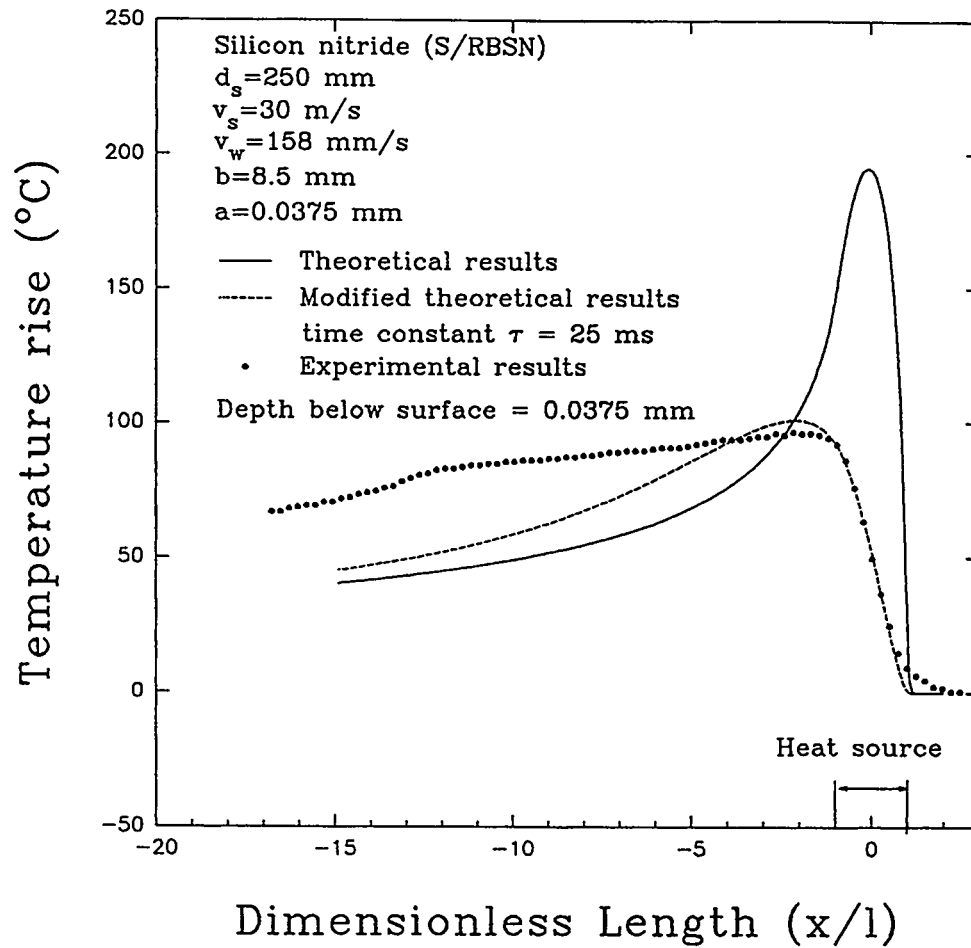


Figure 11. Temperature results with triangular heat source: energy partition $\epsilon = 16\%$.

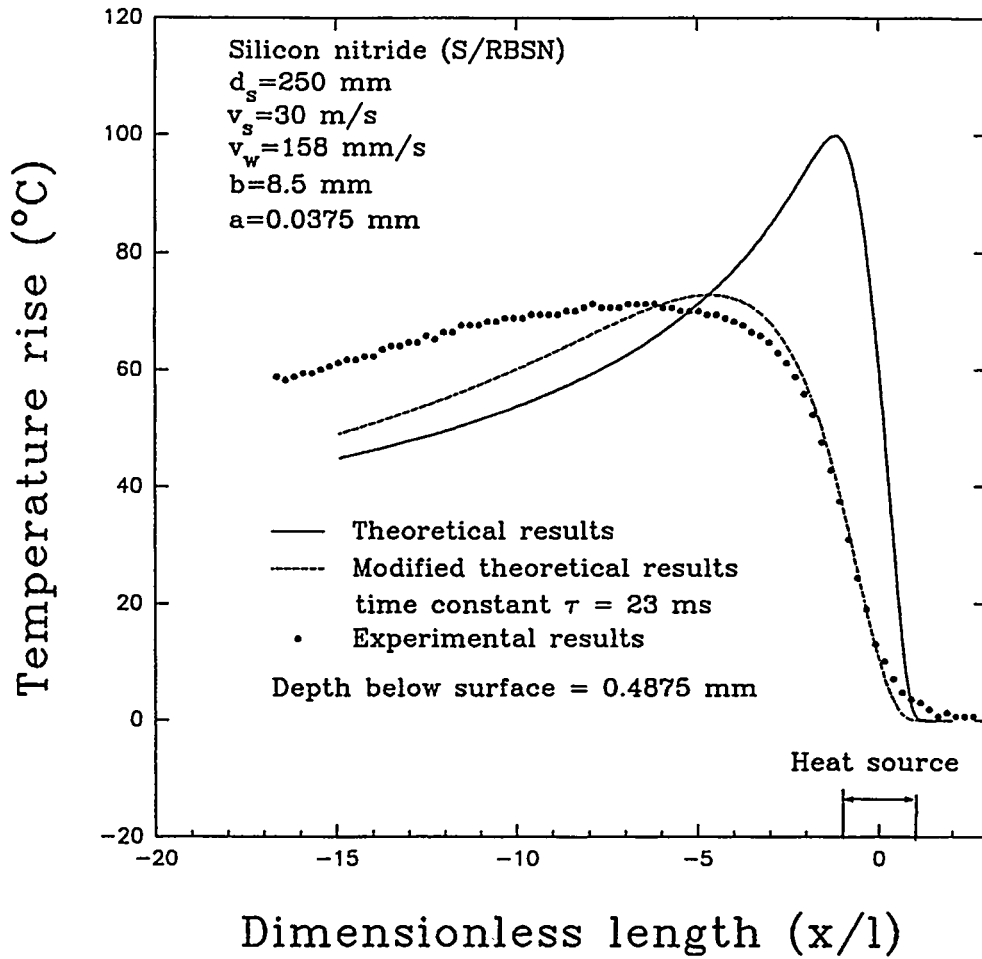


Figure 12. Temperature results with triangular heat source: energy partition $\epsilon = 18\%$.

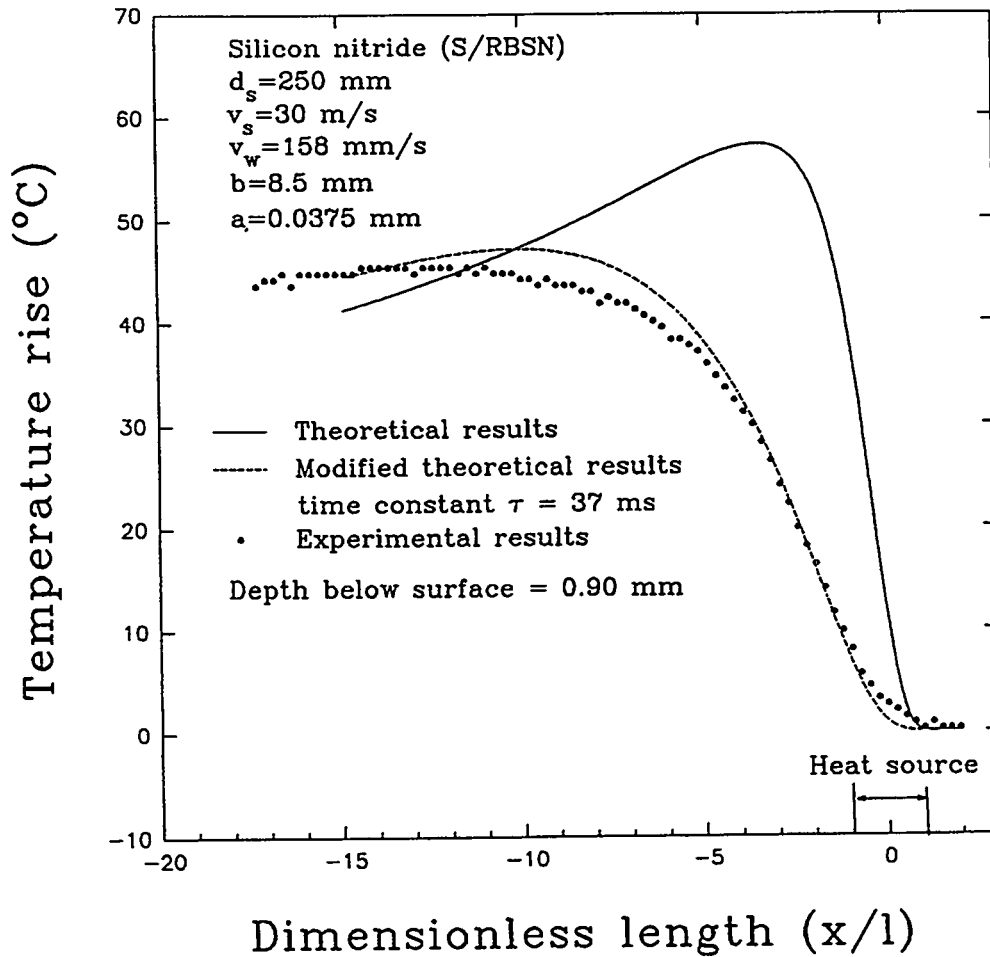


Figure 13. Temperature results with triangular heat source: energy partition $\epsilon = 18\%$.

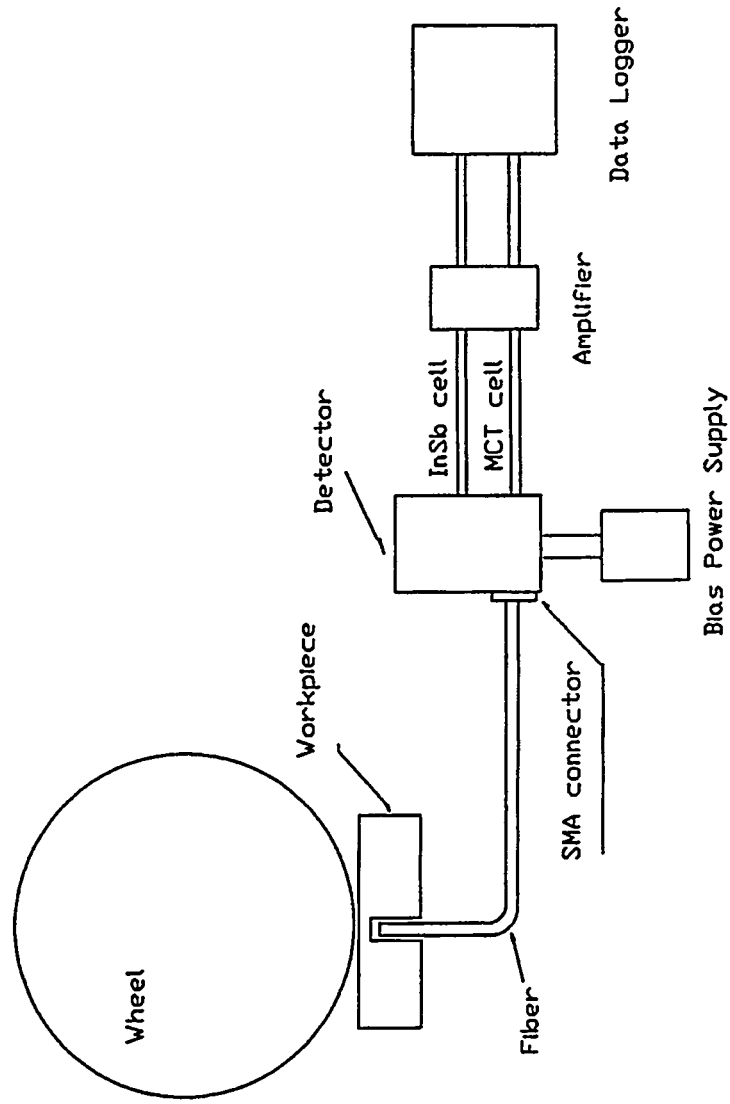


Figure 14. Experimental setup of the infrared two-color detector system.

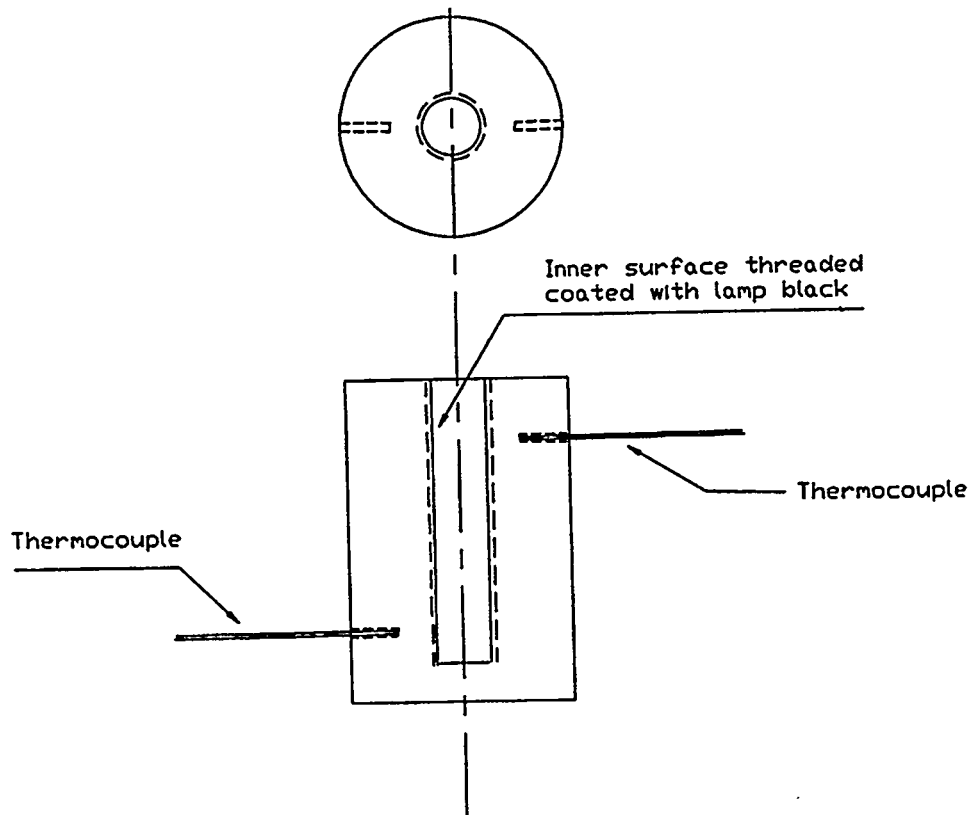


Figure 15. Blackbody for calibration.

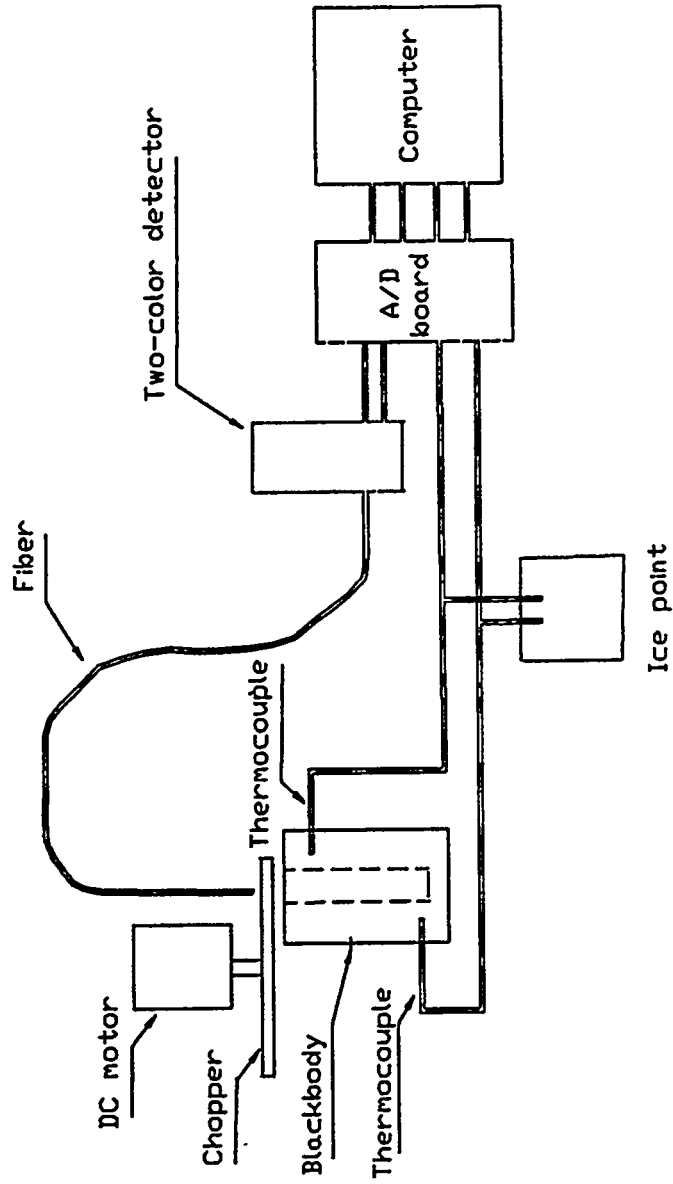


Figure 16. Calibration arrangement for two-color detector system.

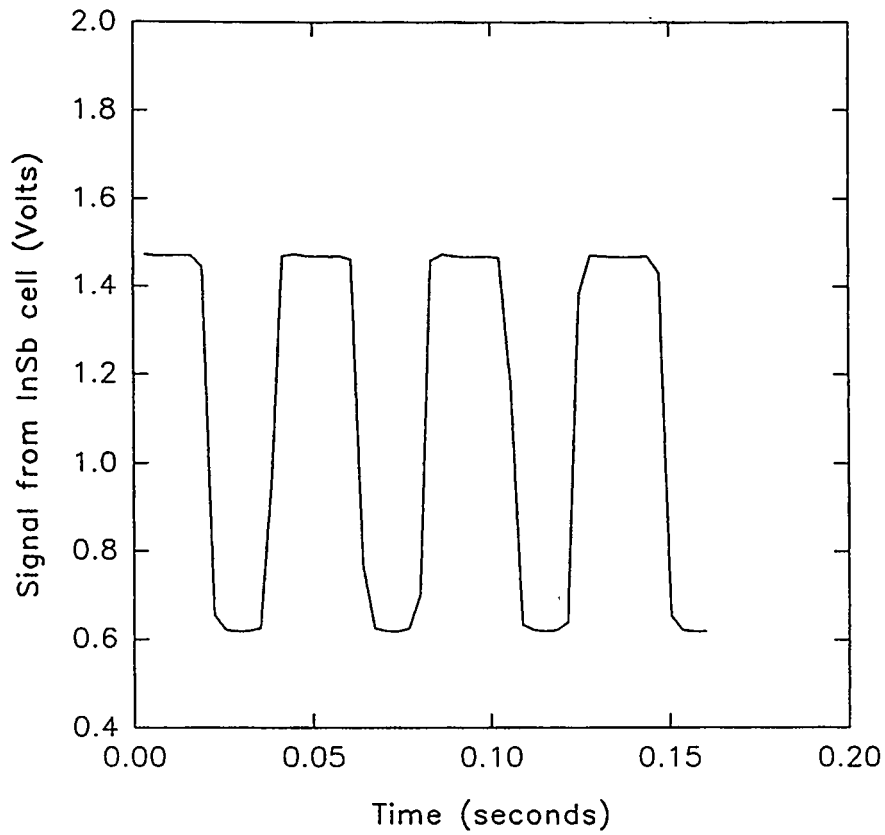


Figure 17. A chopped signal output from InSb cell at temperature of 380°C.

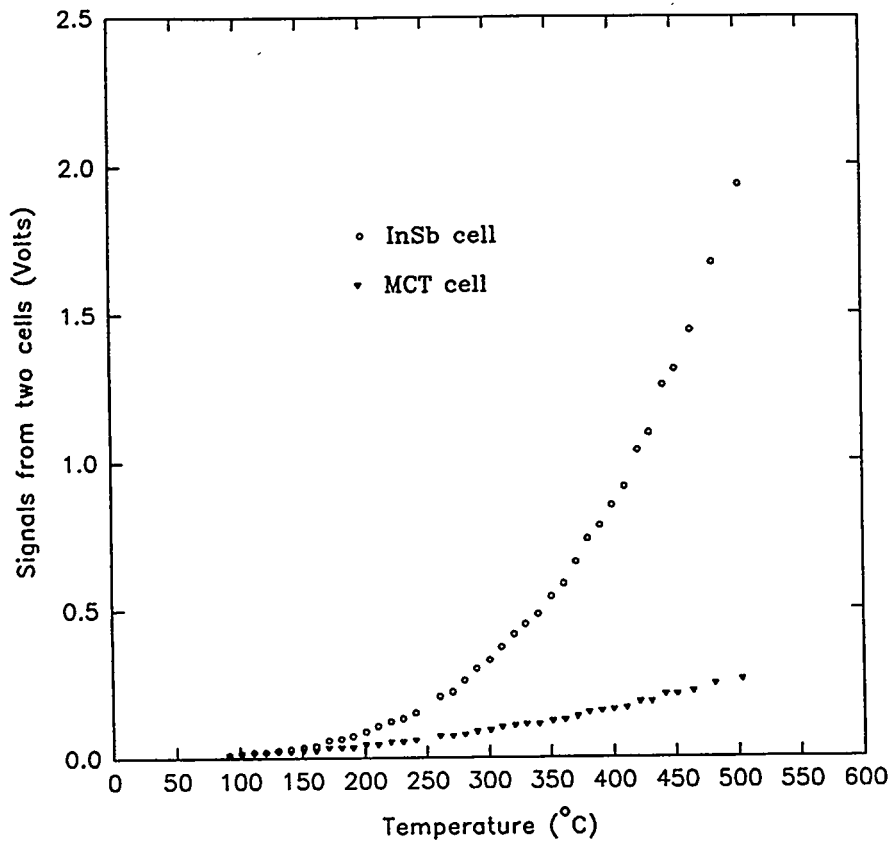


Figure 18. Signals from InSb and MCT cells from first calibration.

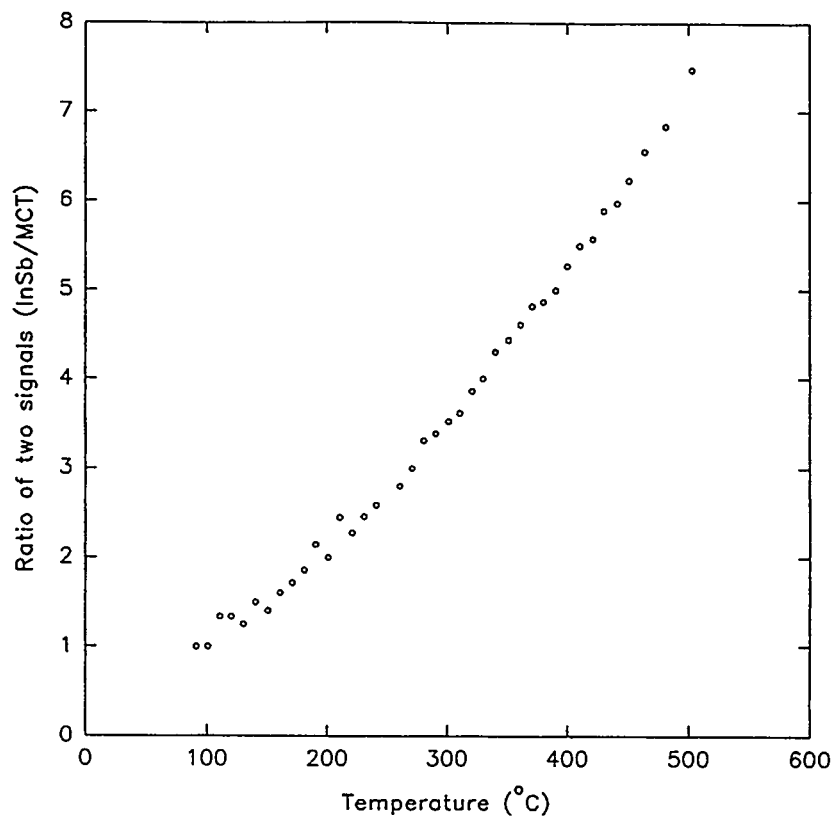


Figure 19. Ratio of signals from InSb and MCT cells versus temperature from first calibration.

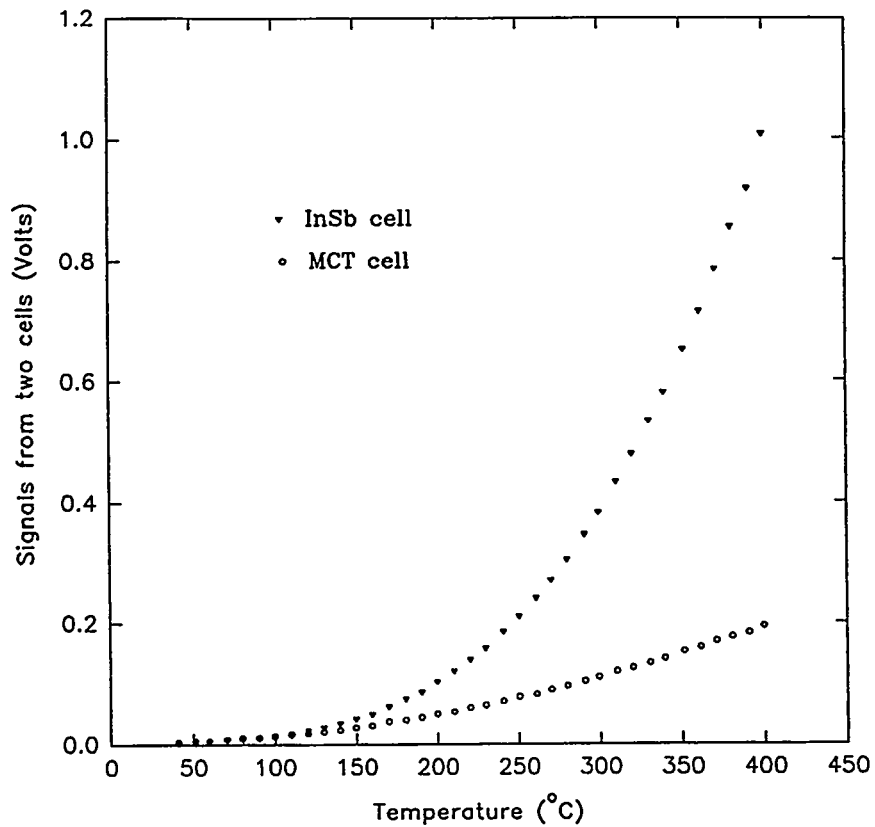


Figure 20. Signals from InSb and MCT cells from second calibration.

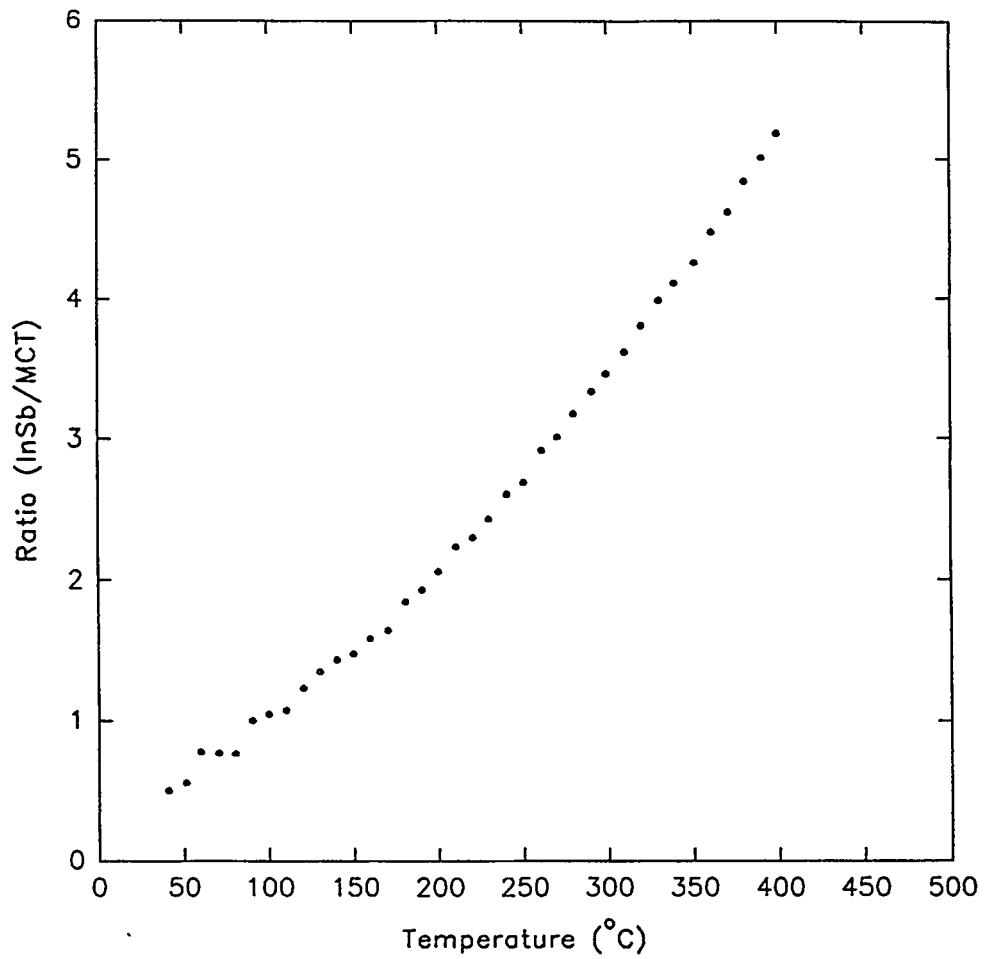


Figure 21. Ratio of signals from InSb and MCT versus temperature from second calibration.

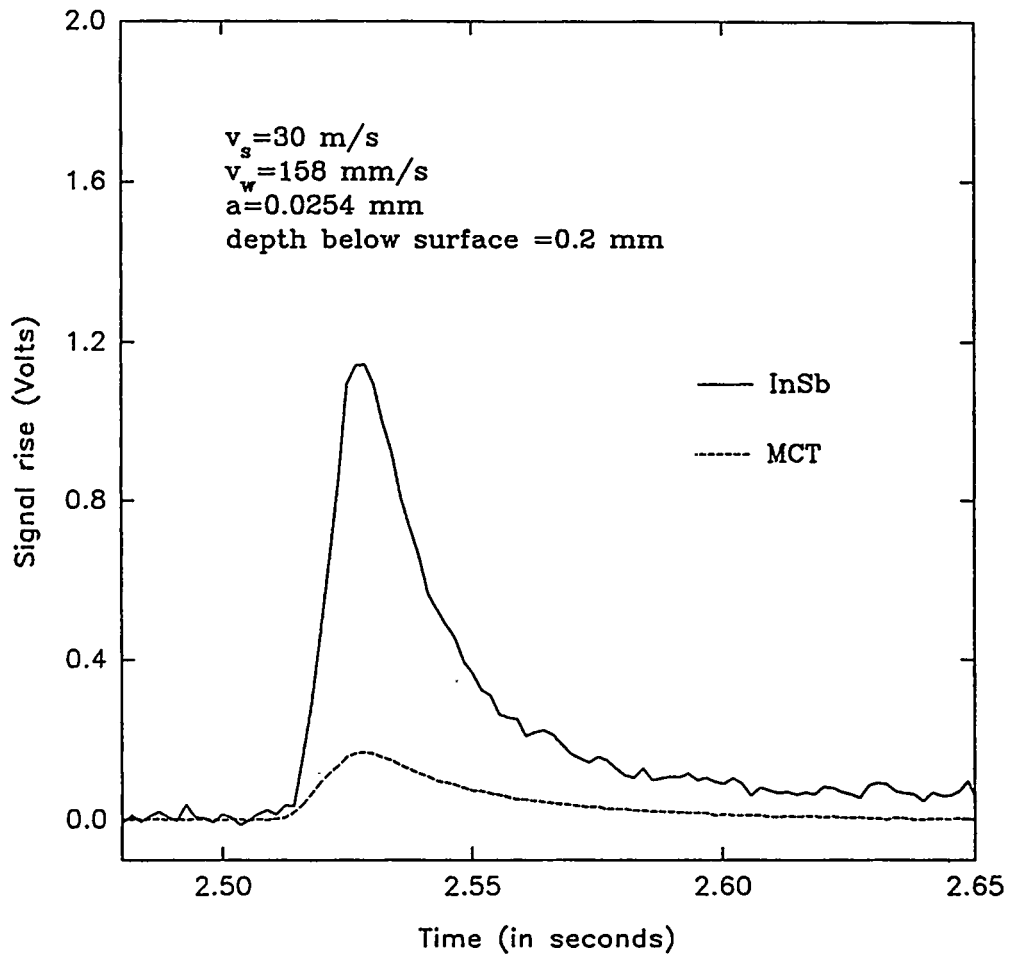


Figure 22. Transient signals from two cells versus time.

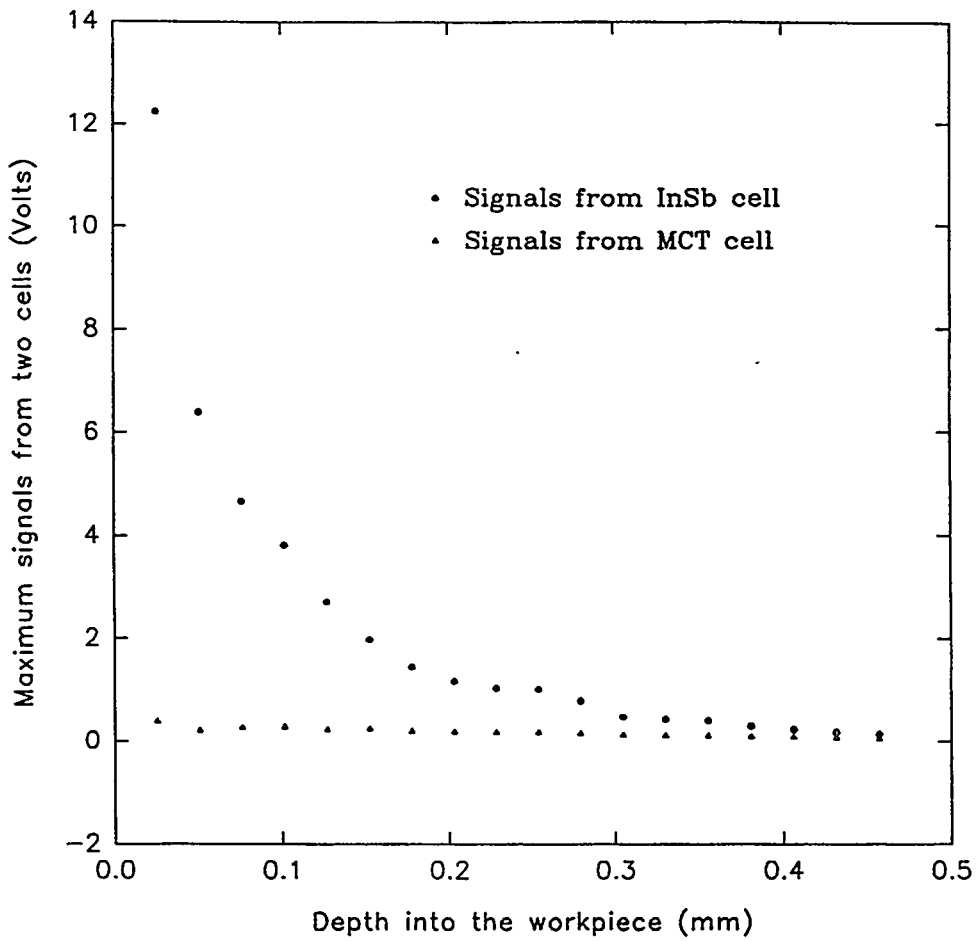


Figure 23. Maximum signal rise from two cells versus depth into workpiece.

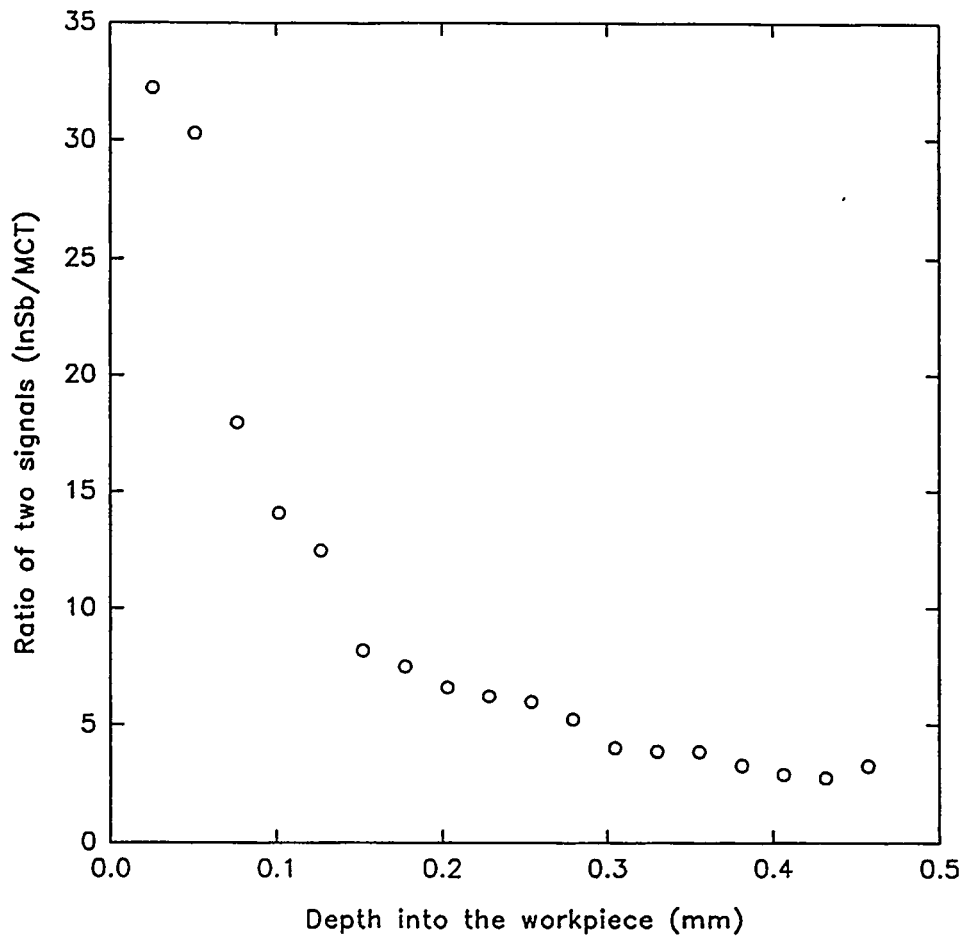


Figure 24. Ratio of two signals (InSb/MCT) versus depth into workpiece.

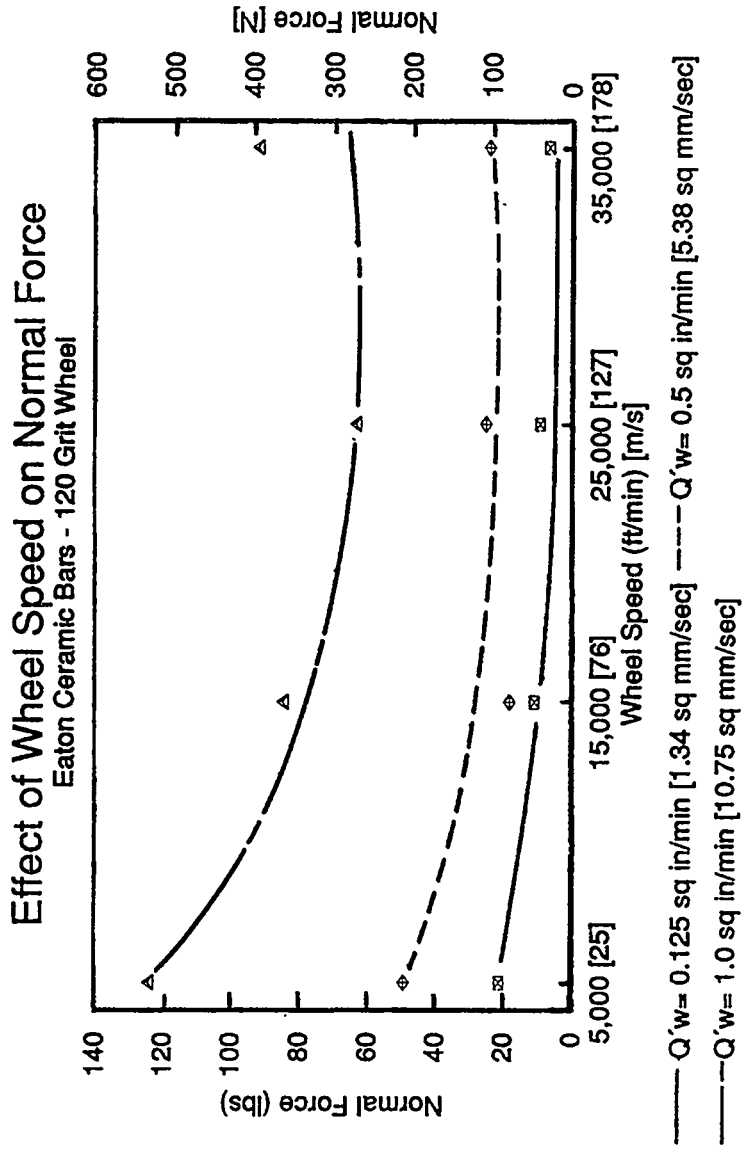


Figure 25A. Effect of wheel speed on normal force.

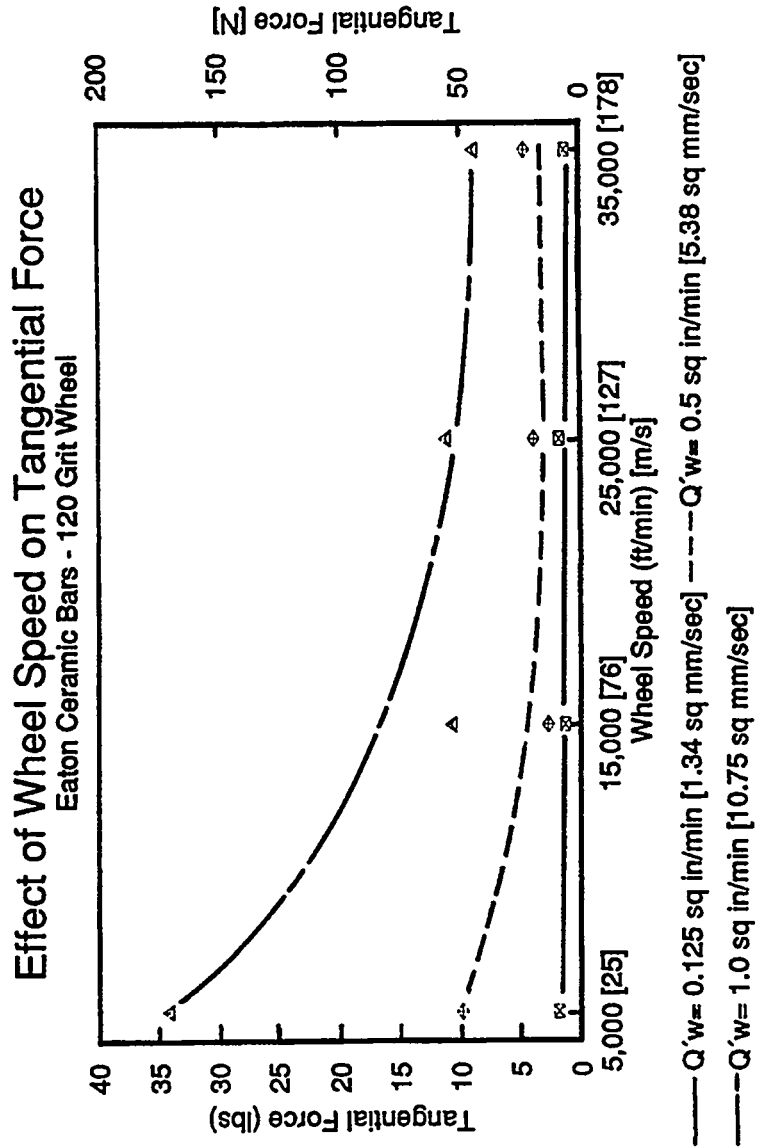


Figure 25B. Effect of wheel speed on tangential force.

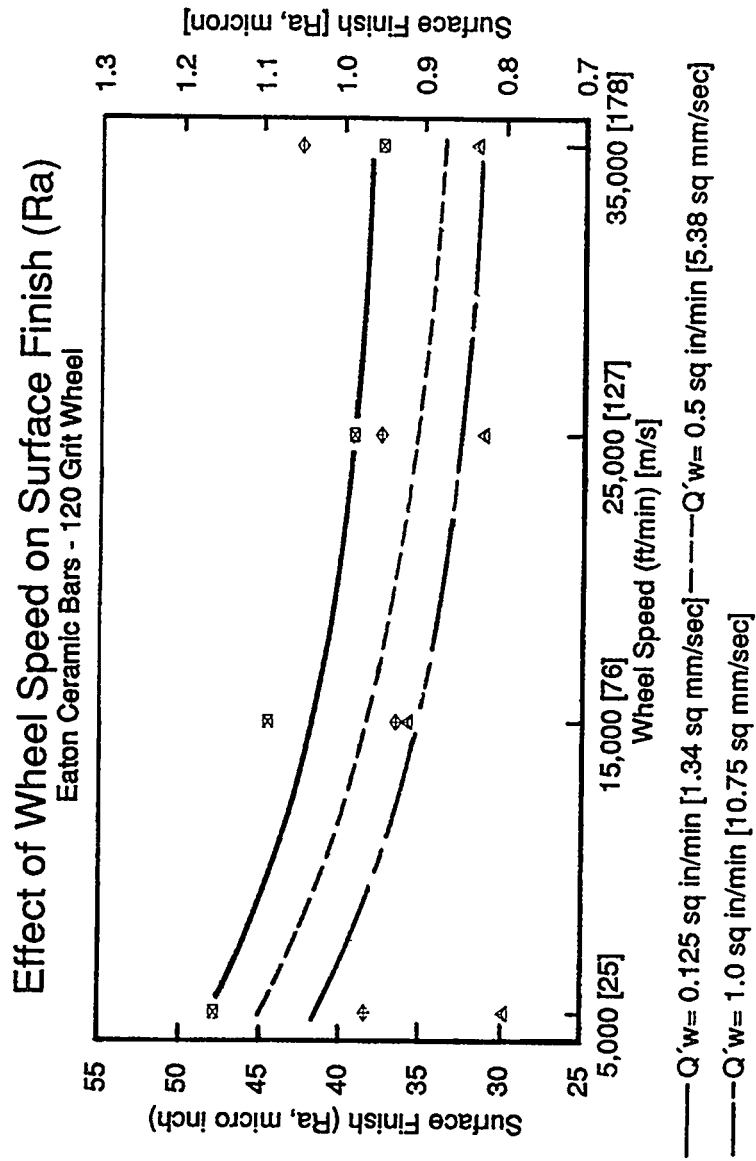


Figure 26. Effect of wheel speed on surface finish (Ra).

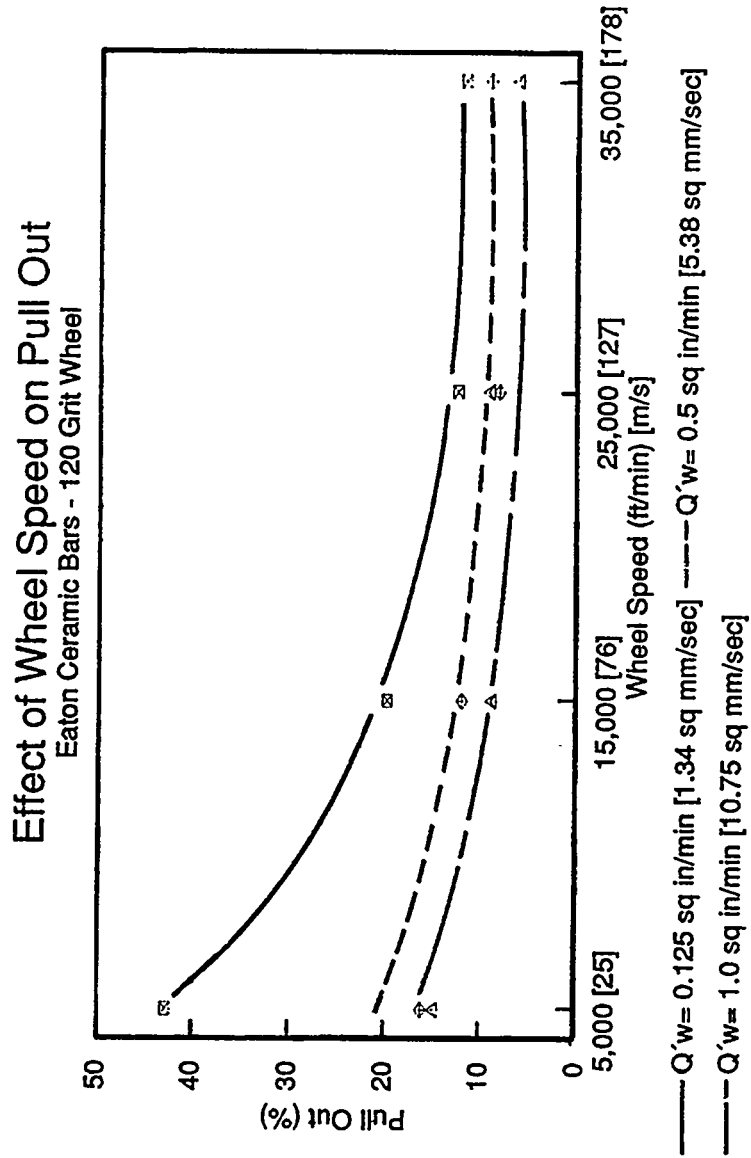


Figure 27. Effect of wheel speed on pull out.

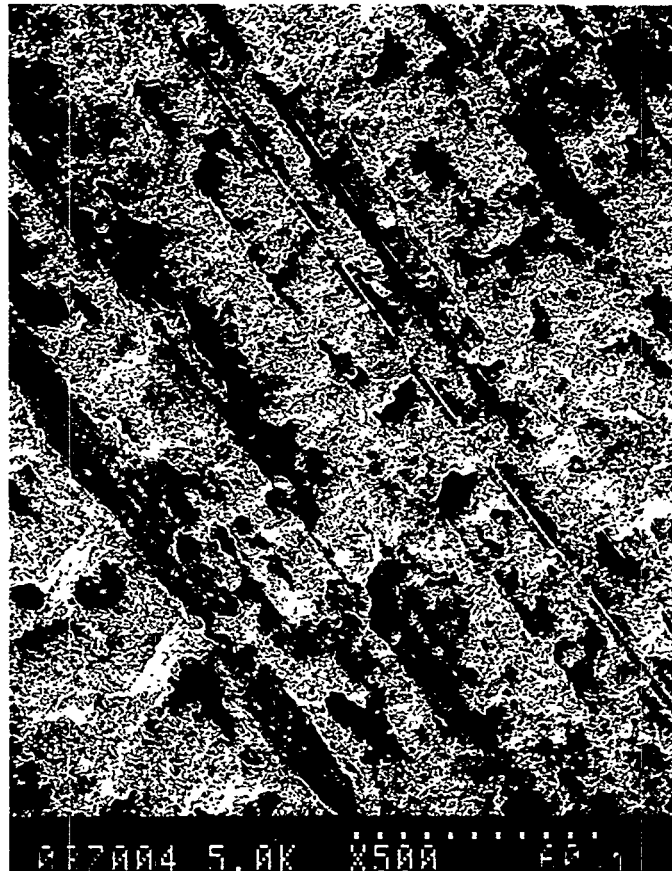


Figure 28A. SEM photomicrograph illustrating 43% surface fragmentation after grinding at $0.125 \text{ in}^2/\text{min}$ ($1.34 \text{ mm}^2/\text{s}$) with a wheel speed of 5,000 SFM (25 m/s).

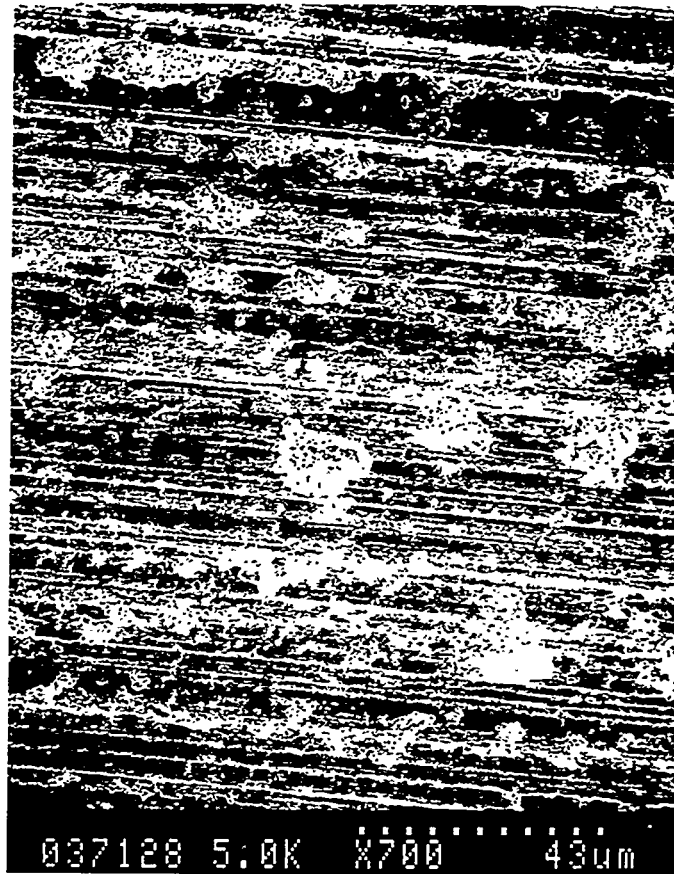


Figure 28B. SEM photomicrograph illustrating 12% surface fragmentation after grinding at $0.125 \text{ in}^2/\text{min}$ ($1.34 \text{ mm}^2/\text{s}$) with a wheel speed of 35,000 SFM (178 m/s).



Figure 28C. SEM photomicrograph illustrating 16% surface fragmentation after grinding at 0.5 in²/min (5.38 mm²/s) with a wheel speed of 5,000 SFM (25 m/s).

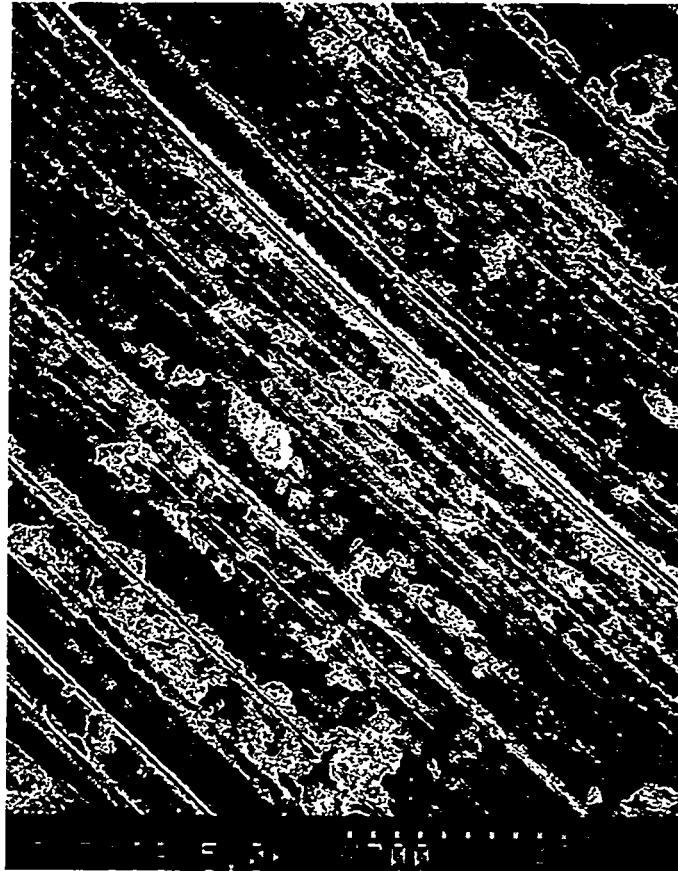


Figure 28D. SEM photomicrograph illustrating 9% surface fragmentation after grinding at 0.5 in²/min (5.38 mm²/s) with a wheel speed of 35,000 SFM (178 m/s).

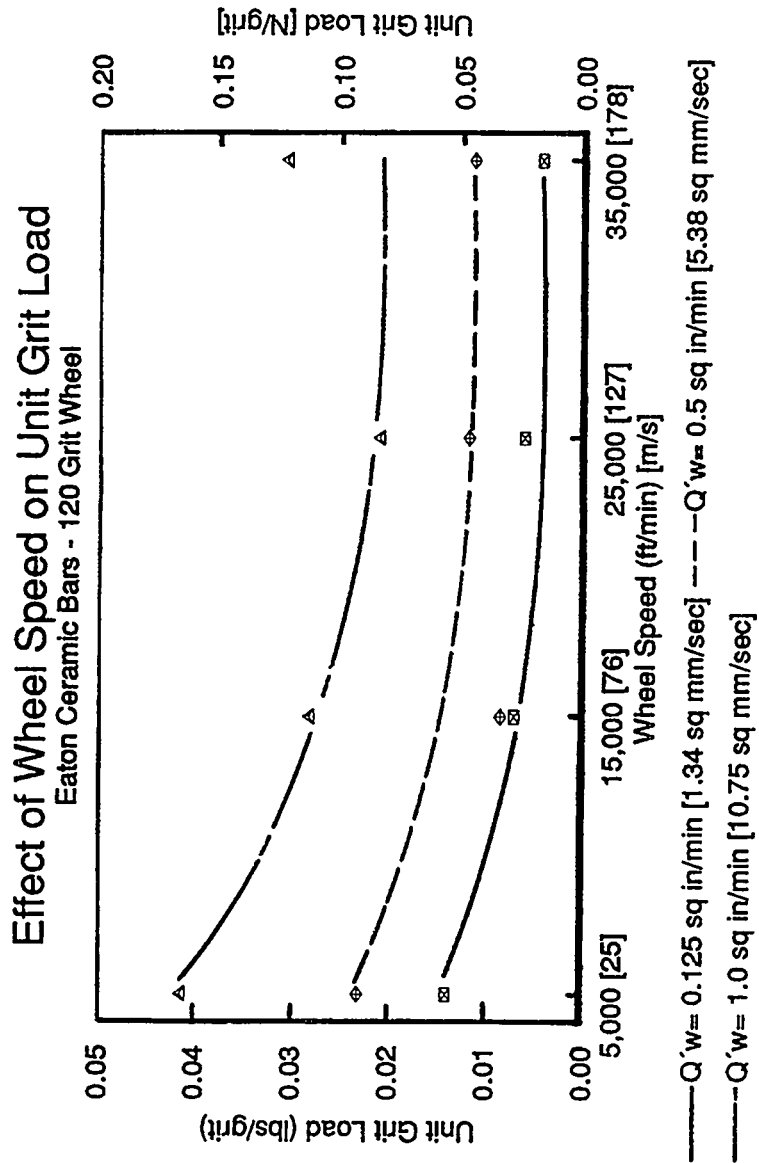


Figure 29. Effect of wheel speed on unit grit load.

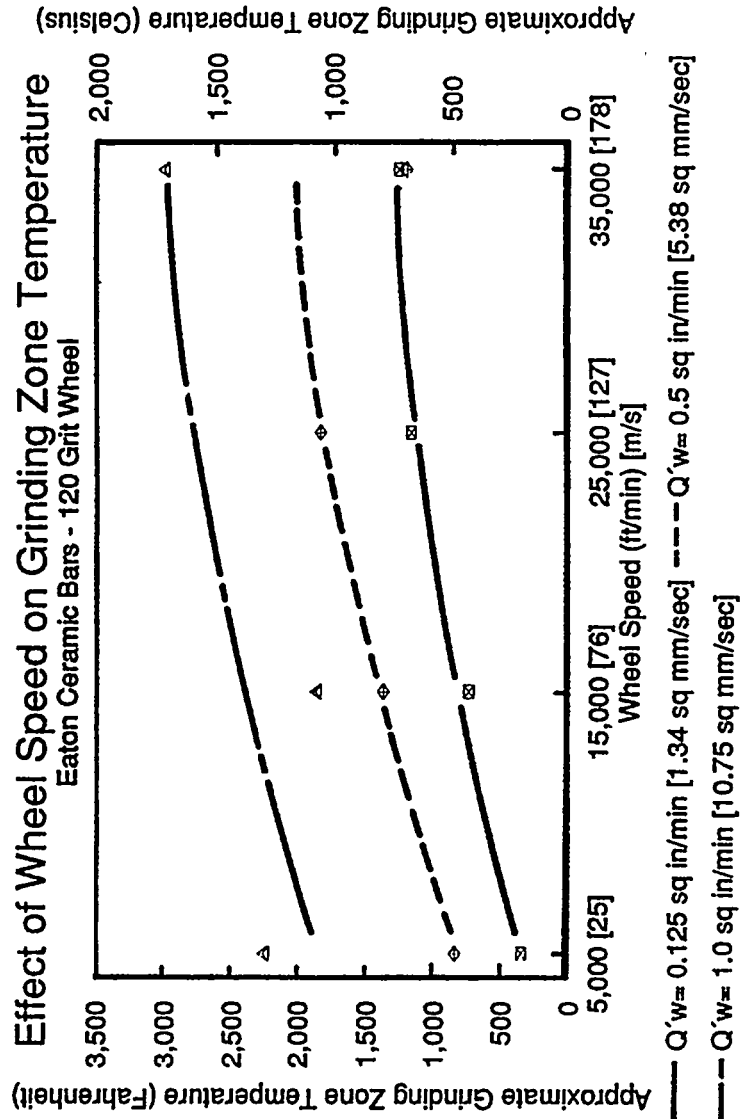


Figure 30. Effect of wheel speed on grinding zone temperature.

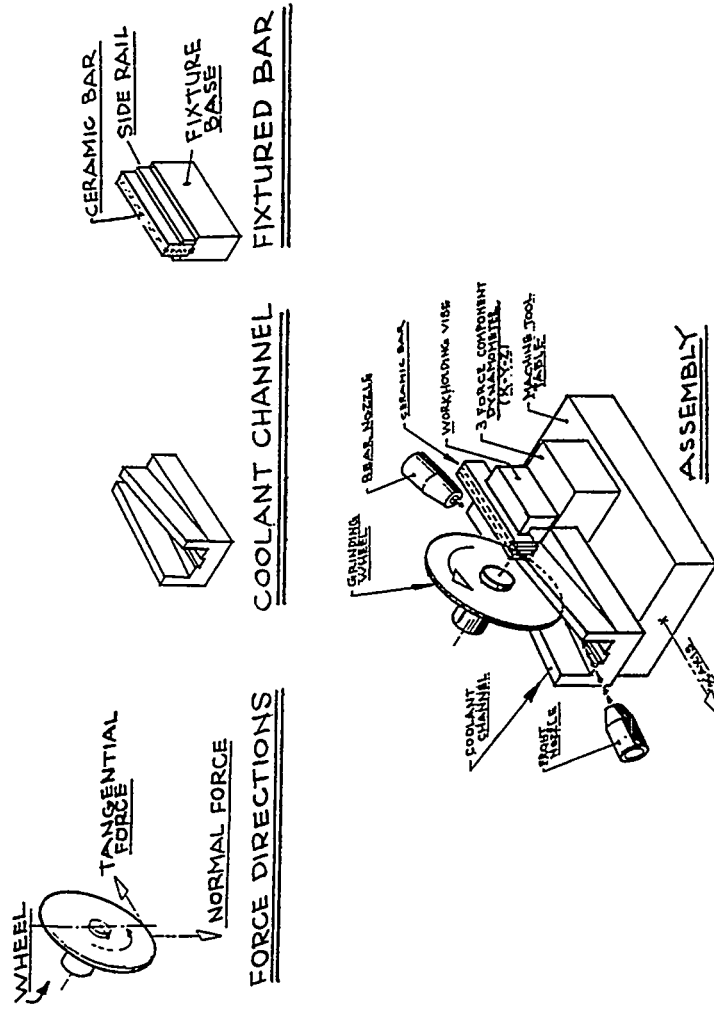


Figure 31. Creep feed grinding setup.

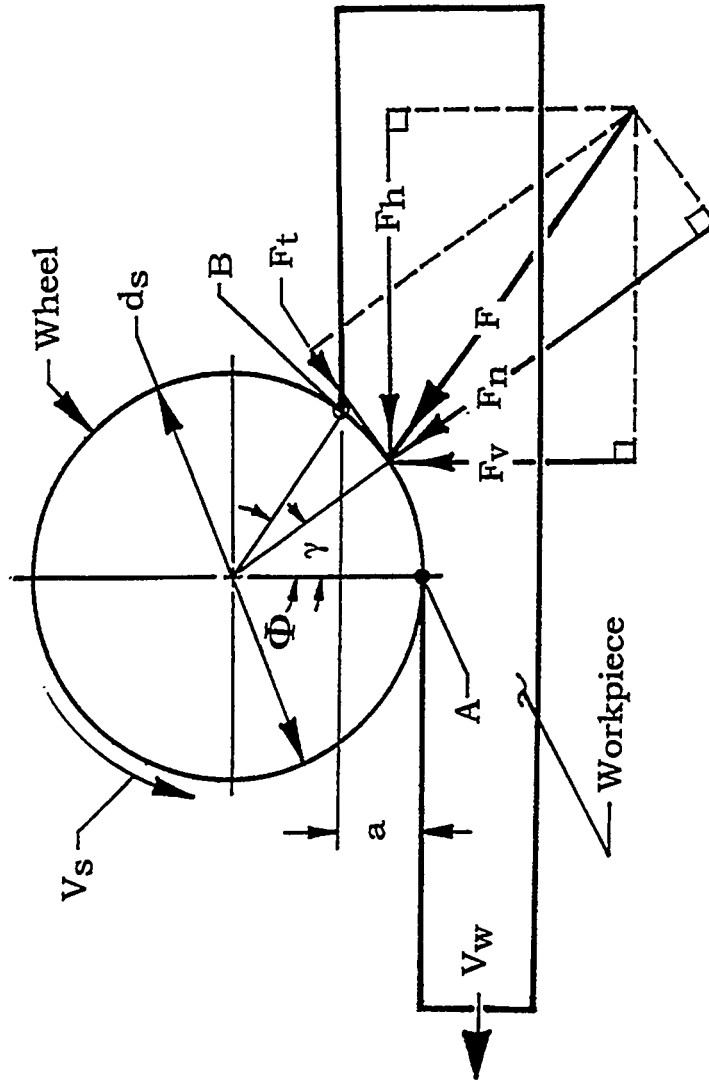
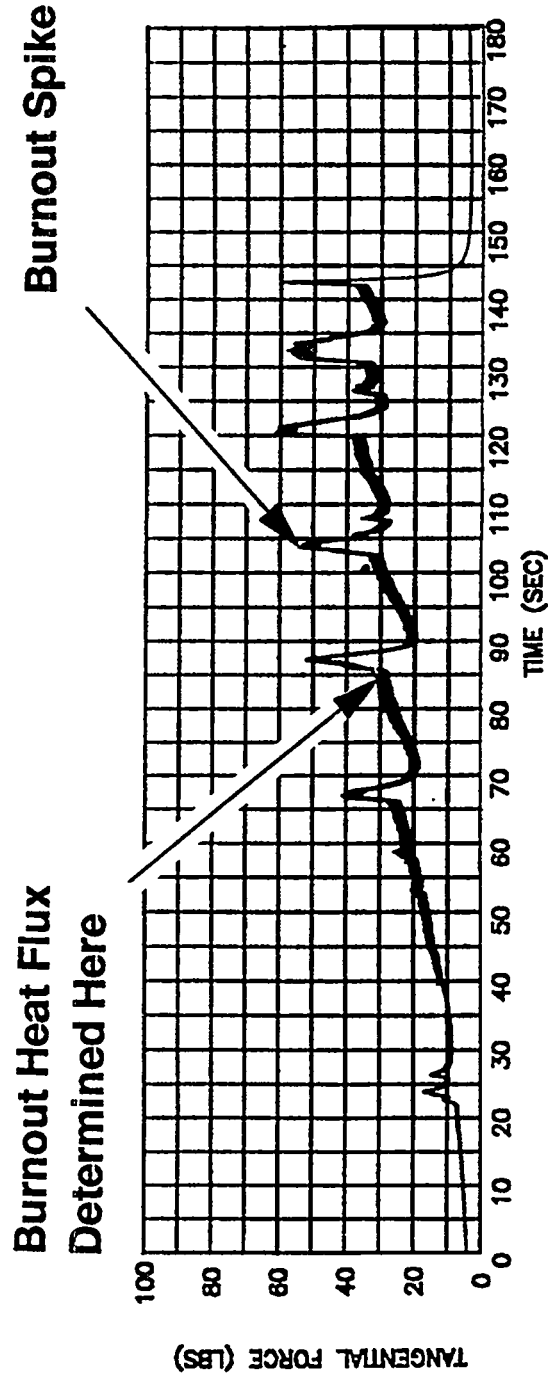


Figure 32. Force components exerted by the workpiece on the wheel.



Wheel: 80 grit diamond, metal bond $V_s = 10,000$ ft/min
Workpiece: $V_w = 0.6$ in/min, $d = 0.437$ in, $b = 0.0625$ in

Figure 33. "Burnout" in creep feed grinding.

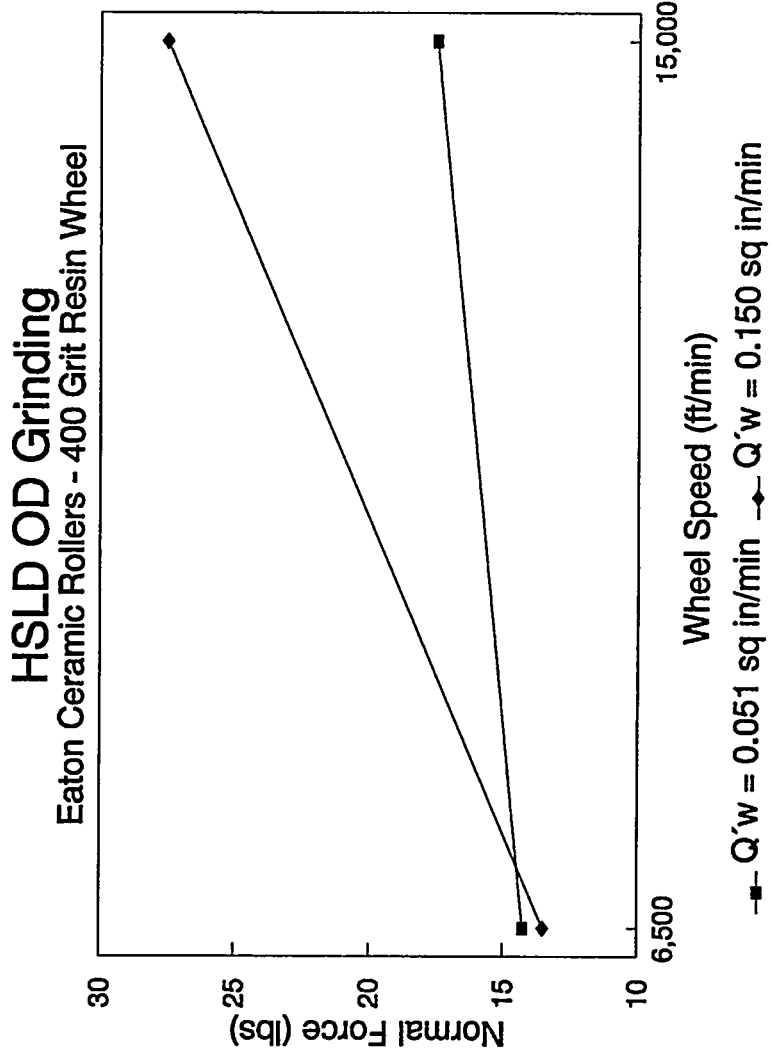


Figure 34A. Effect of wheel speed on normal force for OD grinding.

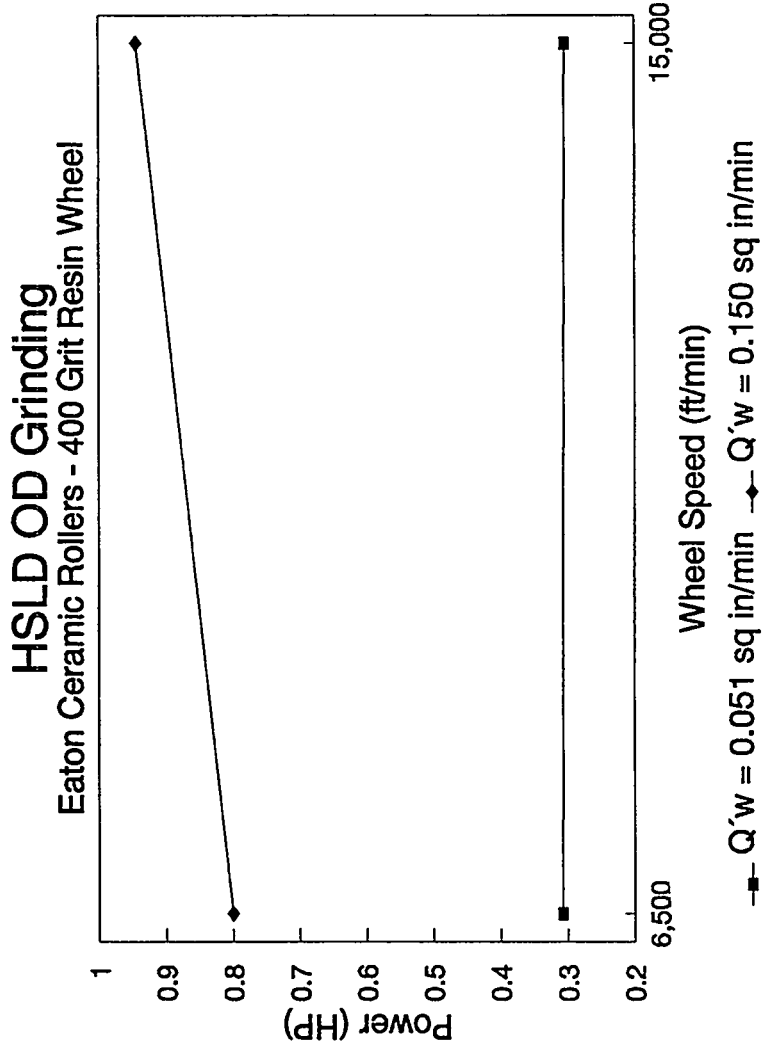


Figure 34B. Effect of wheel speed on power for OD grinding.

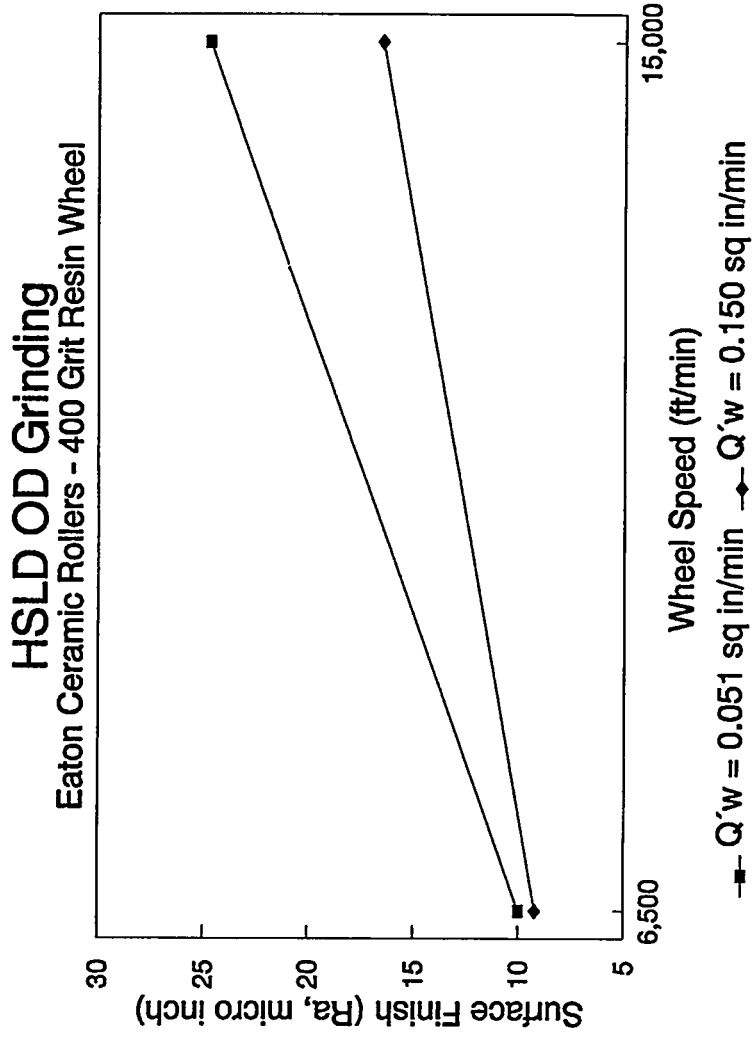


Figure 35A. Effect of wheel speed on surface finish (Ra) for OD grinding.

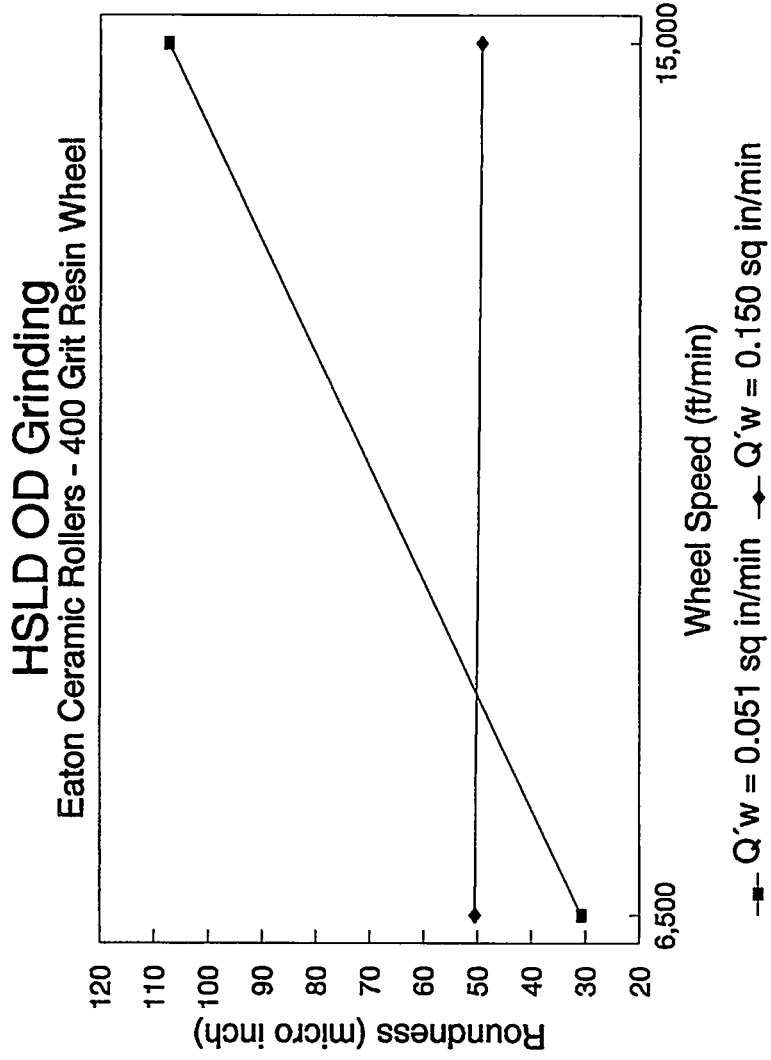
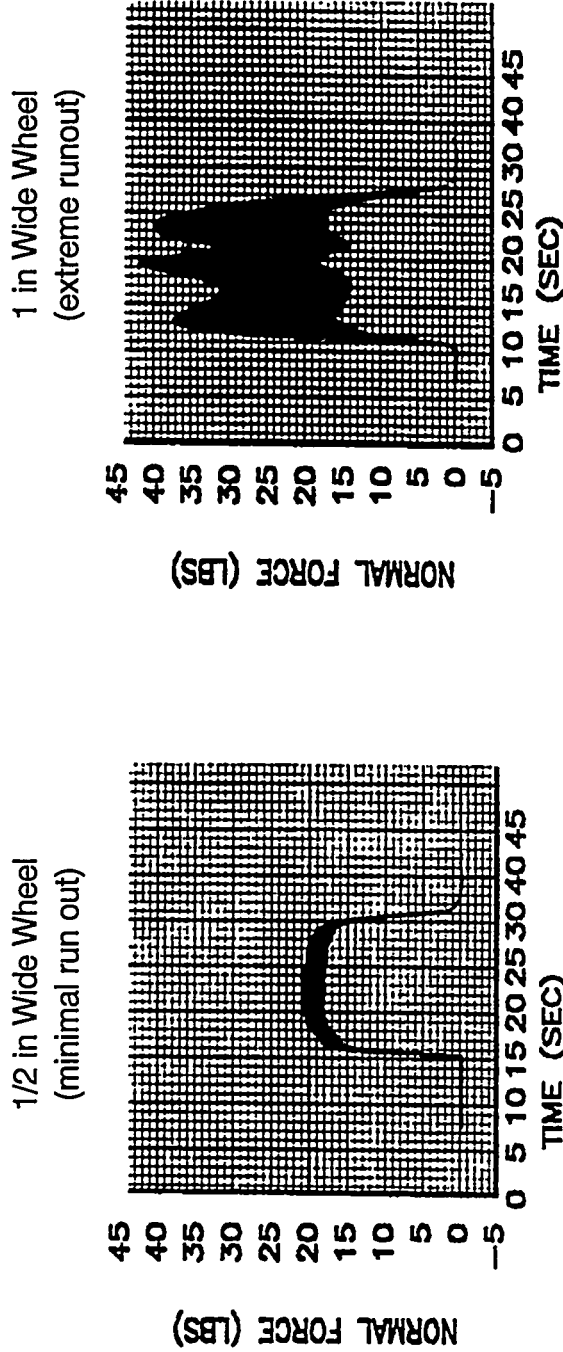


Figure 35B. Effect of wheel speed on roundness for OD grinding.



Wheel: 120 grit diamond brazed, $V_s = 5,000$ ft/min, $d_s = 12$ in
Workpiece: S/RBSN, $V_w = 50$ in/min, $d = 0.0025$ in, $b = 0.357$ in

Figure 36. Comparison of grinding normal forces for two brazed wheels showing effects of wheel run-out.

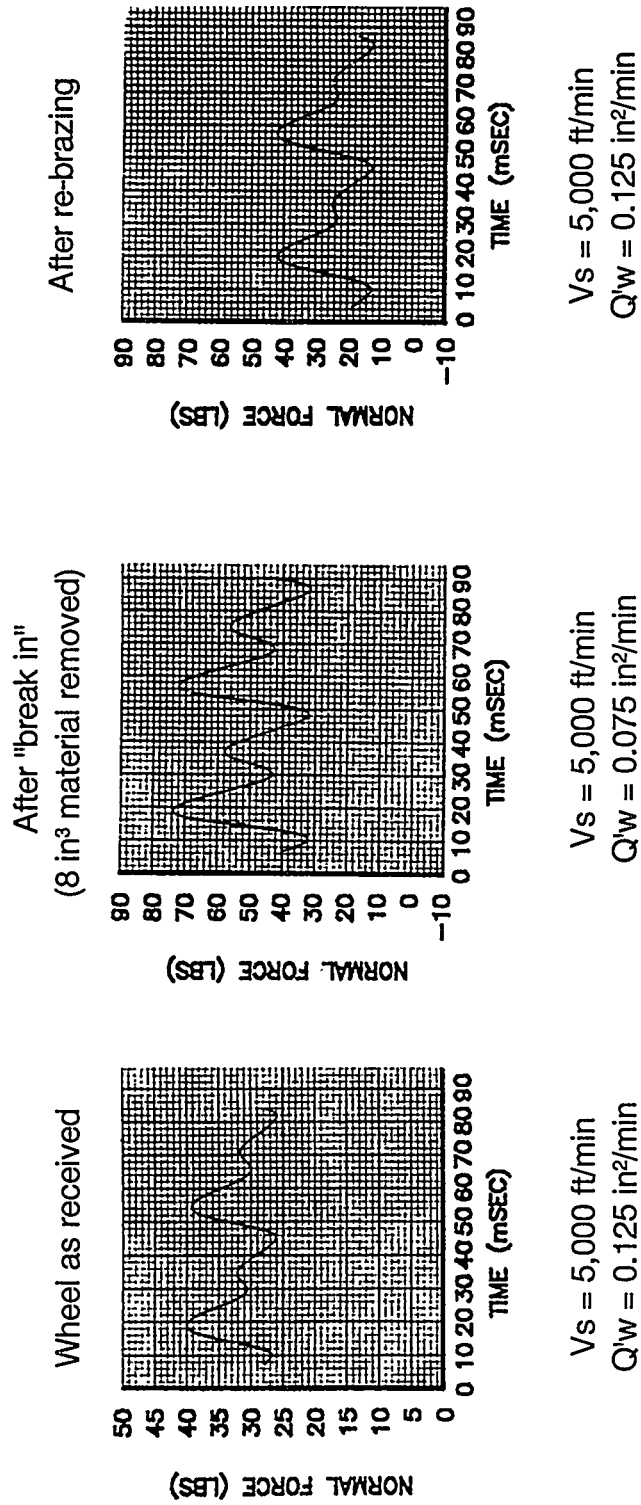
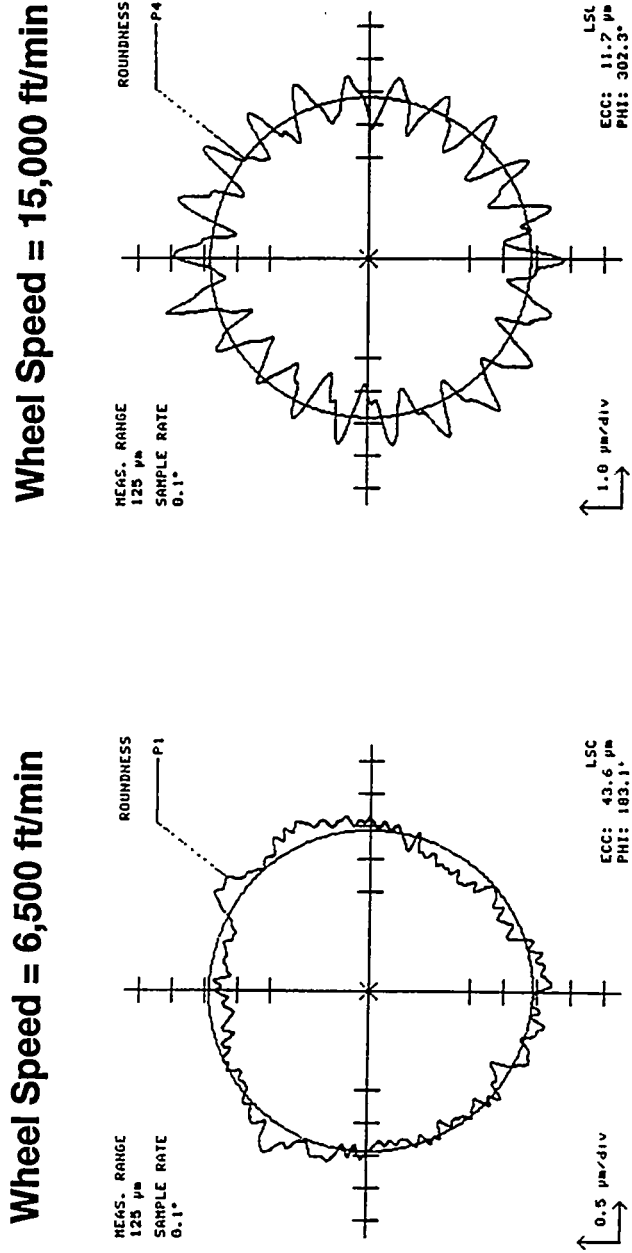


Figure 37. Cyclic forces due to runout.



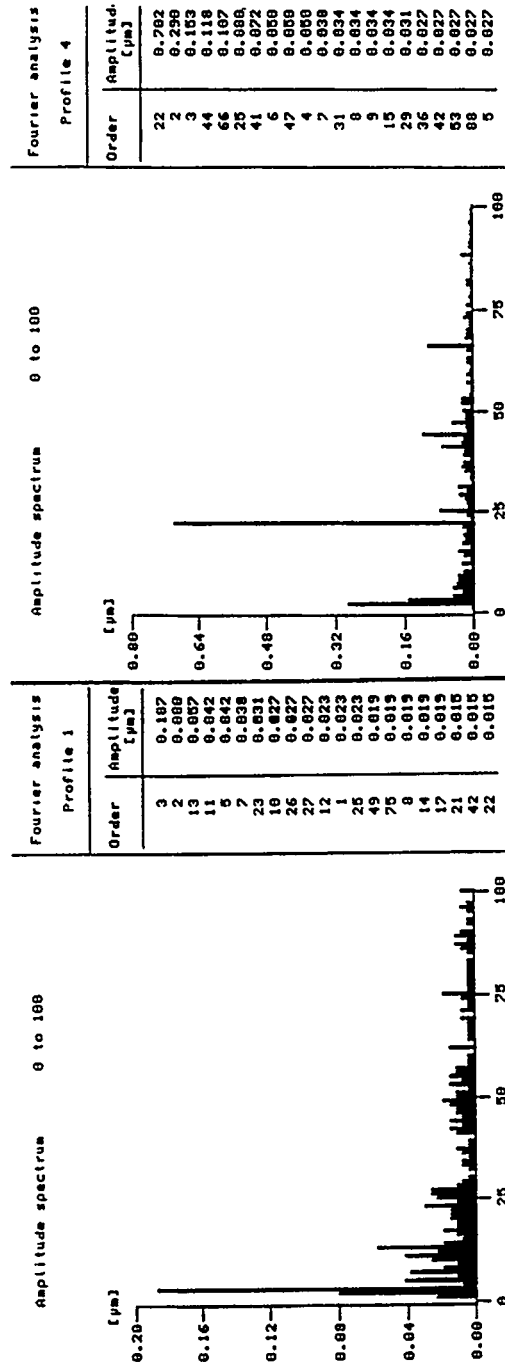
Wheel: Coors 400 grit diamond resin bond
Workpiece speed = 267 ft/min
Infeed rate = 0.000 016 in/rev

Figure 38. Workpiece chatter at high wheel speeds.



Wheel Speed = 6,500 ft/min

Wheel Speed = 15,000 ft/min



Wheel: Coors 400 grit diamond resin bond
Workpiece speed = 267 ft/min
Infeed rate = 0.000 016 in/rev

Figure 39. Chatter determination using fourier analysis of surface profile.



Ceramic Properties Eaton/Coors and Kyocera Materials

		Eaton - Coors		Kyocera
		RBSN	S/RBSN	SN220
Density	g/cc		3.30	3.20
	lb/cu in		0.1192	0.1156
Porosity	%		<0.1	
Flexural strength (Weibull slope)	MPa	175-275	620	590
	ksi	25-40	90.0	85.6
Elastic modulus	GPa	138.0	303.0	294.0
	Msi	20.0	44.0	42.7
Hardness	Hv			
	Other	R45N 58-67	KHN 1500	Ra 91
Fracture toughness (ISB)	MPa rt m . ksi rt in	3.00	6.60	5.70
Poisson's ratio		0.22		0.28
Thermal expansion		Temperature range 25-1000 °C 77-1835 °F		
	10 ⁻⁴ /°C	3.00	3.50	3.20
	10 ⁻⁴ /°F	1.67	1.94	1.78
Thermal shock resistance (delta T critical)	°C		800	550
	°F		1475	1025
Thermal conductivity	W/m K		30.00	25.00
	BTU / hr ft °F		51.90	43.25
Specific heat	J/g k		0.65	0.67
	BTU/lb°F*10 ⁻³		0.1552	0.1600

Table 1. Comparison of ceramic properties for three materials:

- Eaton/Coors RBSN
- Eaton/Coors S/RBSN
- Kyocera SN220



HSLD Surface Grinding Results

Material Removal Rate	0.125 in ² /min 1.34 mm ² /s				0.5 in ² /min 5.38 mm ² /s				1.0 in ² /min 10.75 mm ² /s			
	5,000 (ft/min) [m/sec]	15,000 76	25,000 127	35,000 178	5,000 25	15,000 76	25,000 127	35,000 178	5,000 25	15,000 76	25,000 127	35,000 178
Surface Finish Ra (micro inch) [micron]	48 1.22	45 1.14	39 0.99	38 0.97	38 0.97	37 0.94	38 0.97	43 1.09	30 0.76	36 0.91	31 0.80	32 0.81
Surface Finish Rt (micro inch) [micron]	447 11.35	371 9.42	288 7.32	324 8.23	335 8.51	304 7.72	268 6.81	297 7.54	222 5.64	258 6.55	244 6.20	241 6.12
Pull Out (%)	43	20	12	12	16	12	8	9	15	9	9	6
Normal Force (lbs) [N]	21 93	11 49	9 40	7 31	49 218	18 80	25 111	24 107	124 552	85 378	63 280	92 409
Tangential Force (lbs) [N]	2 9	1 4	2 9	1 4	10 44	3 13	4 18	5 22	34 151	11 49	11 49	9 40
Power (HP) [kW]	0.3 0.2	0.7 0.5	1.1 0.8	1.2 0.9	1.3 1.0	2.2 1.6	3.0 2.2	1.9 1.4	4.5 3.4	3.7 2.8	11.4 8.5	5.9 4.4
Specific Energy (in-lb/in ²)x10 ⁻⁶ [joule/cu mm]	2.6 18	5.3 37	12.5 86	12.3 85	3.6 25	2.9 20	7.0 48	11.7 81	6.1 42	5.8 40	10.3 71	11.5 79
Contact Pressure (psi) [MPa]	369 2.5	185 1.3	161 1.1	115 0.8	612 4.2	222 1.5	311 2.1	298 2.1	1,069 7.4	739 5.1	562 3.9	817 5.6
Unit Grit Load (lbs/grit) [N/grit]	0.014 0.062	0.007 0.031	0.006 0.027	0.004 0.019	0.023 0.103	0.008 0.037	0.012 0.052	0.011 0.050	0.041 0.184	0.028 0.125	0.021 0.094	0.031 0.137
Grind Temperature (Fahrenheit) [Celsius]	351 177	740 393	1,169 632	1,269 687	843 451	1,377 747	1,840 1,004	1,210 654	2,262 1,239	1,876 1,024	5,793 3,201	3,012 1,656

Table 2. Summary of conditions and results for HSLD surface grinding tests.

Notes:

- Eaton S/RBSN ground with Abrasive Technology 120 grit plated wheel
- Specific energy calculated using tangential force.
- Contact pressure calculated using normal force.



Test Number	Wheel Type	Coolant Application	Wheel Speed (ft/min)	Part Speed (in/min)	Depth of Cut (in)	Horizontal Force (lbs)	Vertical Force (lbs)	Power (hp)	Specific Energy (from power) (in-lb/in ³)	Heat Flux (from power) (in-lb/in ² s)
1	Resin	No Channel	10,000	0.5	0.437	19.6	47.0	1.8	51,035,973	99,401B
2	Resin	No Channel	10,000	0.25	0.422	34.0	82.0	2.6	153,745,592	147,130B
3	Resin	No Channel	10,000	0.25	0.437	21.0	58.0	0.8	46,396,339	45,182
4	Metal	No Channel	10,000	0.6	0.437	31.6	85.0	3.0	73,460,870	153,567B
5	Metal	Channel	10,000	0.6	0.437	23.0	62.0	1.4	32,864,073	68,701
6	Metal	Channel	10,000	1.0	0.434	30.0	64.0	2.7	39,709,493	137,876
7	Metal	No Channel	10,000	1.0	0.427	14.0	28.0	1.1	16,619,016	57,236B
8	Metal-Dull	Channel	10,000	1.0	0.425	35.0	100.0	2.2	33,394,447	114,741B
9	Metal	Channel	10,000	1.25	0.433	31.0	66.0	2.6	29,967,963	129,915
10	Metal	Channel	10,000	1.5	0.435	28.0	32.0	2.6	24,858,483	129,616B
11	Metal	Channel	10,000	1.75	0.428	22.0	40.0	2.4	20,302,270	122,505B
12	Metal	Channel	10,000	2.0	0.432	20.0	30.0	2.2	16,426,667	113,807B

Note: "B" after Heat Flux value designates Burnout.

Diamond Slicing Wheel Specifications

Norton Resin Bond (100 grit)	8" OD x 0.0625" wide SD 100 - R 50 B 69 - 1/4
Regal Metal Bond (80 grit)	10" OD x 0.0625" wide MD 80 N 50 M - 1/4

Table 3. Forces and power at burnout or maximum grinding values at full depth of cut (no burnout).



HSLD Cylindrical Grinding Results

Eaton Material	120 Grit Wheel				400 Grit Wheel			
	0.267 in ² /min 2.86 mm ² /sec		0.8 in ² /min 8.6 mm ² /sec		0.267 in ² /min 2.86 mm ² /sec		0.8 in ² /min 8.6 mm ² /sec	
Wheel Speed (ft/min) [m/sec]	3,700 19	11,300 57	3,700 19	11,300 57	3,700 19	11,300 57	3,700 19	11,300 57
Surface Finish Ra (μ in) [micron]	76 1.93	82 2.08	98 2.49	99 2.51	38 0.97	21 0.53	41 1.04	36 0.91
Pull Out (%)	54	76	39	50	20	17	26	19
Power (HP) [kW]	0.4 0.3	0.3 0.2	0.8 0.6	1.0 0.8	0.6 0.5	0.6 0.5	1.6 1.2	2.0 1.5
Normal Force (lbs) [N]	18 82	12 55	55 243	18 78	21 95	7 33	41 182	25 113

Kyocera Material	120 Grit Wheel				400 Grit Wheel			
	0.267 in ² /min 2.86 mm ² /sec		0.8 in ² /min 8.6 mm ² /sec		0.267 in ² /min 2.86 mm ² /sec		0.8 in ² /min 8.6 mm ² /sec	
Wheel Speed (ft/min) [m/sec]	3,700 19	11,300 57	3,700 19	11,300 57	3,700 19	11,300 57	3,700 19	11,300 57
Surface Finish Ra (μ in) [micron]	89 2.26	74 1.88	90 2.29	96 2.44	33 0.84	23 0.58	34 0.86	32 0.81
Pull Out (%)	43	67	32	21	11	10	11	12
Power (HP) [kW]	1.5 1.1	1.1 0.8	1.4 1.0	1.7 1.3	0.9 0.7	1.0 0.8	2.7 2.0	2.8 2.1
Normal Force (lbs) [N]	25 111	24 107	49 218	29 129	27 120	20 89	75 334	45 200

Table 4. HSLD Cylindrical grinding results.



Test Number	Roller Type	Roller Number	Wheel Speed (ft/min)	Part Speed (ft/min)	In-Feed Rate (in/rev)	Material Removal Rate (in ² /min)	Normal Force (lbs)	Power (HP)	Surface Finish-Ra (μ in)	Roundness (μ in)	Specific Energy (in-lb/in ²)
1	Eaton	E-12	6,500	267	0.000016	0.051	14.3	0.31	10.0	30.7	2,569,327
2	Eaton	E-13	15,000	267	0.000016	0.051	17.5	0.30	24.7	107.3	2,544,220
3	Eaton	E-20	6,500	267	0.000046	0.150	13.5	0.80	9.2	50.4	2,328,805
4	Eaton	E-26	15,000	267	0.000046	0.150	27.5	0.94	16.5	49.2	2,747,990
5	Kyocera	K-4	6,500	267	0.000016	0.051	13.0	0.41	7.4	41.1	3,431,349
6	Kyocera	K-13	15,000	267	0.000016	0.051	18.5	0.21	12.7	46.3	1,740,782
7	Kyocera	K-20	6,500	267	0.000046	0.150	16.3	1.01	7.5	42.7	2,925,561
8	Kyocera	K-24	15,000	267	0.000046	0.150	26.0	1.15	14.5	64.0	3,353,479

Table 5. HSLD OD grinding summary data using Coors resin bonded wheel.

INTERNAL DISTRIBUTION

Central Research Library (2)
Document Reference Section
Laboratory Records Department (2)
Laboratory Records, ORNL RC
ORNL Patent Section
M&C Records Office (3)
L. F. Allard, Jr.
L. D. Armstrong
P. F. Becher
R. F. Bernal
T. M. Besmann
P. J. Blau
K. W. Boling
R. A. Bradley
K. Breder
C. R. Brinkman
V. R. Bullington
H. Cai
G. M. Caton
S. J. Chang
R. H. Cooper, Jr.
S. A. David
J. H. DeVan
J. L. Ding
M. K. Ferber
F. M. Foust
W. Fulkerson
R. L. Graves
D. L. Greene
H. W. Hayden, Jr.
E. E. Hoffman
C. R. Hubbard
M. A. Janney
D. R. Johnson (5)
D. Joslin
R. R. Judkins
M. A. Karnitz
M. R. Kass
B. L. Keyes
H. D. Kimrey, Jr.
K. C. Liu
E. L. Long, Jr.
W. D. Manly
R. W. McClung
D. J. McGuire
J. R. Merriman
T. A. Nolan
A. E. Pasto
M. H. Rawlins
M. L. Santella
A. C. Schaffhauser
S. Scott
E. J. Soderstrom
D. P. Stinton
R. W. Swindeman
V. J. Tennery
T. N. Tiegs
J. R. Weir, Jr.
B. H. West
S. G. Winslow
J. M. Wyrick
C. S. Yust

EXTERNAL DISTRIBUTION

Pioneering Research Info. Ctr.
E.I. Dupont de Nemours & Co. Inc.
Experimental Station
P.O. Box 80302
Wilmington DE 19880-0302

Jeffrey Abboud
U.S. Advanced Ceramics Assoc.
1600 Wilson Blvd., Suite 1008
Arlington VA 22209

James H. Adair
University of Florida
Materials Science & Engineering
317 MAE Bldg.
Gainesville FL 32611-2066

Donald F. Adams
University of Wyoming
Mechanical Engineering Department
P.O. Box 3295
Laramie WY 82071

Jalees Ahmad
AdTech Systems Research Inc.
Solid Mechanics
1342 N. Fairfield Road
Dayton OH 45432-2698

Yoshio Akimune
NISSAN Motor Co., Ltd.
Materials Research Laboratory
1 Natsushima-Cho
Yokosuka 237
JAPAN

Mufit Akinc
Iowa State University
322 Spedding Hall
Ames IA 50011

Ilhan A. Aksay
Princeton University
A313 Engineering Quadrangle
Princeton NJ 08544-5263

Charles Aldridge
Heany Industries, Inc.
249 Briarwood Lane
Scottsville NY 14546

Joseph E. Amara
Instron Corporation
Corporate Engineering Office
100 Royale Street
Canton MA 02021

Edward M. Anderson
Aluminum Company of America
N. American Industrial Chemical
P.O. Box 300
Bauxite AR 72011

Norman C. Anderson
Ceradyne, Inc.
Ceramic-to-Metal Division
3169 Redhill Avenue
Costa Mesa CA 92626

Don Anson
BCL
Thermal Power Systems
505 King Avenue
Columbus OH 43201-2693

Thomas Arbanas
G.B.C. Materials Corporation
580 Monastery Drive
Latrobe PA 15650-2698

Frank Armatis
3M Company
Building 60-1N-01
St. Paul MN 55144-1000

Everett B. Arnold
Detroit Diesel Corporation
Mechanical Systems Technology
13400 Outer Drive West
Detroit MI 48239-4001

Bertil Aronsson
Sandvik AB
S-12680
Stockholm Lerkrogsvagen 19
SWEDEN

Dennis Assanis
University of Illinois
Dept. of Mechanical Engineering
1206 W. Green Street
Urbana IL 61801

V. S. Avva
North Carolina A&T State Univ.
Dept. of Mechanical Engineering
Greensboro NC 27411

Patrick Badgley
Sky Technologies, Inc.
2815 Franklin Drive
Columbus IN 47201

Sunggi Baik
Pohang Institute of Sci. & Tech.
P.O. Box 125
Pohang 790-600
KOREA

John M. Bailey
Consultant
Caterpillar, Inc.
P.O. Box 1875
Peoria IL 61656-1875

Bob Baker
Ceradyne, Inc.
3169 Redhill Avenue
Costa Mesa CA 92626

Frank Baker
Aluminum Company of America
Alcoa Technical Center
Alcoa Center PA 15069

Clifford P. Ballard
AlliedSignal Aerospace Company
Ceramics Program
P.O. Box 1021
Morristown NJ 07962-1021

B. P. Bandyopadhyay
ELID Team
Wako Campus
2-1 Hirosawa Wako-shi
Saitama 351-01
JAPAN

P. M. Barnard
Ruston Gas Turbines Limited
P.O. Box 1
Lincoln LN2 5DJ
ENGLAND

Harold N. Barr
Hittman Corporation
9190 Red Branch Road
Columbia MD 21045

Renald D. Bartoe
Vesuvius McDanel
510 Ninth Avenue
Box 560
Beaver Falls PA 15010-0560

David L. Baty
Babcock & Wilcox - LRC
P.O. Box 11165
Lynchburg VA 24506-1165

Donald F. Baxter, Jr.
ASM International
Advanced Materials & Processes
Materials Park OH 44073-0002

M. Brad Beardsley
Caterpillar Inc.
Technical Center Bldg. E
P.O. Box 1875
Peoria IL 61656-1875

John C. Bell
Shell Research Limited
Thornton Research Centre
P.O. Box 1
Chester CH1 3SH
ENGLAND

M. Bentele
Xamag, Inc.
259 Melville Avenue
Fairfield CT 06430

Larry D. Bentsen
BFGoodrich Company
R&D Center
9921 Brecksville Road
Brecksville OH 44141

Louis Beregszazi
Defiance Precision Products
P.O. Drawer 428
Defiance OH 43512

Tom Bernecki
Northwestern University
1801 Maple Avenue
Evanston IL 60201-3135

Charles F. Bersch
Institute for Defense Analyses
1801 N. Beauregard Street
Alexandria VA 22311

Ram Bhatt
NASA Lewis Research Center
21000 Brookpark Road
Cleveland OH 44135

Deane I. Biehler
Caterpillar Inc.
Engineering Research Materials
P.O. Box 1875, Bldg. E
Peoria IL 61656-1875

John W. Bjerklie
Consolidated Natural Gas Service
Co. Inc.
Research Department
Pittsburgh PA 15222-3199

William D. Bjorndahl
TRW, Inc.
One Space Park, MS:R6-2188
Building 01, Room 2040
Redondo Beach CA 90278

Keith A. Blakely
Advanced Refractory Technologies,
Inc.
699 Hertel Avenue
Buffalo NY 14207

Edward G. Blanchard
Netzsch Inc.
119 Pickering Way
Exton PA 19341

Bruce Boardman
Deere and Company Technical Ctr.
3300 River Drive
Moline IL 61265

Russell Bockstedt
Hoechst Celanese Corporation
150 JFK Parkway
Short Hills NJ 07078

M. Boehmer
DLR German Aerospace Research
Estab.
Postfach 90 60 58
D-5000 Koln 90
GERMANY

Lawrence P. Boesch
EER Systems Corp.
1593 Spring Hill Road
Vienna VA 22182-2239

Donald H. Boone
Boone & Associates
2412 Cascade Drive
Walnut Creek CA 94598-4313

Tom Booth
AlliedSignal, Inc.
AiResearch Los Angeles Division
2525 West 190th Street
Torrance CA 90509-2960

Tibor Bornemisza
Sundstrand Power Systems
4400 Ruffin Road
San Diego CA 92186-5757

J.A.M. Boulet
University of Tennessee
Engineering Science and Mechanics
Knoxville TN 37996-2030

H. Kent Bowen
Massachusetts Institute of
Technology
77 Massachusetts Ave., Rm E40-434
Cambridge MA 02139

Leslie J. Bowen
Materials Systems
53 Hillcrest Road
Concord MA 01742

Steven C. Boyce
Air Force Office of Scientific
Research
AFOSR/NA Bldg. 410
Bolling AFB DC 20332-6448

Gary L. Boyd
Ceramic Engineering Consulting
328 Sneath Way
Alpine CA 91901

Steve Bradley
UOP Research Center
50 E. Algonquin Road
Des Plaines IL 60017-6187

Michael C. Brands
Cummins Engine Company, Inc.
P.O. Box 3005, Mail Code 50179
Columbus IN 47201

Raymond J. Bratton
Westinghouse Science & Technology
1310 Beulah Road
Pittsburgh PA 15235

John J. Brennan
United Technologies Corporation
Silver Lane, MS:24
East Hartford CT 06108

Terrence K. Brog
Golden Technologies Company
4545 McIntyre Street
Golden CO 80403

Gunnar Broman
317 Fairlane Drive
Spartanburg SC 29302

Alan Brown
P.O. Box 882
Dayton NJ 08810

Jesse J. Brown
VPI & SU
Ctr. for Advanced Ceram Materials
Blacksburg VA 24061-0256

Sherman D. Brown
University of Illinois
Materials Science and Engineering
105 South Goodwin Avenue
Urbana IL 61801

S. L. Bruner
Ceramatec, Inc.
2425 South 900 West
Salt Lake City UT 84119

Walter Bryzik
U.S. Army Tank Automotive Command
R&D Center, Propulsion Systems
Warren MI 48397-5000

S. J. Burden
2572 Devonwood
Troy MI 48098

Curt V. Burkland
AMERCOM, Inc.
8928 Fullbright Avenue
Chatsworth CA 91311

Bill Bustamante
AMERCOM, Inc.
8928 Fullbright Avenue
Chatsworth CA 91311

Oral Buyukozturk
Massachusetts Institute of
Technology
77 Massachusetts Ave., Room 1-280
Cambridge MA 02139

David A. Caillet
Ethyl Corporation
451 Florida Street
Baton Rouge La 70801

Roger Cannon
Rutgers University
P.O. Box 909
Piscataway NJ 08855-0909

Scott Cannon
P.O. Box 567254
Atlanta GA 30356

Harry W. Carpenter
1844 Fuerte Street
Fallbrook CA 92028

David Carruthers
Kyocera Industrial Ceramics
Company
P.O. Box 2279
Vancouver WA 98668-2279

Calvin H. Carter, Jr.
Cree Research, Inc.
2810 Meridian Parkway
Durham NC 27713

J. David Casey
35 Atlantis Street
West Roxbury MA 02132

Jere G. Castor
J. C. Enterprise
5078 N. 83rd Street
Scottsdale AZ 85250

James D. Cawley
Case Western Reserve University
Materials Science & Engineering
Cleveland OH 44106

Thomas C. Chadwick
Den-Mat Corporation
P.O. Box 1729
Santa Maria CA 93456

Ronald H. Chand
Chand Kare Technical Ceramics
2 Coppage Drive
Worcester MA 01603-1252

Robert E. Chaney
EG&G Idaho, Inc.
Idaho National Engineering Lab
P.O. Box 1625
Idaho Falls ID 83415-3525

Frank C. Chang
U.S. Army Materials Technology
AMTL-EMM
405 Arsenal Street
Watertown MA 02172

Nam S. Chang
Chrysler Corporation
12000 Chrysler Drive
Highland Park MI 48288-0001

William Chapman
Williams International Corp.
2280 W. Maple Road
Walled Lake MI 48390-0200

Ching-Fong Chen
LECO Corporation
3000 Lakeview Avenue
St. Joseph MI 49085

Frank Childs
EG&G Idaho, Inc.
Idaho National Engineering Lab
P.O. Box 1625
Idaho Falls ID 83415-3527

William J. Chmura
Torrington Company
59 Field Street
Torrington CT 06790-4942

Tsu-Wei Chou
University of Delaware
201 Spencer Laboratory
Newark DE 19716

R. J. Christopher
Ricardo Consulting Engineers
Bridge Works
Shoreham-By-Sea W. Sussex BN435FG
ENGLAND

Joel P. Clark
Massachusetts Institute of
Technology
Room 8-409
Cambridge MA 02139

Giorgio Clarotti
Commission of the European Comm
DGXII-C3, M075, 1-53;
200 Rue de la Loi
B-1049 Brussels
BELGIUM

W. J. Clegg
ICI Advanced Materials
P.O. Box 11, The Heath
Runcorn Cheshire WA7 4QE
ENGLAND

William S. Coblenz
Adv. Research Projects Agency
3701 N. Fairfax Drive
Arlington VA 22203

Gloria M. Collins
ASTM
1916 Race Street
Philadelphia PA 19103

William C. Connors
Sundstrand Aviation Operations
Materials Science & Engineering
4747 Harrison Avenue
Rockford IL 61125-7002

John A. Coppola
Carborundum Company
Niagara Falls R&D Center
P.O. Box 832
Niagara Falls NY 14302

Normand D. Corbin
Norton Company
SGNICC/NRDC
Goddard Road
Northboro MA 01532-1545

Douglas Corey
AlliedSignal, Inc.
2525 West 190th Street, MS:T52
Torrance CA 90504-6099

Keith P. Costello
Chand/Kare Technical Ceramics
2 Coppage Drive
Worcester MA 01603-1252

Ed L. Courtright
Pacific Northwest Laboratory
MS:K3-59
Richland WA 99352

Anna Cox
Mitchell Market Reports
P.O. Box 23
Monmouth Gwent NP5 4YG
UNITED KINGDOM

J. Wesley Cox
BIRL
1801 Maple Avenue
Evanston IL 60201-3135

Art Cozens
Instron Corporation
3414 Snowden Avenue
Long Beach CA 90808

Mark Crawford
New Technology Week
4604 Monterey Drive
Annandale VA 22003

Richard A. Cree
Markets & Products, Inc.
P.O. Box 14328
Columbus OH 43214-0328

Les Crittenden
Vesuvius McDanel
Box 560
Beaver Falls PA 15010

William J. Croft
U.S. Army Materials Technology
405 Arsenal Street
Watertown MA 02172

M. J. Cronin
Mechanical Technology, Inc.
968 Albany-Shaker Road
Latham NY 12110

Gary M. Crosbie
Ford Motor Company
20000 Rotunda Drive
MD-2313, SRL Building
Dearborn MI 48121-2053

Floyd W. Crouse, Jr.
U.S. Department of Energy
Morgantown Energy Technology Ctr
P.O. Box 880
Morgantown WV 26505

John Cuccio
AlliedSignal Engines
P.O. Box 52180, MS:1302-2Q
Phoenix AZ 85072-2180

Raymond A. Cutler
Ceramatec, Inc.
2425 South 900 West
Salt Lake City UT 84119

Stephen C. Danforth
Rutgers University
P.O. Box 909
Piscataway NJ 08855-0909

Sankar Das Gupta
Electrofuel Manufacturing Co.
9 Hanna Avenue
Toronto Ontario MGK-1W8
CANADA

Frank Davis
AlliedSignal Aerospace Company
7550 Lucerne Drive, #203
Middleburg Heights OH 44130

Robert F. Davis
North Carolina State University
Materials Engineering Department
P.O. Box 7907
Raleigh NC 27695

Michael DeLuca
RSA Research Group
1534 Claas Ave.
Holbrook NY 11741

Gerald L. DePoorter
Colorado School of Mines
Metallurgical & Materials Engr
Golden CO 80401

J. F. DeRidder
Omni Electro Motive, Inc.
12 Seely Hill Road
Newfield NY 14867

Nick C. Dellow
Materials Technology Publications
40 Sotheron Road
Watford Herts WD1 2QA
UNITED KINGDOM

L. R. Dharani
University of Missouri-Rolla
224 M.E.
Rolla MO 65401

Douglas A. Dickerson
Union Carbide Specialty Powders
1555 Main Street
Indianapolis IN 46224

John Dodsworth
Vesuvius Research & Development
Technical Ceramics Group
Box 560
Beaver Falls PA 15010

B. Dogan
Institut fur Werkstofforschung
GKSS-Forschungszentrum Geesthacht
Max-Planck-Strasse
D-2054 Geesthacht
GERMANY

Alan Dragoo
U.S. Department of Energy
ER-131, MS:F-240
Washington DC 20817

Jean-Marie Drapier
FN Moteurs S.A.
Material and Processing
B-4041 Milmort (Herstal)
BELGIUM

Kenneth C. Dreitlein
United Technologies Research Ctr
Silver Lane
East Hartford CT 06108

Robin A.L. Drew
 McGill University
 3450 University Street
 Montreal Quebec H3A 2A7
 CANADA

Winston H. Duckworth
 BCL
 Columbus Division
 505 King Avenue
 Columbus OH 43201-2693

Bill Durako
 Materials Engineering, Inc.
 P.O. Box 43
 Virgil IL 60182

Ernest J. Duwell
 3M Abrasive Systems Division
 3M Center
 St. Paul MN 55144-1000

Chuck J. Dziedzic
 GTC Process Forming Systems
 4545 McIntyre Street
 Golden CO 80403

Robert J. Eagan
 Sandia National Laboratories
 Engineered Materials & Processes
 P.O. Box 5800
 Albuquerque NM 87185-5800

Jeffrey Eagleson
 Lanxide Corporation
 1001 Connecticut Avenue, N.W.
 Washington DC 20036

Harry E. Eaton
 United Technologies Corporation
 Silver Lane
 East Hartford CT 06108

Harvill C. Eaton
 Louisiana State University
 240 Thomas Boyd Hall
 Baton Rouge LA 70803

Christopher A. Ebel
 Carborundum Company
 Technology Division
 P.O. Box 832
 Niagara Falls NY 14302-0832

J. J. Eberhardt
 U.S. Department of Energy
 Office of Transportation Matrl's
 CE-34, Forrestal Building
 Washington DC 20585

Jim Edler
 Eaton Corporation
 26201 Northwestern Highway
 P.O. Box 766
 Southfield MI 48037

G. A. Eisman
 Dow Chemical Company
 Ceramics and Advanced Materials
 52 Building
 Midland MI 48667

William A. Ellingson
 Argonne National Laboratory
 Energy Technology Division
 9700 S. Cass Avenue
 Argonne IL 60439

Anita Kaye M. Ellis
 Machined Ceramics
 629 N. Graham Street
 Bowling Green KY 42101

Glen B. Engle
 Nuclear & Aerospace Materials
 16716 Martincoit Road
 Poway CA 92064

Jeff Epstein
 Ceramic Technologies, Inc.
 12739 Ashford Knoll
 Houston TX 77082

Kenneth A. Epstein
 Dow Chemical Company
 2030 Building
 Midland MI 48674

Art Erdemir
Argonne National Laboratory
9700 S. Cass Avenue
Argonne IL 60439

E. M. Erwin
Lubrizol Corporation
1819 East 225th Street
Euclid OH 44117

John N. Eustis
U.S. Department of Energy
Industrial Energy Efficiency Div
CE-221, Forrestal Building
Washington DC 20585

W. L. Everitt
Kyocera International, Inc.
8611 Balboa Avenue
San Diego CA 92123

Gordon Q. Evison
332 S. Michigan Avenue
Suite 1730
Chicago IL 60604

John W. Fairbanks
U.S. Department of Energy
Office of Propulsion Systems
CE-322, Forrestal Building
Washington DC 20585

Tim Fawcett
Dow Chemical Company
Advanced Ceramics Laboratory
1776 Building
Midland MI 48674

Robert W. Fawley
Sundstrand Power Systems
Div. of Sundstrand Corporation
P.O. Box 85757
San Diego CA 92186-5757

Jeff T. Fenton
Vista Chemical Company
900 Threadneedle
Houston TX 77079

Larry Ferrell
Babcock & Wilcox
Old Forest Road
Lynchburg VA 24505

Raymond R. Fessler
BIRL
1801 Maple Avenue
Evanston IL 60201

Ross F. Firestone
Ross Firestone Company
188 Mary Street
Winnetka IL 60093-1520

Sharon L. Fletcher
Arthur D. Little, Inc.
15 Acorn Park
Cambridge MA 02140-2390

Thomas F. Foltz
Textron Specialty Materials
2 Industrial Avenue
Lowell MA 01851

Renee G. Ford
Materials and Processing Report
P.O. Box 72
Harrison NY 10528

John Formica
Supermaterials
2020 Lakeside Avenue
Cleveland OH 44114

Edwin Frame
Southwest Research Institute
P.O. Drawer 28510
San Antonio TX 78284

Armanet Francois
French Scientific Mission
4101 Reservoir Road, N.W.
Washington DC 20007-2176

R. G. Frank
Technology Assessment Group
10793 Bentley Pass Lane
Loveland OH 45140

David J. Franus
Forecast International
22 Commerce Road
Newtown CT 06470

Marc R. Freedman
NASA Lewis Research Center
21000 Brookpark Road, MS:49-3
Cleveland OH 44135

Douglas Freitag
Bayside Materials Technology
17 Rocky Glen Court
Brookeville MD 20833

Brian R.T. Frost
Argonne National Laboratory
9700 S. Cass Avenue, Bldg. 900
Argonne IL 60439

Lawrence R. Frost
Instron Corporation
100 Royall Street
Canton MA 02021

Xiren Fu
Shanghai Institute of Ceramics
1295 Ding-xi Road
Shanghai 200050
CHINA

J. P. Gallagher
University of Dayton Research
Institute
300 College Park, JPC-250
Dayton OH 45469-0120

Garry Garvey
Golden Technologies Company Inc.
4545 McIntyre Street
Golden CO 80403

Richard Gates
NIST
Materials Bldg., A-256
Gaithersburg MD 20899

L. J. Gauckler
ETH-Zurich
Sonneggstrasse 5
CH-8092 Zurich 8092
SWITZERLAND

George E. Gazza
U.S. Army Materials Technology
Ceramics Research Division
405 Arsenal Street
Watertown MA 02172-0001

D. Gerster
CEA-DCOM
33 Rue De La Federation
Paris 75015
FRANCE

John Ghinazzi
Coors Technical Ceramics Company
1100 Commerce Park Drive
Oak Ridge TN 37830

Robert Giddings
General Electric Company
P.O. Box 8
Schenectady NY 12301

A. M. Glaeser
University of California
Lawrence Berkeley Laboratory
Hearst Mining Building
Berkeley CA 94720

Joseph W. Glatz
510 Rocksville Road
Holland PA 18966

W. M. Goldberger
Superior Graphite Company
R&D
2175 E. Broad Street
Columbus OH 43209

Allan E. Goldman
U.S. Graphite, Inc.
907 W. Outer Drive
Oak Ridge TN 37830

Stephen T. Gonczy
Allied Signal Research
P.O. Box 5016
Des Plaines IL 60017

Robert J. Gottschall
U.S. Department of Energy
ER-131, MS:G-236
Washington DC 20585

Earl Graham
Cleveland State University
Dept. of Chemical Engineering
Euclid Avenue at East 24th Street
Cleveland OH 44115

John W. Graham
Astro Met, Inc.
9974 Springfield Pike
Cincinnati OH 45215

G. A. Graves
U. of Dayton Research Institute
300 College Park
Dayton OH 45469-0001

Robert E. Green, Jr.
Johns Hopkins University
Materials Science and Engineering
Baltimore MD 21218

Alex A. Greiner
Plint & Partners
Oaklands Park
Wokingham Berkshire RG11 2FD
UNITED KINGDOM

Lance Groseclose
Allison Engine Company
P.O. Box 420, MS:W-5
Indianapolis IN 46206

Thomas J. Gross
U.S. Department of Energy
Transportation Technologies
CE-30, Forrestal Building
Washington DC 20585

Mark F. Gruninger
Union Carbide Corporation
Specialty Powder Business
1555 Main Street
Indianapolis IN 46224

Ernst Gugel
Cremer Forschungsinstitut
GmbH&Co.KG
Oeslauer Strasse 35
D-8633 Roedental 8633
GERMANY

John P. Gyekenyesi
NASA Lewis Research Center
21000 Brookpark Road, MS:6-1
Cleveland OH 44135

Nabil S. Hakim
Detroit Diesel Corporation
13400 Outer Drive West
Detroit MI 48239

Philip J. Haley
Allison Engine Company
P.O. Box 420, MS:T12A
Indianapolis IN 46236

Judith Hall
Fiber Materials, Inc.
Biddeford Industrial Park
5 Morin Street
Biddeford ME 04005

Y. Hamano
Kyocera Industrial Ceramics Corp.
5713 E. Fourth Plain Blvd.
Vancouver WA 98661-6857

Y. Harada
IIT Research Institute
10 West 35th Street
Chicago IL 60616

R. A. Harmon
25 Schalren Drive
Latham NY 12110

Norman H. Harris
Hughes Aircraft Company
P.O. Box 800520
Saugus CA 91380-0520

Alan M. Hart
Dow Chemical Company
1776 Building
Midland MI 48674

Pat E. Hart
Battelle Pacific Northwest Labs
Ceramics and Polymers Development
P.O. Box 999
Richland WA 99352

Michael H. Haselkorn
Caterpillar Inc.
Technical Center, Building E
P.O. Box 1875
Peoria IL 61656-1875

Debbie Haught
U.S. Department of Energy
Off. of Transportation Materials
EE-34, Forrestal Bldg.
Washington DC 20585

N. B. Havewala
Corning Inc.
SP-PR-11
Corning NY 14831

John Haygarth
Teledyne WAA Chang Albany
P.O. Box 460
Albany OR 97321

Norman L. Hecht
U. of Dayton Research Institute
300 College Park
Dayton OH 45469-0172

Peter W. Heitman
Allison Engine Company
P.O. Box 420, MS:W-5
Indianapolis IN 46206-0420

Robert W. Hendricks
VPI & SU
210 Holden Hall
Blacksburg VA 24061-0237

Thomas P. Herbell
NASA Lewis Research Center
21000 Brookpark Road, MS:49-3
Cleveland OH 44135

Marlene Heroux
Rolls-Royce, Inc.
2849 Paces Ferry Road, Suite 450
Atlanta GA 30339-3769

Robert L. Hershey
Science Management Corporation
1255 New Hampshire Ave., N.W.
Suite 1033
Washington DC 20036

Hendrik Heystek
Bureau of Mines
Tuscaloosa Research Center
P.O. Box L
University AL 35486

Robert V. Hillery
GE Aircraft Engines
One Neumann Way, M.D. H85
Cincinnati OH 45215

Arthur Hindman
Instron Corporation
100 Royall Street
Canton MA 02021

Shinichi Hirano
Mazda R&D of North America, Inc.
1203 Woodridge Avenue
Ann Arbor MI 48105

Tommy Hiraoka
NGK Locke, Inc.
1000 Town Center
Southfield MI 48075

Fu H. Ho
General Atomics
P.O. Box 85608
San Diego CA 92186-9784

John M. Hobday
 U.S. Department of Energy
 Morgantown Energy Technology Ctr
 P.O. Box 880
 Morgantown WV 26507

Clarence Hoenig
 Lawrence Livermore National Lab
 P.O. Box 808, Mail Code L-369
 Livermore CA 94550

Thomas Hollstein
 Fraunhofer-Institut für
 Werkstoffmechanik
 Wohlerstrasse 11
 D-79108 Freiburg
 GERMANY

Richard Holt
 National Research Council Canada
 Structures and Materials Lab
 Ottawa Ontario K1A 0R6
 CANADA

Woodie Howe
 Coors Technical Ceramics Company
 1100 Commerce Park Drive
 Oak Ridge TN 37830

Stephen M. Hsu
 NIST
 Gaithersburg MD 20899

Hann S. Huang
 Argonne National Laboratory
 9700 S. Cass Avenue
 Argonne IL 60439-4815

Gene Huber
 Precision Ferrites & Ceramics
 5576 Corporate Drive
 Cypress CA 90630

Harold A. Huckins
 Princeton Advanced Technology
 4 Bertram Place
 Hilton Head SC 29928

Fred R. Huettig
 Advanced Magnetics Inc.
 45 Corey Lane
 Mendham NJ 07945

Brian K. Humphrey
 Lubrizol Petroleum Chemicals Co.
 3000 Town Center, Suite 1340
 Southfield MI 48075-1201

Robert M. Humrick
 Dylon Ceramic Technologies
 3100 Edgehill Road
 Cleveland Heights OH 44118

Lorretta Inglehart
 National Science Foundation
 Division of Materials Research
 1800 "G" Street, N.W., Room 408
 Washington DC 20550

Michael S. Inoue
 Kyocera International, Inc.
 8611 Balboa Avenue
 San Diego CA 92123-1580

Joseph C. Jackson
 U.S. Advanced Ceramics Assoc.
 1600 Wilson Blvd., Suite 1008
 Arlington VA 22209

Osama Jadaan
 U. of Wisconsin-Platteville
 1 University Plaza
 Platteville WI 53818

Said Jahanmir
 NIST
 Materials Bldg., Room A-237
 Gaithersburg MD 20899

Curtis A. Johnson
 General Electric Company
 P.O. Box 8
 Schenectady NY 12301

Sylvia Johnson
 SRI International
 333 Ravenswood Avenue
 Menlo Park CA 94025

Thomas A. Johnson
Lanxide Corporation
P.O. Box 6077
Newark DE 19714-6077

W. S. Johnson
Indiana University
One City Centre, Suite 200
Bloomington IN 47405

Walter F. Jones
AFOSR/NA
110 Duncan Ave., Ste. B115
Washington DC 20332-0001

Jill E. Jonkouski
U.S. Department of Energy
9800 S. Cass Avenue
Argonne IL 60439-4899

L. A. Joo
Great Lakes Research Corporation
P.O. Box 1031
Elizabethton TN 37643

A. David Joseph
SPX Corporation
700 Terrace Point
Muskegon MI 49443

Adam Jostsons
Australian Nuclear Science &
Technology
New Illawarra Road
Lucas Heights New South Wales
AUSTRALIA

Tom Kalamasz
Norton/TRW Ceramics
7A-4 Raymond Avenue
Salem NH 03079

Lyle R. Kallenbach
Phillips Petroleum
Mail Drop:123AL
Bartlesville OK 74004

Nick Kamiya
Kyocera Industrial Ceramics Corp.
25 Northwest Point Blvd., #450
Elk Grove Village IL 60007

Roy Kamo
Adiabatics, Inc.
3385 Commerce Park Drive
Columbus IN 47201

Chih-Chun Kao
Industrial Technology Research
Institute
195 Chung-Hsing Road, Sec. 4
Chutung Hsinchu 31015 R.O.C.
TAIWAN

Keith R. Karasek
AlliedSignal Aerospace Company
50 E. Algonquin Road
Des Plaines IL 60017-5016

Martha R. Kass
U.S. Department of Energy
Oak Ridge Operations
Building 4500N, MS:6269
Oak Ridge TN 37831-6269

Robert E. Kassel
Ceradyne, Inc.
3169 Redhill Avenue
Costa Mesa CA 92626

Allan Katz
Wright Laboratory
Metals and Ceramics Division
Wright-Patterson AFB OH 45433

R. Nathan Katz
Worcester Polytechnic Institute
100 Institute Road
Worcester MA 01609

Tony Kaushal
Detroit Diesel Corporation
13400 Outer Drive, West
Detroit MI 48239-4001

Ted Kawaguchi
Tokai Carbon America, Inc.
375 Park Avenue, Suite 3802
New York NY 10152

Noritsugu Kawashima
TOSHIBA Corporation
4-1 Ukishima-Cho
Kawasaki-Ku Kawasaki, 210
JAPAN

Lisa Kempfer
Penton Publishing
1100 Superior Avenue
Cleveland OH 44114-2543

Frederick L. Kennard, III
AC Rochester
1300 N. Dort Highway
Flint MI 48556

David O. Kennedy
Lester B. Knight Cast Metals Inc.
549 W. Randolph Street
Chicago IL 60661

George Keros
Photon Physics
3175 Penobscot Building
Detroit MI 48226

Thomas Ketcham
Corning, Inc.
SP-DV-1-9
Corning NY 14831

Pramod K. Khandelwal
Allison Engine Company
P.O. Box 420, MS:T10B
Indianapolis IN 46206

Jim R. Kidwell
AlliedSignal Engines
P.O. Box 52180
Phoenix AZ 85072-2180

Shin Kim
The E-Land Group
19-8 ChangJeon-dong
Mapo-gu, Seoul 121-190
KOREA

W. C. King
Mack Truck, Z-41
1999 Pennsylvania Avneue
Hagerstown MD 21740

Carol Kirkpatrick
MSE, Inc.
P.O. Box 3767
Butte MT 59702

Tony Kirn
Caterpillar Inc.
Defense Products Department, JB7
Peoria IL 61629

James D. Kiser
NASA Lewis Research Center
21000 Brookpark Road, MS:49-3
Cleveland OH 44135

Max Klein
900 24th Street, N.W., Unit G
Washington DC 20037

Richard N. Kleiner
Golden Technologies Company
4545 McIntyre Street
Golden CO 80403

Stanley J. Klima
NASA Lewis Research Center
21000 Brookpark Road, MS:6-1
Cleveland OH 44135

Albert S. Kobayashi
University of Washington
Mechanical Engineering Department
Mail Stop:FU10
Seattle WA 98195

Shigeki Kobayashi
Toyota Central Research Labs
Nagakute Aichi, 480-11
JAPAN

Richard A. Kole
Z-Tech Corporation
8 Dow Road
Bow NH 03304

Joseph A. Kovach (5)
Eaton Corporation
32500 Chardon Road
Willoughby Hills OH 44094

Kenneth A. Kovaly
Technical Insights Inc.
P.O. Box 1304
Fort Lee NJ 07024-9967

Ralph G. Kraft
Spraying Systems Company
North Avenue at Schmale Road
Wheaton IL 60189-7900

Arthur Kranish
Trends Publishing Inc.
1079 National Press Building
Washington DC 20045

A. S. Krieger
Radiation Science, Inc.
P.O. Box 293
Belmont MA 02178

Pieter Krijgsman
Ceramic Design International
Holding B.V.
P.O. Box 68
Hattem 8050-AB
THE NETHERLANDS

Waltraud M. Kriven
University of Illinois
105 S. Goodwin Avenue
Urbana IL 61801

Edward J. Kubel, Jr.
ASM International
Advanced Materials & Processes
Materials Park OH 44073

Dave Kupperman
Argonne National Laboratory
9700 S. Cass Avenue
Argonne IL 60439

Oh-Hun Kwon
North Company
SGNICC/NRDC
Goddard Road
Northboro MA 01532-1545

W. J. Lackey
GTRI
Materials Science and Tech. Lab
Atlanta GA 30332

Jai Lalā
Tenmat Ltd.
40 Somers Road
Rugby Warwickshire CV22 7DH
ENGLAND

Hari S. Lamba
General Motors Corporation
9301 West 55th Street
LaGrange IL 60525

Richard L. Landingham
Lawrence Livermore National Lab
P.O. Box 808, L-369
Livermore CA 94550

James Lankford
Southwest Research Institute
6220 Culebra Road
San Antonio TX 78228-0510

Stanley B. Lasday
Business News Publishing Co.
1910 Cochran Road, Suite 630
Pittsburgh PA 15220

S. K. Lau
Carborundum Company
Technology Division
P.O. Box 832, B-100
Niagara Falls NY 14302

J. Lawrence Lauderdale
Babcock & Wilcox
1850 "K" Street, Suite 950
Washington DC 20006

Jean F. LeCostaouec
Textron Specialty Materials
2 Industrial Avenue
Lowell MA 01851

Benson P. Lee
Technology Management, Inc.
4440 Warrensville Rd., Suite A
Cleveland OH 44128

Burtrand I. Lee
Clemson University
Olin Hall
Clemson SC 29634-0907

June-Gunn Lee
KIST
P.O. Box 131, Cheong-Ryang
Seoul 130-650
KOREA

Ran-Rong Lee
Ceramics Process Systems
Corporation
155 Fortune Boulevard
Mildford MA 01757

Stan Levine
NASA Lewis Research Center
21000 Brookpark Road, MS:49-3
Cleveland OH 44135

David Lewis, III
Naval Research Laboratory
Code 6370
Washington DC 20375-5343

Ai-Kang Li
Materials Research Labs., ITRI
195-5 Chung-Hsing Road, Sec. 4
Chutung Hsinchu 31015 R.O.C.
TAIWAN

Robert H. Licht
Norton Company
SGNICC/NRDC
Goddard Road
Northboro MA 01532-1545

E. Lilley
Norton Company
SGNICC/NRDC
Goddard Road
Northboro MA 01532-1545

Chih-Kuang Lin
National Central University
Dept. of Mechanical Engineering
Chung-Li 32054
TAIWAN

Laura J. Lindberg
AlliedSignal Aerospace Company
Garrett Fluid Systems Division
P.O. Box 22200
Tempe AZ 85284-2200

Hans A. Lindner
Cremer Forschungsinstitut
GmbH&Co.KG
Oeslauer Strasse 35
D-8633 Rodental 8866
GERMANY

Ronald E. Loehman
Sandia National Laboratories
Chemistry & Ceramics Dept. 1840
P.O. Box 5800
Albuquerque NM 87185

Jeffrey C. Logas
Winona State University
115 Pasteur Hall
Winona MN 55987

Bill Long
Babcock & Wilcox
P.O. Box 11165
Lynchburg VA 24506

L. A. Lott
EG&G Idaho, Inc.
Idaho National Engineering Lab
P.O. Box 1625
Idaho Falls ID 83415-2209

Raouf O. Loutfy
MER Corporation
7960 S. Kolb Road
Tucson AZ 85706

Gordon R. Love
Aluminum Company of America
Alcoa Technical Center
Alcoa Center PA 15960

Lydia Luckevich
Ortech International
2395 Speakman Drive
Mississauga Ontario L5K 1B3
CANADA

James W. MacBeth
Carborundum Company
Structural Ceramics Division
P.O. Box 1054
Niagara Falls NY 14302

George Maczura
Aluminum Company of America
3450 Park Lane Drive
Pittsburgh PA 15275-1119

David Maginnis
Tinker AFB
OC-ALC/LIIRE
Tinker AFB OK 73145-5989

Frank Maginnis
Aspen Research, Inc.
220 Industrial Boulevard
Moore OK 73160

Tai-il Mah
Universal Energy Systems, Inc.
4401 Dayton-Xenia Road
Dayton OH 45432

Kenneth M. Maillar
Barbour Stockwell Company
83 Linskey Way
Cambridge MA 02142

S. G. Malghan
NIST
I-270 & Clopper Road
Gaithersburg MD 20899

S. Malkin (5)
University of Massachusetts
Amherst, MA 01003

Lars Malmrup
United Turbine AB
Box 13027
Malmo S-200 44
SWEDEN

John Mangels
Ceradyne, Inc.
3169 Redhill Avenue
Costa Mesa CA 92626

Murli Manghnani
University of Hawaii
2525 Correa Road
Honolulu HI 96822

Russell V. Mann
Matec Applied Sciences, Inc.
75 South Street
Hopkinton MA 01748

William R. Manning
Champion Aviation Products Div
P.O. Box 686
Liberty SC 29657

Ken Marnoch
Amercom, Inc.
8928 Fullbright Avenue
Chatsworth CA 91311

Robert A. Marra
Aluminum Company of America
Alcoa Technical Center
Alcoa Center PA 15069

Chauncey L. Martin
3M Company
3M Center, Building 60-1N-01
St. Paul MN 55144

Steve C. Martin
Advanced Refractory Technologies
699 Hertel Avenue
Buffalo NY 14207

Kelly J. Mather
William International Corporation
2280 W. Maple Road
Walled Lake MI 48088

James P. Mathers
3M Company
3M Center, Bldg. 201-3N-06
St. Paul MN 55144

Ron Mayville
Arthur D. Little, Inc.
15-163 Acorn Park
Cambridge MA 02140

F. N. Mazadarany
General Electric Company
Bldg. K-1, Room MB-159
P.O. Box 8
Schenectady NY 12301

James W. McCauley
Alfred University
Binns-Merrill Hall
Alfred NY 14802

Louis R. McCreight
2763 San Ramon Drive
Rancho Palos Verdes CA 90274

Colin F. McDonald
McDonald Thermal Engineering
1730 Castellana Road
La Jolla CA 92037

B. J. McEntire
Norton Company
10 Airport Park Road
East Granby CT 06026

Chuck McFadden
Coors Ceramics Company
600 9th Street
Golden CO 80401

Thomas D. McGee
Iowa State University
110 Engineering Annex
Ames IA 50011

Carol McGill
Corning Inc.
Sullivan Park, FR-02-08
Corning NY 14831

James McLaughlin
Sundstrand Power Systems
4400 Ruffin Road
P.O. Box 85757
San Diego CA 92186-5757

Matt McMonigle
U.S. Department of Energy
Improved Energy Productivity
CE-231, Forrestal Building
Washington DC 20585

J. C. McVickers
AlliedSignal Engines
P.O. Box 52180, MS:9317-2
Phoenix AZ 85072-2180

D. B. Meadowcroft
"Jura," The Ridgeway
Oxshott
Leatherhead Surrey KT22 0LG
UNITED KINGDOM

Joseph J. Meindl
Reynolds International, Inc.
6603 W. Broad Street
P.O. Box 27002
Richmond VA 23261-7003

Michael D. Meiser
AlliedSignal, Inc.
Ceramic Components
P.O. Box 2960, MS:T21
Torrance CA 90509-2960

George Messenger
National Research Council of
Canada
Building M-7
Ottawa Ontario K1A 0R6
CANADA

D. Messier
U.S. Army Materials Technology
SLCMT-EMC
405 Arsenal Street
Watertown MA 02172-0001

Arthur G. Metcalfe
Arthur G. Metcalfe and
Associates, Inc.
2108 East 24th Street
National City CA 91950

R. Metselaar
Eindhoven University
P.O. Box 513
Eindhoven 5600 MB
THE NETHERLANDS

David J. Michael
Harbison-Walker Refractories Co.
P.O. Box 98037
Pittsburgh PA 15227

Ken Michaels
Chrysler Motors Corporation
P.O. Box 1118, CIMS:418-17-09
Detroit MI 48288

Bernd Michel
Institute of Mechanics
P.O. Box 408
D-9010 Chemnitz
GERMANY

D. E. Miles
Commission of the European Comm.
rue de la Loi 200
B-1049 Brussels
BELGIUM

Carl E. Miller
AC Rochester
1300 N. Dort Highway, MS:32-31
Flint MI 48556

Charles W. Miller, Jr.
Centorr Furnaces/Vacuum
Industries
542 Amherst Street
Nashua NH 03063

R. Minimmi
Enichem America
2000 Cornwall Road
Monmouth Junction NJ 08852

Michele V. Mitchell
AlliedSignal, Inc.
Ceramic Components
P.O. Box 2960, MS:T21
Torrance CA 90509-2960

Howard Mizuhara
WESGO
477 Harbor Boulevard
Belmont CA 94002

Helen Moeller
Babcock & Wilcox
P.O. Box 11165
Lynchburg VA 24506-1165

Francois R. Mollard
Concurrent Technologies Corp.
1450 Scalp Avenue
Johnstown PA 15904-3374

Phil Mooney
Panametrics
221 Crescent Street
Waltham MA 02254

Geoffrey P. Morris
3M Company
3M Traffic Control Materials
Bldg. 209-BW-10, 3M Center
St. Paul MN 55144-1000

Jay A. Morrison
Rolls-Royce, Inc.
2849 Paces Ferry Road, Suite 450
Atlanta GA 30339-3769

Joel P. Moskowitz
Ceradyne, Inc.
3169 Redhill Avenue
Costa Mesa CA 92626

Brij Moudgil
University of Florida
Material Science & Engineering
Gainesville FL 32611

Christoph J. Mueller
Sprehsaal Publishing Group
P.O. Box 2962, Mauer 2
D-8630 Coburg
GERMANY

Thomas W. Mullan
Vapor Technologies Inc.
345 Route 17 South
Upper Saddle River NJ 07458

Theresa A. Mursick-Meyer
Norton Company
SGNICC/NRDC
Goddard Road
Northboro MA 01532-1545

M. K. Murthy
MkM Consultants International
10 Avoca Avenue, Unit 1906
Toronto Ontario M4T 2B7
CANADA

David L. Mustoe
Custom Technical Ceramics
8041 West I-70 Service Rd. Unit 6
Arvada CO 80002

Curtis V. Nakaishi
U.S. Department of Energy
Morgantown Energy Technology Ctr.
P.O. Box 880
Morgantown WV 26507-0880

Yoshio Nakamura
Faicera Research Institute
3-11-12 Misono
Sagamihara, Tokyo
JAPAN

Stefan Nann
Roland Berger & Partner GmbH
Georg-Glock-Str. 3
40474 Dusseldorf
GERMANY

K. S. Narasimhan
Hoeganaes Corporation
River Road
Riverton NJ 08077

Robert Naum
Applied Resources, Inc.
P.O. Box 241
Pittsford NY 14534

Malcolm Naylor
Cummins Engine Company, Inc.
P.O. Box 3005, Mail Code 50183
Columbus IN 47202-3005

Fred A. Nichols
Argonne National Laboratory
9700 S. Cass Avenue
Argonne IL 60439

H. Nickel
Forschungszentrum Juelich (KFA)
Postfach 1913
D-52425 Juelich
GERMANY

Dale E. Niesz
Rutgers University
Center for Ceramic Research
P.O. Box 909
Piscataway NJ 08855-0909

Paul W. Niskanen
Lanxide Corporation
P.O. Box 6077
Newark DE 19714-6077

David M. Nissley
United Technologies Corporation
Pratt & Whitney Aircraft
400 Main Street, MS:163-10
East Hartford CT 06108

Bruce E. Novich
Ceramics Process Systems Corp.
155 Fortune Boulevard
Milford MA 01757

Daniel Oblas
50 Meadowbrook Drive
Bedford MA 01730

Don Ohanehi
Magnetic Bearings, Inc.
1908 Sussex Road
Blacksburg VA 24060

Hitoshi Ohmori
ELID Team
Itabashi Branch
1-7 13 Kaga Itabashi
Tokyo 173
JAPAN

Robert Orenstein
General Electric Company
55-112, River Road
Schenectady NY 12345

Norb Osborn
Aerodyne Dallas
151 Regal Row, Suite 120
Dallas TX 75247

Richard Palicka
Cercom, Inc.
1960 Watson Way
Vista CA 92083

Joseph N. Panzarino
Norton Company
SGNICC/NRDC
Goddard Road
Northboro MA 01532-1545

Pellegrino Papa
Corning Inc.
MP-WX-02-1
Corning NY 14831

Terry Paquet
Boride Products Inc.
2879 Aero Park Drive
Traverse City MI 49684

E. Beth Pardue
MPC
8297 Williams Ferry Road
Lenoir City TN 37771

Soon C. Park
3M Company
Building 142-4N-02
P.O. Box 2963
St. Paul MN 55144

Vijay M. Parthasarathy
Caterpillar/Solar Turbines
2200 Pacific Highway
P.O. Box 85376
San Diego CA 92186-5376

Harmut Paschke
Schott Glaswerke
Christoph-Dorner-Strasse 29
D-8300 Landshut
GERMANY

James W. Patten
Cummins Engine Company, Inc.
P.O. Box 3005, Mail Code 50183
Columbus IN 47202-3005

Robert A. Penty
Eastman Kodak Company
Kodak Park
Bldg., 326, 3rd Floor
Rochester NY 14652-5120

Robert W. Pepper
Textron Specialty Materials
2 Industrial Avenue
Lowell MA 01851

Peter Perdue
Detroit Diesel Corporation
13400 Outer Drive West,
Speed Code L-04
Detroit MI 48239-4001

John J. Petrovic
Los Alamos National Laboratory
Group MST-4, MS:G771
Los Alamos NM 87545

Frederick S. Pettit
University of Pittsburgh
Pittsburgh PA 15261

Richard C. Phoenix
Ohmtek, Inc.
2160 Liberty Drive
Niagara Falls NY 14302

Bruce J. Pletka
Michigan Technological University
Metallurgical & Materials Engr.
Houghton MI 49931

John P. Pollinger
AlliedSignal, Inc.
Ceramic Components
P.O. Box 2960, MS:T21
Torrance CA 90509-2960

P. Popper
 High Tech Ceramics International
 Journal
 22 Pembroke Drive - Westlands
 Newcastle-under-Lyme
 Staffs ST5 2JN
 ENGLAND

F. Porz
 Universitat Karlsruhe
 Institut fur Keramik Im
 Maschinendau
 Postfach 6980
 D-76128 Karlsruhe
 GERMANY

Harry L. Potma
 Royal Netherlands Embassy
 Science and Technology
 4200 Linnean Avenue, N.W.
 Washington DC 20008

Bob R. Powell
 General Motors Corporation
 Metallurgy Department
 Box 9055
 Warren MI 48090-9055

Stephen C. Pred
 Biesterfeld U.S., Inc.
 500 Fifth Avenue
 New York NY 10110

Karl M. Prewo
 United Technologies Research Ctr.
 411 Silver Lane, MS:24
 East Hartford CT 06108

Vimal K. Pujari
 Norton Company
 SGNICC/NRDC
 Goddard Road
 Northboro MA 01532-1545

George Quinn
 NIST
 Ceramics Division, Bldg. 223
 Gaithersburg MD 20899

Ramas V. Raman
 Ceracon, Inc.
 1101 N. Market Boulevard, Suite 9
 Sacramento CA 95834

Charles F. Rapp
 Owens Corning Fiberglass
 2790 Columbus Road
 Granville OH 43023-1200

Dennis W. Readey
 Colorado School of Mines
 Metallurgy and Materials Engr.
 Golden CO 80401

Wilfred J. Rebello
 PAR Enterprises, Inc.
 12601 Clifton Hunt Lane
 Clifton VA 22024

Harold Rechter
 Chicago Fire Brick Company
 7531 S. Ashland Avenue
 Chicago IL 60620

Robert R. Reeber
 U.S. Army Research Office
 P.O. Box 12211
 Research Triangle Park NC
 27709-2211

K. L. Reifsnider
 VPI & SU
 Engineering Science and Mechanics
 Blacksburg VA 24061

Paul E. Rempes
 McDonnell Douglass Aircraft Co.
 P.O. Box 516, Mail Code:0642263
 St. Louis MO 63166-0516

Gopal S. Revankar
 John Deere Company
 3300 River Drive
 Moline IL 61265

K. Y. Rhee
 Rutgers University
 P.O. Box 909
 Piscataway NJ 08854

James Rhodes
Advanced Composite Materials Corp
1525 S. Buncombe Road
Greer SC 29651

Roy W. Rice
W. R. Grace and Company
7379 Route 32
Columbia MD 21044

David W. Richerson
2093 E. Delmont Drive
Salt Lake City UT 84117

Tomas Richter
J. H. France Refractories
1944 Clarence Road
Snow Shoe PA 16874

Michel Rigaud
Ecole Polytechnique
Campus Universite De Montreal
P.O. Box 6079, Station A
Montreal, P.Q. Quebec H3C 3A7
CANADA

John E. Ritter
University of Massachusetts
Mechanical Engineering Department
Amherst MA 01003

Frank L. Roberge
AlliedSignal Engines
P.O. Box 52180
Phoenix AZ 85072-2180

W. Eric Roberts
Advanced Ceramic Technology, Inc.
990 "F" Enterprise Street
Orange CA 92667

Y. G. Roman
TNO TPD Keramick
P.O. Box 595
Eindhoven 5600 AN
HOLLAND

Michael Rossetti
Arthur D. Little, Inc.
15 Acorn Park
Cambridge MA 01240

Barry Rossing
Lanxide Corporation
P.O. Box 6077
Newark DE 19714-6077

Steven L. Rotz
Lubrizol Corporation
29400 Lakeland Boulevard
Wickliffe OH 44092

Robert Ruh
Wright Laboratory
WL/MLLM
Wright-Patterson AFB OH 45433

Robert J. Russell
17 Highgate Road
Framingham MA 01701

Jon A. Salem
NASA Lewis Research Center
21000 Brookpark Road
Cleveland OH 44135

W. A. Sanders
NASA Lewis Research Center
21000 Brookpark Road, MS:49-3
Cleveland OH 44135

J. Sankar
North Carolina A&T State Univ.
Dept. of Mechanical Engineering
Greensboro NC 27406

Yasushi Sato
NGK Spark Plugs (U.S.A.), Inc.
1200 Business Center Drive, #300
Mt. Prospect IL 60056

Maxine L. Savitz
AlliedSignal, Inc.
Ceramic Components
P.O. Box 2960, MS:T21
Torrance CA 90509-2960

Ashok Saxena
GTRI
Materials Engineering
Atlanta GA 30332-0245

David W. Scanlon
Instron Corporation
100 Royall Street
Canton MA 02021

Charles A. Schacht
Schacht Consulting Services
12 Holland Road
Pittsburgh PA 15235

Robert E. Schafrik
National Materials Advisory Board
2101 Constitution Ave., N.W.
Washington DC 20418

James Schienle
AlliedSignal Engines
P.O. Box 52180, MS:1302-2P
Phoenix AZ 85072-2180

John C. Schneider
San Juan Technologies, Inc.
3210 Arena Road
Colorado Springs CO 80921-1503

Gary Schnittgrund
Rocketdyne, BA05
6633 Canoga Avenue
Canoga Park CA 91303

Mark Schomp
Lonza, Inc.
17-17 Route 208
Fair Lann NJ 07410

Joop Schoonman
Delft University of Technology
P.O. Box 5045
2600 GA Delft
THE NETHERLANDS

Robert B. Schulz
U.S. Department of Energy
Office of Transportation Matrls.
CE-34, Forrestal Building
Washington DC 20585

Murray A. Schwartz
Materials Technology Consulting
30 Orchard Way, North
Potomac MD 20854

Peter Schwarzkopf
SRI International
333 Ravenswood Avenue
Menlo Park CA 94025

William T. Schwessinger
Multi-Arc Scientific Coatings
1064 Chicago Road
Troy MI 48083-4297

W. D. Scott
University of Washington
Materials Science Department
Mail Stop:FB10
Seattle WA 98195

Nancy Scoville
Thermo Electron Technologies
P.O. Box 9046
Waltham MA 02254-9046

Thomas M. Sebestyen
U.S. Department of Energy
Advanced Propulsion Division
CE-322, Forrestal Building
Washington DC 20585

Brian Seegmiller
Coors Ceramics Company
600 9th Street
Golden CO 80401

T. B. Selover
AICRE/DIPPR
3575 Traver Road
Shaker Heights OH 44122

Charles E. Semler
Semler Materials Services
4160 Mumford Court
Columbus OH 43220

Thomas Service
Service Engineering Laboratory
324 Wells Street
Greenfield MA 01301

Kish Seth
Ethyl Corporation
P.O. Box 341
Baton Rouge LA 70821

William J. Shack
Argonne National Laboratory
9700 S. Cass Avenue, Bldg. 212
Argonne IL 60439

Peter T.B. Shaffer
Technical Ceramics Laboratories,
4045 Nine/McFarland Drive
Alpharetta GA 30201

Richard K. Shaltens
NASA Lewis Research Center
21000 Brookpark Road, MS:302-2
Cleveland OH 44135

Robert S. Shane
1904 NW 22nd Street
Stuart FL 34994-9270

Ravi Shankar
Chromalloy
Research and Technology Division
Blaisdell Road
Orangeburg NY 10962

Terence Sheehan
Alpex Wheel Company
727 Berkley Street
New Milford NJ 07646

Dinesh K. Shetty
University of Utah
Materials Science and Engineering
Salt Lake City UT 84112

Masahide Shimizu
New Ceramics Association
Shirasagi 2-13-1-208, Nakano-ku
Tokyo, 165
JAPAN

Thomas Shreves
American Ceramic Society, Inc.
735 Ceramic Place
Westerville OH 43081-8720

Jack D. Sibold
Coors Ceramics Company
4545 McIntyre Street
Golden CO 80403

Johann Siebels
Volkswagen AG
Werkstofftechnologie
Postfach 3180
Wolfsburg 1
GERMANY

George H. Siegel
Point North Associates, Inc.
P.O. Box 907
Madison NJ 07940

Richard Silbergliitt
FM Technologies, Inc.
10529-B Braddock Road
Fairfax VA 22032

Mary Silverberg
Norton Company
SGNICC/NRDC
Goddard Road
Northboro MA 01532-1545

Gurpreet Singh
Department of the Navy
Code 56X31
Washington DC 20362-5101

Maurice J. Sinnott
University of Michigan
5106 IST Building
Ann Arbor MI 48109-2099

John Skildum
3M Company
3M Center
Building 224-2S-25
St. Paul MN 55144

Richard H. Smoak
Smoak & Associates
3554 Hollislope Road
Altadena CA 91001-3923

Jay R. Smyth
AlliedSignal Engines
111 S. 34th Street, MS:503-412
Phoenix AZ 85034

Rafal A. Sobotowski
British Petroleum Company
Technical Center, Broadway
3092 Broadway Avenue
Cleveland OH 44115

S. Somiya
Nishi Tokyo University
3-7-19 Seijo, Setagaya
Tokyo, 157
JAPAN

Boyd W. Sorenson
DuPont Lanxide Composites
1300 Marrows Road
Newark DE 19711

Charles A. Sorrell
U.S. Department of Energy
Advanced Industrial Concepts
CE-232, Forrestal Building
Washington DC 20585

C. Spencer
EA Technology
Capenhurst Chester CH1 6ES
UNITED KINGDOM

Allen Spizzo
Hercules Inc.
Hercules Plaza
Wilmington DE 19894

Richard M. Spriggs
Alfred University
Center for Advanced Ceramic
Technology
Alfred NY 14802

Charles Spuckler
NASA Lewis Research Center
21000 Brookpark Road, MS:5-11
Cleveland OH 44135-3191

M. Srinivasan
Material Solutions
P.O. Box 663
Grand Island NY 14702-0663

Gordon L. Starr
Cummins Engine Company, Inc.
P.O. Box 3005, Mail Code:50182
Columbus IN 47202-3005

Tom Stillwagon
AlliedSignal, Inc.
Ceramic Components
P.O. Box 2960, MS:T21
Torrance CA 90509-2960

H. M. Stoller
TPL Inc.
3754 Hawkins, N.E.
Albuquerque NM 87109

Paul D. Stone
Dow Chemical USA
1776 "Eye" Street, N.W., #575
Washington DC 20006

F. W. Stringer
Aero & Industrial Technology Ltd.
P.O. Box 46, Wood Top
Burnley Lancashire BB11 4BX
UNITED KINGDOM

Thomas N. Strom
NASA Lewis Research Center
21000 Brookpark Road, MS:86-6
Cleveland OH 44135

M. F. Stroosnijder
Institute for Advanced Materials
Joint Research Centre
21020 Ispra (VA)
ITALY

Karsten Styhr
30604 Ganado Drive
Rancho Palos Verdes CA 90274

T. S. Sudarshan
Materials Modification, Inc.
2929-P1 Eskridge Center
Fairfax VA 22031

M. J. Sundaresan
University of Miami
P.O. Box 248294
Coral Gables FL 33124

Patrick L. Sutton
U.S. Department of Energy
Office of Propulsion Systems
CE-322, Forrestal Building
Washington DC 20585

Willard H. Sutton
United Technologies Corporation
Silver Lane, MS:24
East Hartford CT 06108

J. J. Swab
U.S. Army Materials Technology
Ceramics Research Division,
SLCMT-EMC
405 Arsenal Street
Watertown MA 02172

Robert E. Swanson
Metalworking Technology, Inc.
1450 Scalp Avenue
Johnstown PA 15904

Steve Szaruga
Air Force Wright Aeronautical Lab
WL/MLBC
Wright-Patterson AFB OH
45433-6533

Yo Tajima
NGK Spark Plug Company
2808 Iwasaki
Komaki-shi Aichi-ken, 485
JAPAN

Fred Teeter
5 Tralee Terrace
East Amherst NY 14051

Monika O. Ten Eyck
Carborundum Microelectronics
P.O. Box 2467
Niagara Falls NY 14302-2467

David F. Thompson
Corning Glass Works
SP-DV-02-1
Corning NY 14831

Merle L. Thorpe
Hobart Tafa Technologies, Inc.
20 Ridge Road
Concord NH 03301-3010

T. Y. Tien
University of Michigan
Materials Science and Engineering
Dow Building
Ann Arbor MI 48103

D. M. Tracey
Norton Company
SGNICC/NRDC
Goddard Road
Northboro MA 01532-1545

Marc Tricard
Norton Company, WGTC
1 New Bond Street
Worcester MA 01615-0008

L. J. Trostel, Jr.
Box 199
Princeton MA 01541

W. T. Tucker
General Electric Company
P.O. Box 8, Bldg. K1-4C35
Schenectady NY 12301

Masanori Ueki
Nippon Steel Corporation
1618 Ida
Nakahara-Ku Kawasaki, 211
JAPAN

Filippo M. Ugolini
ATA Studio
Via Degli Scipioni, 268A
ROMA, 00192
ITALY

Donald L. Vaccari
Allison Gas Turbines
P.O. Box 420, Speed Code S49
Indianapolis IN 46206-0420

Carl F. Van Conant
 Boride Products, Inc.
 2879 Aero Park Drive
 Traverse City MI 49684

Marcel H. Van De Voorde
 Commission of the European Comm.
 P.O. Box 2
 1755 ZG Petten
 THE NETHERLANDS

O. Van Der Biest
 Katholieke Universiteit Leuven
 Dept. Metaalkunde en Toegepaste
 de Croylaan 2
 B-3030 Leuven
 BELGIUM

Michael Vannier
 Washington University, St. Louis
 510 S. Kings Highway
 St. Louis MO 63110

Stan Venkatesan
 Southern Coke & Coal Corporation
 P.O. Box 52383
 Knoxville TN 37950

V. Venkateswaran
 Carborundum Company
 Niagara Falls R&D Center
 P.O. Box 832
 Niagara Falls NY 14302

Dennis Viechnicki
 U.S. Army Materials Technology
 405 Arsenal Street
 Watertown MA 02172-0001

Ted Vojnovich
 U.S. Department of Energy, ST-311
 Office of Energy Research, 3F077P
 Washington DC 20585

John D. Volt
 E.I. Dupont de Nemours & Co. Inc.
 P.O. Box 80262
 Wilmington DE 19880

John B. Wachtman
 Rutgers University
 P.O. Box 909
 Piscataway NJ 08855

Shigetaka Wada
 Toyota Central Research Labs
 Nagakute Aichi, 480-11
 JAPAN

Janet Wade
 AlliedSignal Engines
 P.O. Box 52180, MS:1303-2
 Phoenix AZ 85072-2180

Richard L. Wagner
 Ceramic Technologies, Inc.
 537 Turtle Creek South Dr., #24D
 Indianapolis IN 46227

J. Bruce Wagner, Jr.
 Arizona State University
 Center for Solid State Science
 Tempe AZ 85287-1704

Daniel J. Wahlen
 Kohler, Co.
 444 Highland Drive
 Kohler WI 53044

Ingrid Wahlgren
 Royal Institute of Technology
 Studsvik Library
 S-611 82 Nykoping
 SWEDEN

Ron H. Walecki
 AlliedSignal, Inc.
 Ceramic Components
 P.O. Box 2960, MS:T21
 Torrance CA 90509-2960

Michael S. Walsh
 Vapor Technologies Inc.
 6300 Gunpark Drive
 Boulder CO 80301

Chien-Min Wang
 Industrial Technology Research
 Institute
 195 Chung-Hsing Road, Sec. 4
 Chutung Hsinchu 31015 R.O.C.
 TAIWAN

Robert M. Washburn
 ASMT
 11203 Colima Road
 Whittier CA 90604

Gerald Q. Weaver
 Carborundum Specialty Products
 42 Linus Allain Avenue
 Gardner MA 01440-2478

Kevin Webber
 Toyota Technical Center, U.S.A.
 1410 Woodridge, RR7
 Ann Arbor MI 48105

Karen E. Weber
 Detroit Diesel Corporation
 13400 Outer Drive West
 Detroit MI 48239-4001

James K. Weddell
 Du Pont Lanxide Composites Inc.
 P.O. Box 6100
 Newark DE 19714-6100

R. W. Weeks
 Argonne National Laboratory
 MCT-212
 9700 S. Cass Avenue
 Argonne IL 60439

Ludwig Weiler
 ASEA Brown Boveri AG
 Eppelheimer Str. 82
 D-6900 Heidelberg
 GERMANY

James Wessel
 Dow Corning Corporation
 1800 "M" Street, N.W., #325 South
 Washington DC 20036

Robert D. West
 Therm Advanced Ceramics
 P.O. Box 220
 Ithaca NY 14851

Thomas J. Whalen
 1845 Cypress Pointe Court
 Ann Arbor MI 48108

Ian A. White
 Hoeganaes Corporation
 River Road
 Riverton NJ 08077

Sheldon M. Wiederhorn
 NIST
 Building 223, Room A329
 Gaithersburg MD 20899

John F. Wight
 Alfred University
 McMahan Building
 Alfred NY 14802

D. S. Wilkinson
 McMaster University
 1280 Main Street, West
 Hamilton Ontario L8S 4L7
 CANADA

James C. Williams
 General Electric Company
 Engineering Materials Technology
 One Neumann Way, Mail Drop:H85
 Cincinnati OH 45215-6301

Steve J. Williams
 RCG Hagler Bailly, Inc.
 1530 Wilson Boulevard, Suite 900
 Arlington VA 22209-2406

Thomas A. Williams
 National Renewable Energy Lab
 1617 Cole Boulevard
 Golden CO 80401

Craig A. Willkens
 Norton Company
 SGNICC/NRDC
 Goddard Road
 Northboro MA 01532-1545

Roger R. Wills
Ohio Aerospace Institute (OAI)
22800 Cedar Point Road
Brook Park OH 44142

David Gordon Wilson
Massachusetts Institute of
Technology
77 Massachusetts Ave., Room 3-455
Cambridge MA 02139

Matthew F. Winkler
Seaworthy Systems, Inc.
P.O. Box 965
Essex CT 06426

Gerhard Winter
Hermann C. Starck Berlin GmbH
P.O. Box 25 40
D-3380 Goslar 3380
GERMANY

William T. Wintucky
NASA Lewis Research Center
Terrestrial Propulsion Office
21000 Brookpark Road, MS:86-6
Cleveland OH 44135

Thomas J. Wissing
Eaton Corporation
Engineering and Research Center
P.O. Box 766
Southfield MI 48037

James C. Withers
MER Corporation
7960 S. Kolb Road
Building F
Tucson AZ 85706

Dale E. Wittmer
Southern Illinois University
Mechanical Engineering Department
Carbondale IL 62901

Warren W. Wolf
Owens Corning Fiberglass
2790 Columbus Road, Route 16
Granville OH 43023

Egon E. Wolff
Caterpillar Inc.
Technical Center
P.O. Box 1875
Peoria IL 61656-1875

George W. Wolter
Howmet Turbine Components Corp.
Technical Center
699 Benston Road
Whitehall MI 49461

James C. Wood
NASA Lewis Research Center
21000 Brookpark Road, MS:86-6
Cleveland OH 44135

Wayne L. Worrell
University of Pennsylvania
3231 Walnut Street
Philadelphia PA 19104

John F. Wosinski
Corning Inc.
ME-2 E-5 H8
Corning NY 14830

Ruth Wroe
ERDC
Capenhurst Chester CH1 6ES
ENGLAND

Bernard J. Wrona
Advanced Composite Materials Corp
1525 S. Buncombe Road
Greer SC 29651

Carl C. M. Wu
Naval Research Laboratory
Ceramic Branch, Code 6373
Washington DC 20375

John C. Wurst
U. of Dayton Research Institute
300 College Park
Dayton OH 45469-0101

Neil Wyant
ARCH Development Corp.
9700 S. Cass Avenue, Bldg. 202
Argonne IL 60439

Roy Yamamoto
 Texaco Inc.
 P.O. Box 509
 Beacon NY 12508-0509

John Yamanis
 AlliedSignal Aerospace Company
 P.O. Box 1021
 Morristown NJ 07962-1021

Harry C. Yeh
 AlliedSignal, Inc.
 Ceramic Components
 P.O. Box 2960, MS:T21
 Torrance CA 90509-2960

Hiroshi Yokoyama
 Hitachi Research Lab
 4026 Kuji-Cho
 Hitachi-shi Ibaraki 319-12
 JAPAN

Thomas M. Yonushonis
 Cummins Engine Company, Inc.
 P.O. Box 3005, Mail Code 50183
 Columbus IN 47202-3005

Thomas J. Yost
 Corning Inc.
 Technical Products Div., 21-1-2
 Corning NY 14831

Jong Yung
 Sundstrand Aviation Operations
 4747 Harrison Avenue
 Rockford IL 61125

A. L. Zadoks
 Caterpillar Inc.
 Technical Center, Building L
 P.O. Box 1875
 Peoria IL 61656-1875

Avi Zangvil
 University of Illinois
 104 S. Goodwin Avenue
 Urbana IL 61801

Charles H. Zenuk
 Transtech
 6662 E. Paseo San Andres
 Tucson AZ 85710-2106

Carl Zweben
 General Electric Company
 P.O. Box 8555, VFSC/V4019
 Philadelphia PA 19101

Department of Energy
 Oak Ridge Operations Office
 Asst. Manager for Energy
 Research and Development
 P.O. Box 2001
 Oak Ridge, TN 37831-8600

Department of Energy
 Office of Scientific and
 Technical Information
 Office of Information Services
 P.O. Box 62
 Oak Ridge, TN 37831